UMTA-CO-06-0009-83-2

TRANSIT CAR DEMONSTRATION TEST PROGRAM ON THE ROLL DYNAMICS UNIT

Volume I

PREPARED FOR

U.S. DEPARTMENT OF TRANSPORTATION

URBAN MASS TRANSPORTATION ADMINISTRATION
Office of Technical Assistance

WASHINGTON, D.C. 20590

NOTICE

This document is disseminated under the sponsorship of the Department of Transportation in the interest of information exchange. The United States Government assumes no liability for its contents or use thereof.

The United States Government does not endorse products or manufacturers. Trade or manufacturers' names appear herein solely because they are considered essential to the object of this report.

Technical Report Documentation Page

1. Report No.	2. Government Accession No.	3. Recipient's Catalog No.
UMTA-CO-06-0009-83-2		

4. Title and Subtitle	5. Report Date
Transit Car Test Program on the Roll Dynamics Unit	6. Performing Organization Code: TTC-004

7. Author(s)	8. Performing Organization Report No.
(I) N.K. Cooperrider, E.H. Law, R.H. Fries, I. Haque * (II) G. Arnold, S. Nelson **	(I) CR-R-82037 (II) TTC-004

9. Performing Organization Name and Address	10. Work Unit No. (TRAIS)
Transportation Test Center P.O. Box 11130 Pueblo, Colorado 81001	CO-06-0009
	11. Contract or Grant No.
	13. Type of Report and Period Covered: FINAL March 3 thru 18, 1981
12. Sponsoring Agency Name and Address U.S. Department of Transportation Urban Mass Transportation Administration	14. Sponsoring Agency Code: URT-12

15. Supplementary Notes

* Authors (I) College of Engineering & Applied Sciences, Arizona State University
** Authors (II) Boeing Services International, O&M Contractor, TTC

16. Abstract

This report documents two separate studies aimed at verifying and demonstrating the capabilities of the Roll Dynamics Unit (RDU). The RDU is part of the Rail Dynamics Laboratory (RDL), located at the Transportation Test Center (TTC), in Pueblo, Colorado. During testing, the RDU's potential for simulating actual track conditions was explored and results were correlated with measurements taken during in-track testing. Other efforts focused on the RDU's use as a laboratory instrument, by which selected performance parameters can be varied, and the responses of a single rail vehicle measured, under controlled conditions.

Sponsored by the Urban Mass Transportation Administration (UMTA), testing involved use of the Number One SOAC (State-of-the-Art Car), one of two such vehicles developed under UMTA's Urban Rail Vehicle and Systems Program (URRVS). The 90,000-pound intra-city, rapid transit vehicle, configured as an "A" Car (capable of independent or two-car operation), was operated on the TTC's Transit Test Track (TTT) to provide in-track data. It was then installed on the RDU for the testing described in this report. Information on SOAC technical/historical development and URRVS Program highlights are presented as background for the discussion of the results.

The first study was conducted by TTC personnel under the technical counsel of University of Arizona and Clemson University personnel and concerned itself with rail vehicle stability. Test methodology and software requirements were developed and analytical models evaluated. RDU mechanical characteristics were assessed in terms of their influence on measured vehicle responses during studies of hunting, creep forces, and forced sinusoidal responses.

The other study involved separate testing, done by TTC personnel, in such traditional performance areas of transit vehicle operation as traction, acceleration/deceleration, energy consumption, and spin/slide performance. In-track results were compared to RDU measured responses and the resulting excellent correlation demonstrated the feasibility of RDU testing.

17. Key Words	18. Distribution Statement
Analytical Modelling Creep Forces Eigenvalue-Eigenvector Energy Consumption Rail Dynamics Roll Dynamics Spin/Slide Traction Resistance	Document may be purchased from the National Technical Information Service, 5285 Port Royal Road, Springfield, Virginia 22161

19. Security Classif. (of this report)	20. Security Classif. (of this page)	21. No. of Pages	22. Price
Unclassified	Unclassified	208	

TRANSIT CAR DEMONSTRATION TEST PROGRAM ON THE ROLL DYNAMICS UNIT

Volume I

State-of-the-Art-Car (SOAC) Creep Forces and Dynamic Response on the Roll Dynamics Unit

N. K. Cooperrider, E. H. Law, R. H. Fries, I. Haque

September 1982

Prepared for
Boeing Services International
Pueblo, Colorado
Contract No. F-401285-6940

(Reproduced from Report No. CR-R-82037,
College of Engineering & Applied Sciences,
Arizona State University
Tempe, Arizona 85287)

TRANSIT CAR DEMONSTRATION TEST PROGRAM ON THE ROLL DYNAMICS UNIT

EXECUTIVE SUMMARY

Introduction. An important key to the successful operation of a given rail transportation system is the safe, reliable, and efficient performance of its rail vehicles. Many complex relationships of wheel/rail interface and truck suspension dynamics have been observed during on-track testing. Instability and erratic behavior of transit cars, brought on by poor interaction between wheel and rail, not only causes rough rides for passengers, but is also responsible for accidents, derailments, and excessive maintenance costs.

Development of the Rail Dynamics Laboratory (RDL) at the Transportation Test Center (TTC), in Pueblo, Colorado gave the opportunity to test and identify improvements for today's railroad and transit systems. The Roll Dynamics Unit (RDU), which is part of the RDL, can be used to investigate the wheel/rail dynamics of acceleration, adhesion, braking, and hunting while simulating a vehicle's forward motion on rollers rather than on conventional rails. The RDU has the capacity to apply rotating forces or absorb forces from a powered vehicle's wheels. Through a system of drive motors, flywheels, gearboxes, and rollers, the RDU is capable of simulating relative motion - for both self-propelled and unpowered vehicles of various truck spacings, axle spacings, and rail gauge - up to speeds of 144 mph.

Electronic equipment controls both the rotational speed and torque of the drive train by the manipulation of thumb wheel switches. During a test, operating conditions are monitored both automatically and manually. The automatic monitors are interconnected to control circuitry to prevent damage to the RDU or test vehicle.

Whereas the RDU can be applied to studies of acceleration, adhesion, braking, and lateral dynamics, dynamometer tests to characterize motor performance of self-propelled vehicles can also be performed. Accordingly, validation of analytical models of these phenomena can be accomplished. The effects of various components on the hunting threshold speed for a particular truck can be precisely assessed on the RDU. It can also be used to evaluate given designs relative to standard performance criteria.

The purpose of the test programs described in this report was to demonstrate the RDL's capabilities through the use of the RDU to evaluate propulsion systems, braking, energy consumption characteristics, and dynamic stability parameters of a transit vehicle. The State of the Art Car (SOAC), representing a typical transit car, was used to accomplish this task.

The RDU Transit Car Demonstration Test Program, funded by the Urban Mass Transit Administration (UMTA), consisted of two distinct, separate portions, both conducted between March 3rd and 18th of 1981. Reports on these two portions have been designated Volumes I and II and are presented herein.

Volume I. The first portion of the test program concerned itself with the study of rail vehicle stability. This part of the test program was conducted by TTC personnel under the technical counsel of Arizona State University and Clemson University personnel who were under contract with UMTA. Volume I of

this document, entitled STATE-OF-THE-ART-CAR (SOAC) CREEP FORCES AND DYNAMIC RESPONSE ON THE ROLL DYNAMICS UNIT, deals with this section of the test program. The specific objectives of this part of the test program were:

1. To measure the steady forces and resultant vehicle displacements under constant speed conditions and to formalize test requirements, methods and software development for the purpose of estimating the creep force characteristics of the SOAC on the RDU.

2. To determine test requirements to evaluate the vehicle's hunting characteristics and to measure vehicle reponses to known perturbations for comparison and enhancement of analytical vehicle dynamic models.

The major conclusions drawn from these sets of test runs were:

1. This program successfully showed that the testing methods, creep coefficient identification technique, and dynamic theory validation approach all produced useful results.

2. The actuator configuration, used for the forced sinusoidal response tests; i.e., use of only the leading actuator on the truck, was found to be nearly optimum.

3. Since the swept frequency tests did not produce clear resonances or modal frequencies, the utility of the single frequency sinusoidal response tests was minimal. Besides, the frequency sweep test data were sufficient to characterize the vehicle response.

4. The creep coefficient estimates from runs under the same conditions were consistent with the available theory for rolling contact and showed good repeatability, which lends confidence to the values derived and the test methods employed.

5. A need for careful determination of wheel and roller cross-sectional curvatures in future creep coefficient identification was illustrated.

6. Based on the comparisons of the Dynamic Response data and the theoretical model, the Kinematic mode damping ratios are underestimated, but there is good agreement between frequencies. The roll restraint system used on the RDU made predicting the body mode frequencies difficult. Analytical and experimental transfer functions, for several cases, agreed quite well over the entire frequency range of the tests.

7. The dynamic model showed that the roller rig terms were relatively unimportant for the SOAC vehicle, and that the critical speed on the RDU is only about 10 mph lower than it would be on track whose profile is the same as the rollers' profile.

The report details the test program, vehicle modelling, creep force and dynamic response results and analysis along with summary conclusions and recommendations.

Volume II. The second portion of the test program concentrated on the traditional performance characterization of transit vehicles. TTC personnel were responsible for the conduct of the test and the analysis and reporting of the

findings. Volume II of this document, entitled DEMONSTRATION OF A TRANSIT CAR PERFORMANCE TEST ON THE ROLL DYNAMICS UNIT, deals with this subject matter.

The performance tests carried out were as follows:

1. Traction Resistance
2. Acceleration
3. Deceleration
4. Spin/Slide Protection System Tests
5. Energy Consumption and Undercar Temperature Tests

The objectives of this series of tests were:

1. To identify advantages and disadvantages of performance testing on the rollers as highlighted by the SOAC tests.
2. Compare the results from the RDU tests with results of a similar test conducted, using the same SOAC car, on the Transit Test Track (TTT).

Encouraging conclusions were drawn as follows:

1. The tests, although of limited scope in comparison to the track tests performed on the same car, showed excellent correlation and demonstrated feasibility of RDU testing.
2. The tractive resistance, acceleration, and power consumption tests were highly successful, while the spin/slide test was of limited success. An alternate method of spin/slide testing has been proposed which could improve this deficiency.

Volume II includes background information, details of the test program, analysis and results, conclusions, and recommendations.

TABLE OF CONTENTS

TABLE OF CONTENTS
(continued)

Chapter 1

INTRODUCTION

BACKGROUND

The potential for unstable running of rail vehicles is well known. Unstable running, or "hunting", is highly undesirable, and ensuring stable behavior within normal operating speeds is a major vehicle design objective. Although the theory of rail vehicle lateral dynamics can predict the effects of design changes on stability with reasonable accuracy, the actual limits of stable operation can depend on factors such as rail surface conditions, suspension friction levels and roadbed alignment that are highly variable and difficult to measure. Actual testing is always needed to confirm the stability properties of a rail vehicle.

Field testing to determine rail vehicle stability properties is difficult. The roadbed geometry and rail surface condition must be carefully measured, as they have a strong influence on stability. Vehicle instrumentation and data recording equipment must be installed and carried on board the test vehicle or an adjacent vehicle. Furthermore, it is difficult or impossible to visually observe the vehicle component motions during the tests. It is also difficult to introduce controlled disturbances into the vehicle. Although instrumented field tests can be carried out, they require careful planning and execution, and they generally involve large expenses and long periods of time to complete.

The Roll Dynamics Unit (RDU) at the Transportation Test Center (TTC) is intended to reduce the difficulty of rail vehicle stability testing by providing a stationary facility for such tests. The four rollersets of this facility can be driven up to 144 mph while the vehicle body is held stationary. Prescribed disturbances can be imposed on the vehicle with hydraulic actuators mounted between ground and the vehicle or between vehicle components. Instrumentation is mounted between fixed references and the vehicle, and a computerized data recording system is provided.

Questions concerning the differences in rail vehicle operation on roller rig and track must be answered when using facilities such as the RDU for vehicle stability testing. Differences are introduced due to the geometry of the rollers, the fact that they are moving rather than stationary, and the laboratory rather than field wheel-rail (roller) surface conditions. The dynamics of the roller rig system and the flexibility of the rollers may also affect the vehicle behavior on the roller rig. To extrapolate the results of tests on the RDU to behavior in the field requires an understanding of these differences and their influence on vehicle stability. The project reported here was intended to be the first stage in developing that understanding and methodology.

Demonstration tests were conducted on the State-of-the-Art-Car (SOAC) on the RDU during March of 1981. As part of this project, tests were performed to determine the wheel-roller contact forces and to establish the stability properties of the SOAC.

OBJECTIVES

The specific objectives of the project reported here were the following:

1. To determine test requirements for measuring the creep force characteristics of the SOAC on the RDU.
2. To determine test requirements for dynamic tests of the SOAC on the RDU. These tests were intended to provide data for comparison and improvement of analytical vehicle dynamic models.
3. To develop software for estimation of the creep force characteristics of the SOAC on the RDU, and to use this software to make a preliminary analysis of the RDU creep force characteristics.

This work was planned as the first phase of a longer project to develop testing procedures for vehicles on the RDU, and to provide a method, using the theory of rail vehicle lateral dynamics, to extrapolate roller rig test results to behavior in the field. This report discuss the tests, test results, creep force identification processes, and preliminary comparisons of dynamic test results with theoretical results.

TEST DESCRIPTION

The instrumentation, data recording, test conduct, and data analysis for this project were carried out by Boeing Services International following our Test Requirements document [1].

The test program involved static vehicle characterization tests to determine vehicle parameters as well as the dynamic tests on the RDU. The characterization tests included efforts to determine the following properties:

- o Primary suspension stiffnesses
- o Secondary yaw stiffness and friction
- o Wheel and roller profiles
- o Interaxle misalignments

The RDU testing was designed to provide data for identification of the wheel-rail creep forces and for validation of a theory for vehicle lateral dynamics on the RDU. Altogether, 32 test runs were made. These runs involved the following four types of tests:

- o Creep force identification
- o Initial condition response
- o Swept sinusoidal response
- o Single frequency sinusoidal response.

Each type of test was conducted at more than one speed, with two or three different wheel/roller surface preparations, and at different levels of applied forces.

APPROACH

Our responsibilities on this project were to specify the test requirements and to analyze the data obtained from the tests. The test requirements were given in an earlier document [1]. This report is devoted to describing the tests, the test results, the creep force identification process, and the dynamic model verification efforts. Chapter 2 describes the SOAC properties, the test instrumentation, the test conduct and the data recording and processing procedures. Chapter 3 presents the theoretical models of vehicle behavior used for the creep force identification and dynamic behavior prediction. Chapter 4 contains a discussion of several identification methods that could be used for the creep force laws, while the creep force identification

results are given in Chapter 5. The dynamic response test results and comparisons with theory appear in Chapter 6. Conclusions and recommendations for future work are found in the last chapter.

The reader should be aware that this project was intended to be the first stage of a longer effort to develop methods for testing rail vehicles on the RDU and for extrapolating those results to expected behavior in the field. The present project involved identification of creep coefficients and initial comparisons of test results with the dynamic theory. It is intended that future efforts would entail completion of the identification and validation efforts, extrapolation of test results on the RDU to to vehicle behavior in the field, and development of recommendations for RDU test procedures.

Chapter 2

TEST PROGRAM

INTRODUCTION

The creep force and dynamic reponse portions of the "Transit Vehicle Demonstration Tests" were performed during March 1981. Additional tests were carried out later in 1981 to characterize the vehicle components that strongly influence vehicle dynamic behavior. The vehicle and RDU characterization, test instrumentation, test conduct and data handling procedures are discussed in this chapter.

The SOAC vehicle in place on the RDU during these tests is shown in Figure 2-1. The vehicle was placed on the RDU with the motorman's end running in the forward direction. This end was designated the "A-end." The axles were numbered from the leading end, i.e. Axles 1 and 2 in the A-truck and Axles 3 and 4 in the B-truck. The majority of the instrumentation for these tests was placed on the A-truck.

Two hydraulic actuators were attached to the frame of the A-truck at axle level. These were configured to apply specified lateral forces to the frame.

In the creep force tests, steady forces were applied to the vehicle at different speeds and with different wheel-rail surface conditions. The resulting displacements of the vehicle components were measured by position transducers at many locations on the vehicle. Data was recorded on analog and digital magnetic tape during these tests.

The dynamic response tests involved single sinusoid, swept sinusoid and initial condition excitation of the vehicle. In the sinusoidal excitation tests, the actuator was driven in position control mode at two excitation amplitude levels. The initial condition tests involved application of a steady force to displace the vehicle components, and quick release to allow a free transient response. Forced and transient response tests were carried out at different speeds and with different wheel-rail surface conditions. Displacement measurements were recorded on analog and digital magnetic tape.

Analysis and use of these test results requires knowledge of the RDU characteristics, vehicle characteristics, instrumentation, test conduct and data processing methods. The requirements for these areas

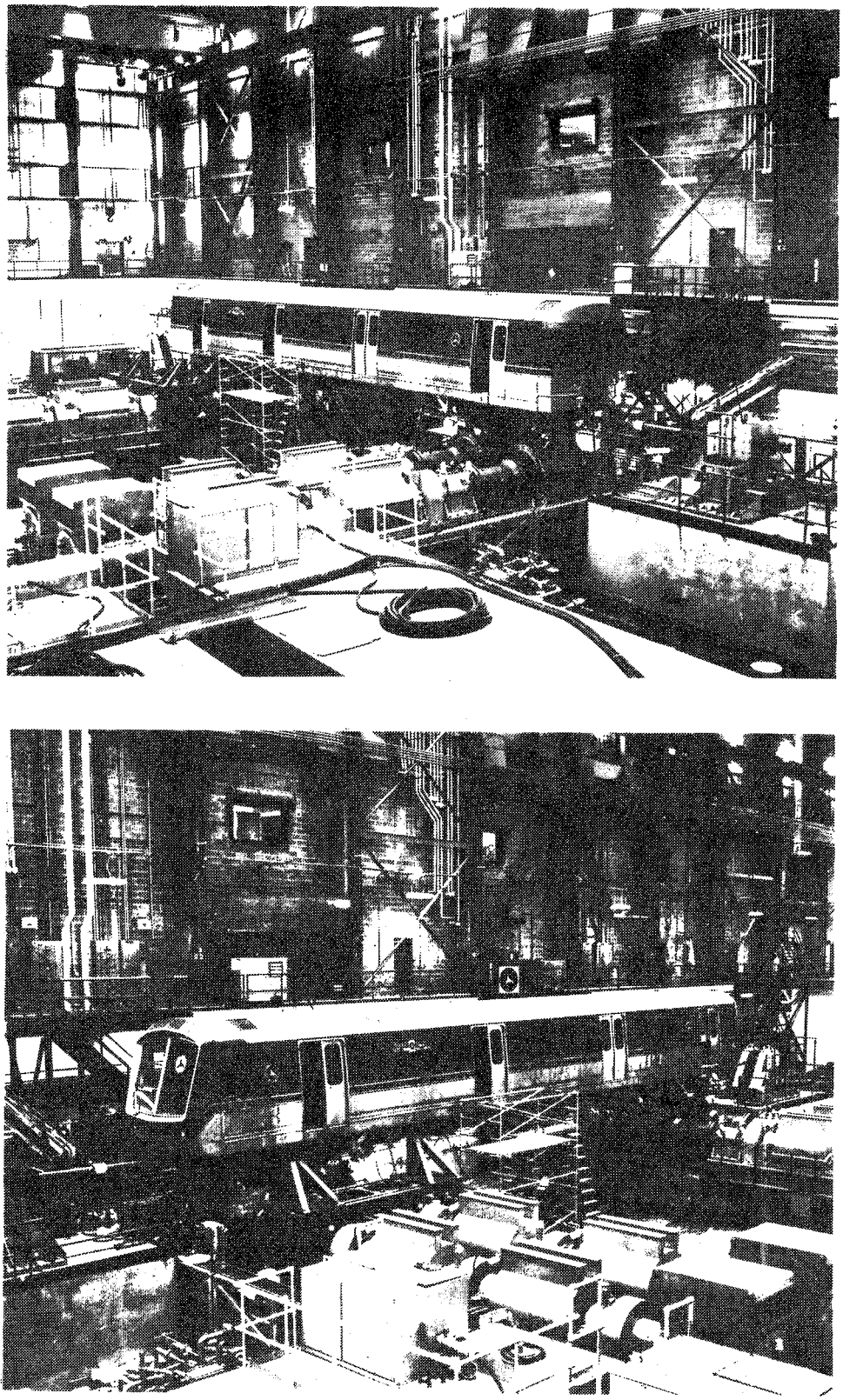

Figure 2-1. SOAC Vehicle in Place on the RDU. (Photographs by TTC)

were initially defined in test planning documents [1,2]. These subjects are taken up in the following sections.

ROLL DYNAMICS UNIT (RDU)

The RDU provides the capability for driving or absorbing power from the wheelsets of the vehicle. In these tests the vehicle was unpowered and the rollersets driven. One roller module is provided for each wheelset. The major sub-systems of the RDU are the following:

- Drive train
- Roller module units
- Vehicle restraint system
- Service structures
- Control and monitoring system.

A general description of these features may be found in [3].

Each of the four drive trains is powered by a 600 horsepower variable speed motor. Synchronous operation of the drive train is accomplished with a master control system. The sixty inch rollers can be operated at surface speeds up to 144 mph. Detailed knowledge of the RDU sub-systems was not needed for this project.

The most critical RDU geometric parameters are the lateral and yaw offsets between the two rollersets under each truck. Although measurement of these quantities was requested in the test requirements document, these measurements were not made. This was an unfortunate shortcoming, because very small angular misalignments between the rollers, on the order of one milliradian, give rise to substantial lateral offsets of the wheelsets relative to the rollersets.

The dynamics of the RDU system were not expected to have a significant influence on the vehicle dynamic response. The structural vibrations of the roller and drive line are expected to be well above 10 Hz, the upper frequency of interest in this project. Further information on the drive line dynamics may be found in the drive train manufacturer's documentation [4].

SOAC VEHICLE CHARACTERISTICS

Those vehicle characteristics that determine the system dynamic behavior must be known in order to understand the test results, estimate the wheel-rail creep coefficients, and to provide theoretical results for comparison with test results. This required information includes geometric parameters, inertia properties, suspension characteristics and car body bending and torsion model frequencies. Many of these parameters were available from the vehicle manufacturer or could be estimated adequately. Additional tests were performed at the Transportation Test Center to determine the axle misalignments and to verify the suspension parameters.

Vehicle Geometry

All the required geometry information, with the exception of the axle misalignments, was obtained from the vehicle and truck manufacturer. Table 2-1 lists these geometry values.

The offsets in the lateral and yaw directions between the two axles of the leading (instrumented) truck were obtained by an optical measurement procedure. The wheelsets were placed on air bearings that were repetitively inflated to remove any residual loads in the suspension. Misalignment measurements were then made against an optical reference. The results are summarized in Table 2-2.

These offsets are extremely small, on the same order as the measurement errors in the process, and should not significantly influence the truck equilibrium position on the rollers. Further details concerning this test are given in [2-5].

Inertia Properties

The masses of the truck components were obtained from the manufacturer, and the vehicle body mass found by weighing the assembled car. Estimates for the moments of inertia were found by scaling available values for similar truck and car components. The resulting values are given in Table 2-3.

Table 2-1. SOAC Geometric Parameters

Symbol	Description	Value	Source
d_p	Primary suspension semi-spacing	1.885 ft	A
d_s	Secondary suspension semi-spacing	3.375 ft	A
ℓ	Truck semi-wheelbase	3.75 ft	A
h_T	Height of truck c.g. above primary suspension	0	B
h_{TB}	Height of truck bolster above truck c.g.	1.05 ft	B, A
h_{BC}	Height of body c.g. above bolster	3.0 ft	B
ℓ_F	Distance from car c.g. to front truck center	27.0 ft	A
ℓ_R	Distance from car c.g. to rear truck center	27.0 ft	A
r_o	Nominal wheel tread radius	1.75 ft	C

A. General Steel Industries Drawing No. 34700 (12-30-71)

B. Estimate

C. Measurement

Table 2-2. Relative Wheelset Lateral and Yaw Offsets for A-Truck

Trial	Lateral Offset, in.	Yaw Offset, millirad
1	-0.006	0.006
2	-0.003	0.148
3	0.002	0.000
4	0.000	0.000

Table 2-3. SOAC Inertia Properties

Symbol	Description	Value	Source
I_{cyy}	Car body yaw moment of inertia	0.8581×10^6 slug- ft^2	B
I_{czz}	Car body roll moment of inertia	0.3135×10^6 slug- ft^2	B
I_{Ty}	Truck frame yaw moment of inertia	1250 slug- ft^2	B
I_{Tz}	Truck frame roll moment of inertia	703 slug- ft^2	B
I_{wy}	Wheelset yaw moment of inertia	301 slug- ft^2	B
I_{Wx}	Wheelset moment of inertia about axle	54 slug- ft^2	B
W_c	Car body weight	59300 lb	A
W_T	Truck frame weight	8150 lb	A
W_w	Wheelset weight	3810 lb	A

A - manufacturer

B - estimate

Suspension Properties

Design values for the suspension properties were obtained from the truck manufacturer. These suspension design values are given in Table 2-4. In order to verify the secondary yaw, primary lateral and primary longitudinal values, which have the strongest influence on the vehicle dynamics, characterization tests were conducted on the A-truck shortly after completing the tests on the RDU.

The primary suspension is provided by means of four rubber chevrons per axle, two on each side placed at the axle boxes. The lateral primary suspension test was performed by applying a lateral force at each of the wheelsets and measuring the relative wheelset to side frame lateral displacement. The truck was lifted free of the rails on an air table during these tests and the truck frame held fixed to a reaction mass. Details of the test are given in [6].

After initial set up and cycling, two test sequences, each involving increasing and decreasing the applied load, were carried out. Straight lines were fit to the load increasing and load decreasing data points to obtain lateral stiffness values. The average values for both tests for the front and rear wheelsets are the following:

Primary lateral stiffness/wheel: K_{xp1} and K_{xp2}

Axle 1, K_{xp1} = 22,860 lb/in (274,300 lb/ft)

Axle 2, K_{xp2} = 24,320 lb/in (291,800 lb/ft)

These values are in good agreement with the design values given in Table 2-4.

The longitudinal stiffness of these primary suspension elements was measured by a similar test on the A-truck. These tests were conducted by applying a longitudinal force across the primary suspension with the braking system of the truck while the vehicle was in place on the RDU. The roller drive system was disengaged to allow the wheelsets free longitudinal movement, and the truck frame was anchored longitudinally to a reaction mass. The suspension displacements were recorded by dial gauges. A test conduct procedure that involved pre-cycling and measurements with the load increasing and the load decreasing was followed to obtain the force-displacement values. Details of the test are given in [7].

Table 2-4 SOAC Suspension Design Values

PRIMARY SUSPENSION	
Vertical Stiffness/wheel	96,000 lb/ft
Laternal Stiffness/wheel	264,000 lb/ft
Longitudinal Stiffness/wheel	864,000 lb/ft
SECONDARY SUSPENSION	
Vertical Stiffness/side	
Light	25,092 lb/ft
Loaded	33,924 lb/ft
Lateral Stiffness/side	
Light	10,500 lb/ft
Loaded	11,640 lb/ft
Vertical Damping/side	1,720 lb/(ft/sec)
Lateral Damping/side	2,366 lb/(ft/sec)

Individual straight line fits to the test data over the load increasing and load decreasing regions of the data provided stiffness values that excluded hysteresis effects. Averaging these values over the different runs provided the following stiffness values:

Primary longitudinal stiffness/wheel: K_{zp1} and K_{zp2},

Axle 1, K_{zp1} = 145,200 lb/in (1,742,000 lb/ft)

Axle 2, K_{zp2} = 159,900 lb/in (1,919,000 lb/ft)

The values are approximately twice the design values given in Table 2-4. Several checks, including a second test series on the B-truck, were made to verify the test values. The checks and second test series corroborate the values given above.

The secondary yaw suspension tests were conducted to determine the effective yaw stiffness and the friction force level between truck frame and bolster. The secondary yaw system consists of longitudinal anchor rods with rubber bushings between the car body and bolster and a friction centerplate between bolster and truck frame. The stiffness in the bushings provides a resisting torque up to a limit dictated by maximum friction level at the centerplate. In the creep and dynamic tests, the bolts holding the anchor rod bushings were backed off to reduce the effective secondary yaw stiffness. On the B-truck these bolts were loosened completely then "snugged" again with a wrench. On the A-truck the bolts were loosened completely and then "hand-tightened" prior to Run 4.

The yaw suspension tests were conducted with the anchor rod nuts in "loose", "hand-tight", and "fully tightened" conditions. The A-truck was placed on an air table, and hydraulic actuators used to apply a yaw torque to the truck frame. LVDT's measured displacements across the anchor rods and at the centerplate. As in the other suspension tests, the applied loads were cycled. Tests details are given in [8].

Three runs were made in the "hand-tightened" condition and one run in each of the other conditions. The yaw friction level was determined by observing when large deflections occurred as the load was increased. Rotational stiffness values were calculated with linear regression methods. The following average values were found:

Secondary Yaw Stiffness: $K_{\theta s}$

Anchor bolt hand tight = 3,380 ft-lb/milliradian

Anchor bolt loose = 1,720 "

Anchor bolt fully tightened = 24,380 ft-lb/milliradian

Secondary Yaw Friction Torque: $T_{\theta s}$

Average friction torque = 5500 ft-lb

As design values for these quantities were not available, no comparisons can be made.

Car Body Flexibility

In evaluating dynamic test results it is important to know all the dominant modes of vehicle motion. These motions may include vertical, and lateral bending on torsion of the car body. A vibration test of the car body was conducted at the time of manufacture to establish this information. The following frequencies and modal shapes were found in these tests [2-9]:

Car Body Flexible Modes:

Vertical: Body bending first mode = 8.1 Hz

Body bending second mode = 12.3 Hz

Body bending third mode = 15.0 Hz

Lateral: No modes below 20 Hz

Torsion: No modes below 20 Hz

WHEEL-ROLLER GEOMETRY

The wheel and roller profile geometries play a dominant role in vehicle on roller rig dynamics [2-10]. The RDU rollers were machined to the 136 lb/yd RE rail head profile with a 1/40 cant angle in 1978. The Canadian National (CN) Profile A was selected for the test vehicle and the wheelsets turned to this profile on a Hegensheidt wheel lathe shortly before the tests. These specifications for the roller and wheel profiles are shown in Figure 2-2 and 2-3. The actual profiles differ from the specification due to machining tolerances and 3 years of wear, while the actual wheel profiles differ from the specification due to errors inherent in the machining equipment and processes used. It is important, in such tests, to measure the actual wheel and rail profiles.

In order to determine the actual geometric characteristics, the wheel and rail profiles were directly measured before the creep and

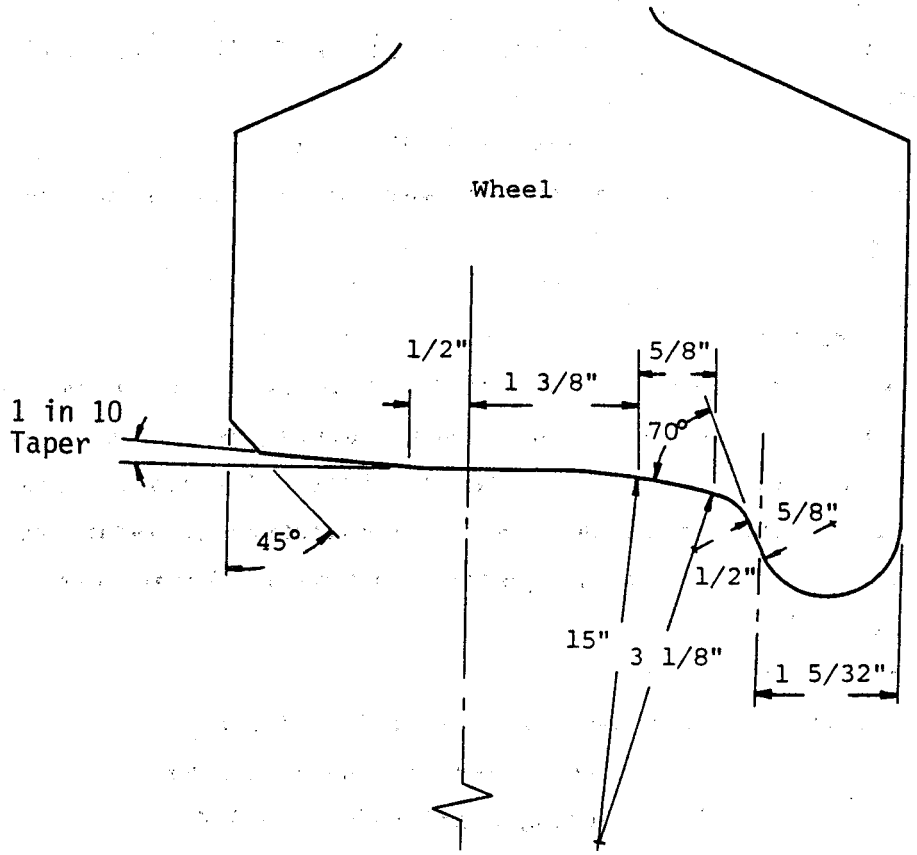

Figure 2-2. Ideal CNA Wheel Profile.

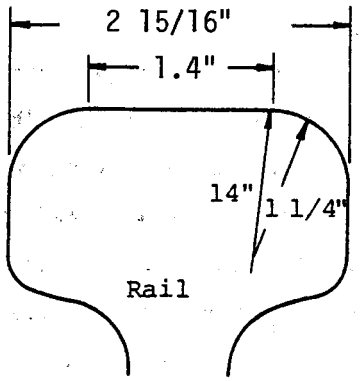

Figure 2-3. Ideal AREA 136 RE Rail Profile.

dynamic response tests, and the wheel profiles were again measured after the tests. The wheel and roller profiles measurements were taken with the Transportation Test Center's "British Rail" profilometer. The measured profiles for the A-truck and corresponding rollers are shown in Figures 2-4 and 2-5.

The measured wheel and roller profile data, as well as data generated for the specified 136 lb/yd rail head and the CNA wheel profile were processed with the WHRAILA program [2-11] to obtain the following geometric constraint functions needed in the creep force and dynamic response analyses:

$(r_L - r_R)/2a$ - normalized wheelset rolling radii difference

$(R_L - R_R)/2a$ - normalized roller rolling radii difference

$(\delta_L - \delta_R)/2$ - wheelset contact angle difference

ϕ - wheelset roll angle

where 2a is the nominal rail gauge. These functions are shown for Axle 1 in Figure 2-6 and Axle 2 in Figure 2-7.

These geometric constraint function plots demonstrate that the wheel-roller geometry differs considerably between the two axles. Axle 1 has a rolling radius offset of approximately 0.15 inches and more discontinuities in the functions due to contact point jumps on wheel and roller surfaces.

The creep force and forced response analyses utilized linear representations of these constraint functions. Straight line fits to the depicted functions in the wheel tread contact region provided the wheelset conicity, λ, the roller conicity, λ_R, the contact angle coefficient, Δ, and the roll coefficient, Γ. These coefficients are the slopes of the linear approximations. For the creep test analysis, where the wheelsets were forced into flange contact, straight line fits to the entire tread contact region were used. In the dynamic response test analysis, where smaller wheelset lateral motions occurred, straight line fits in the vicinity of the equilibrium position were used. These estimated values, as well as values obtained from analysis of the specified wheel and roller profiles (Fig. 2-2 and 2-3) are given in Table 2-5.

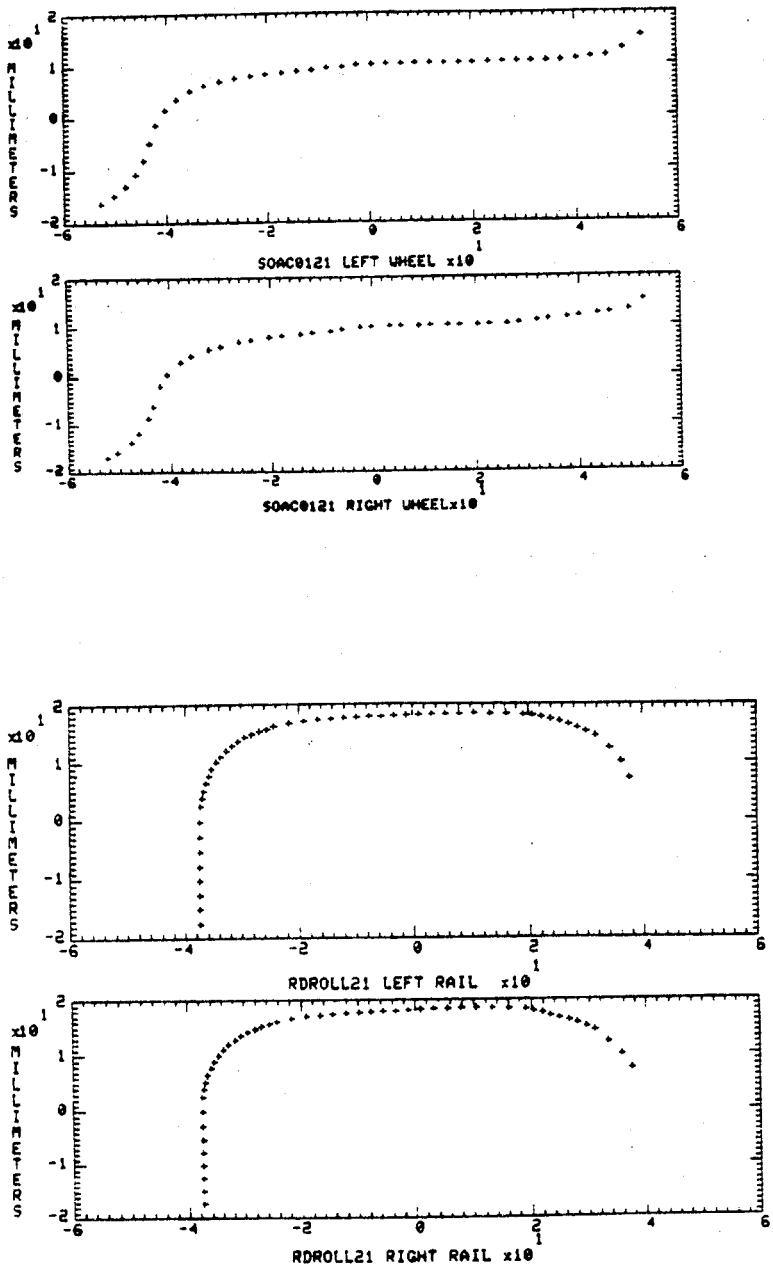

Figure 2-4. Actual Wheel and Roller Profiles for Wheelset 2 and Rollerset 2.

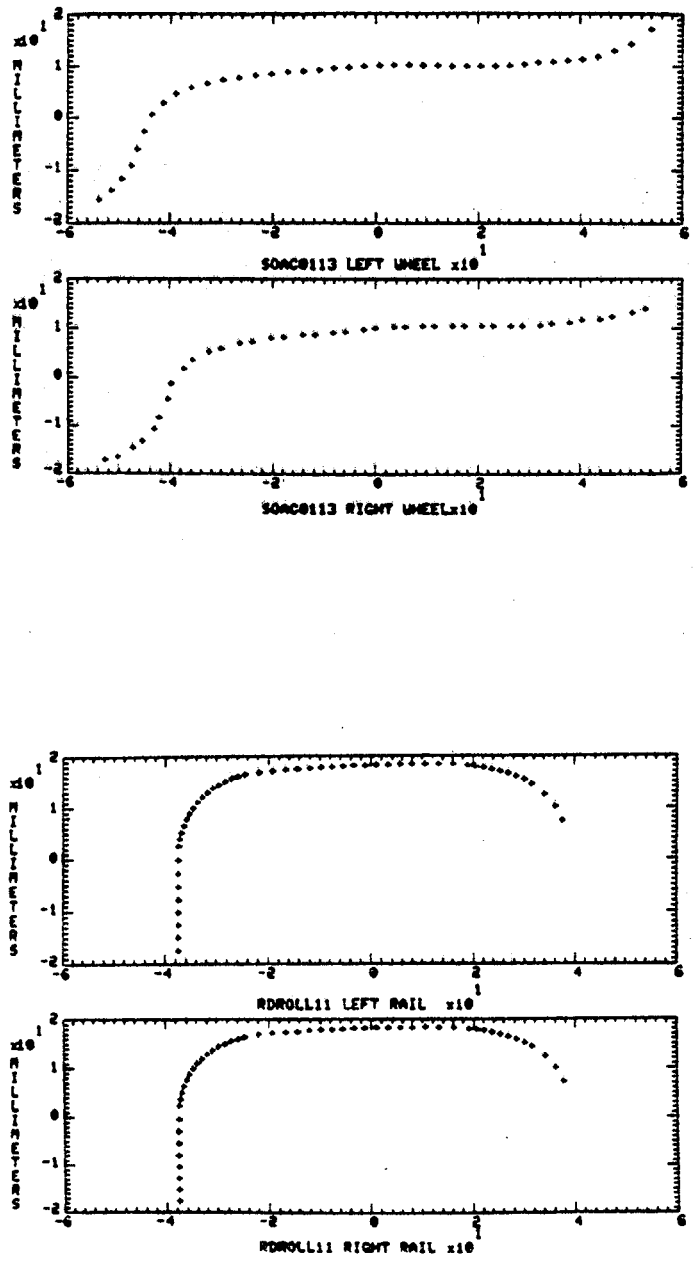

Figure 2-5: Actual Wheel and Roller Profiles for Wheelset 1 and Rollerset 1.

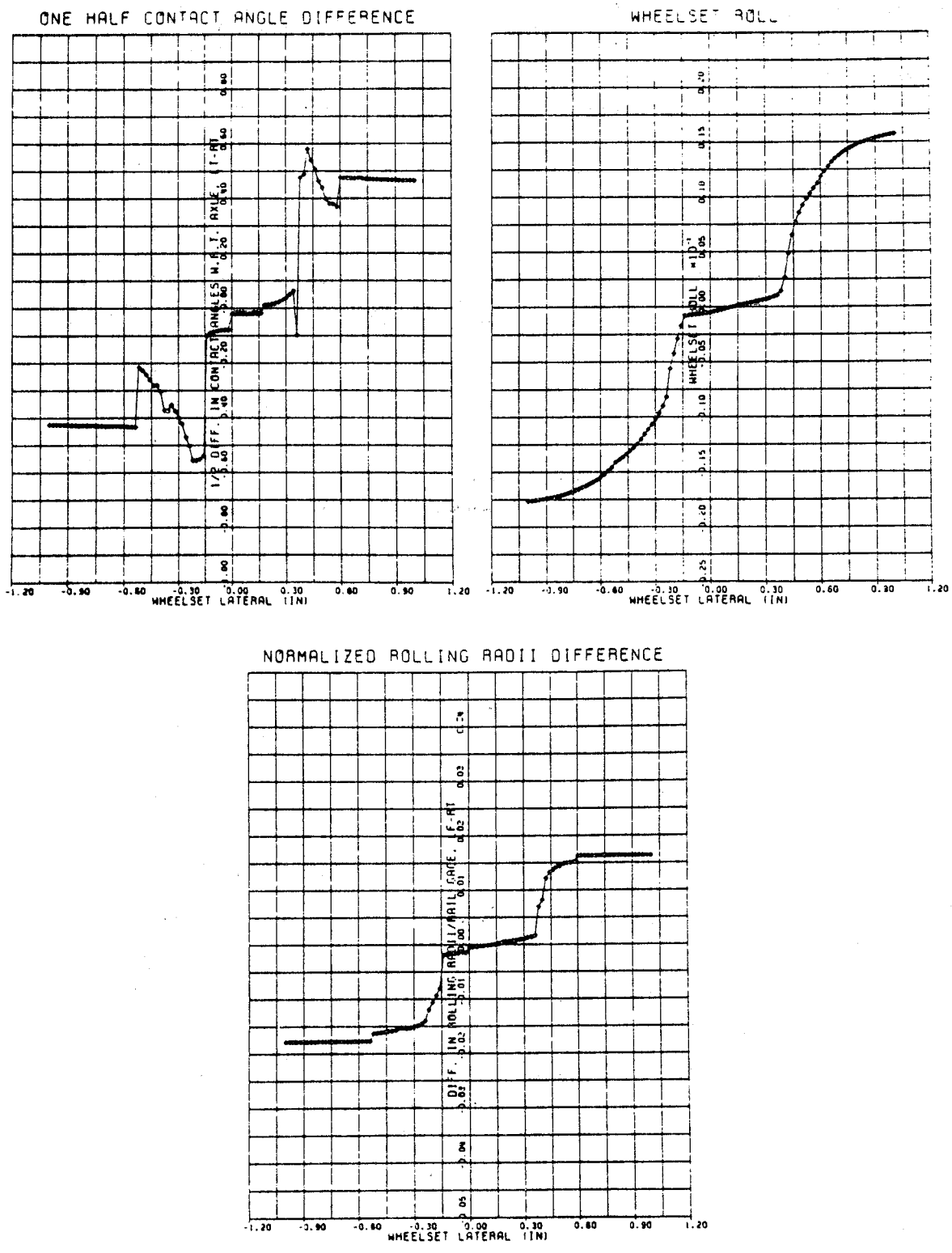

Figure 2-6. Actual Wheel-Rail Geometry Parameters for Wheelset 1.

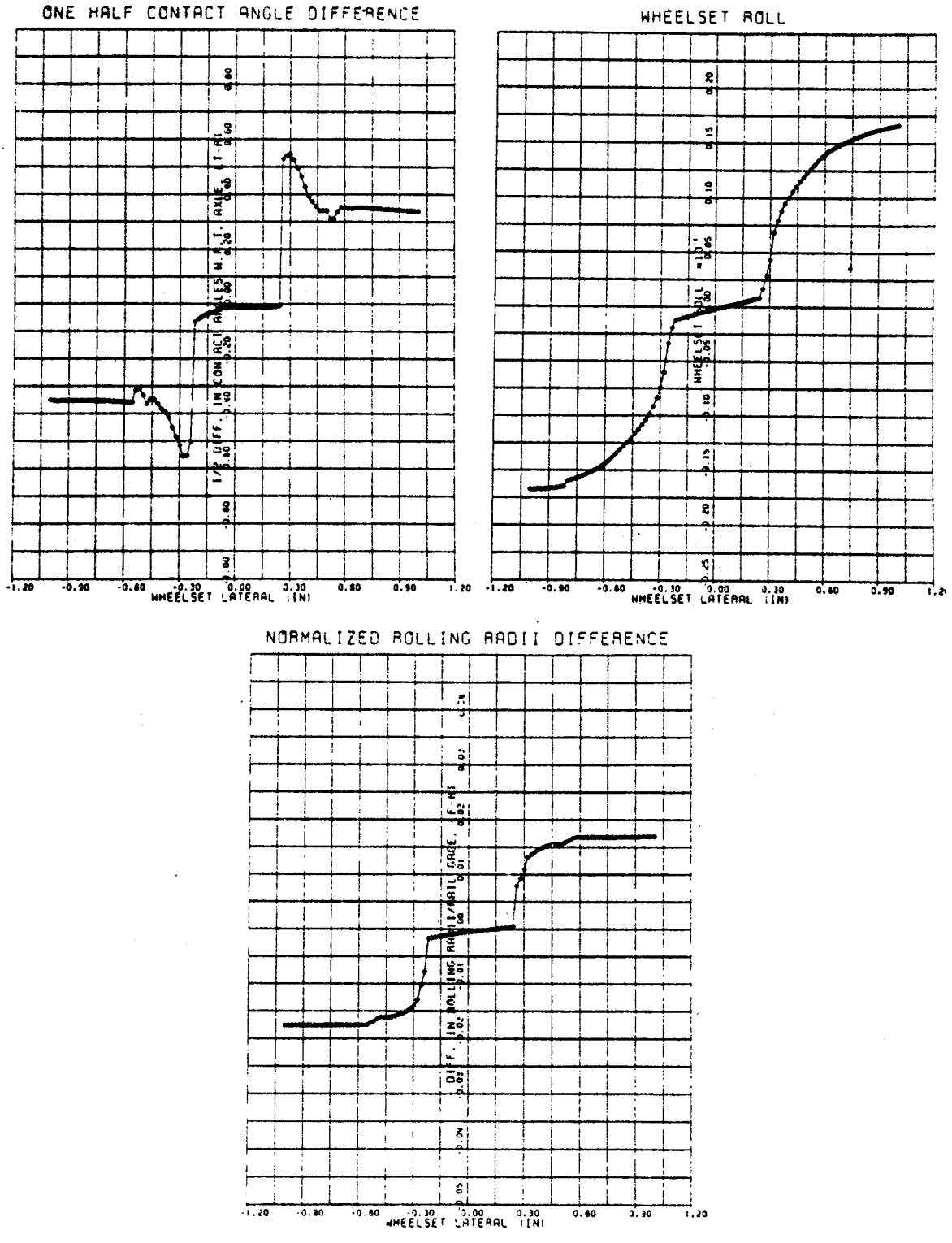

Figure 2-7. Actual Wheel-Rail Geometry Parameters for Wheelset 2.

Table 2-5. Linear Coefficients for Wheel-Rail Geometric Constraint Functions

	Wheelset Conicity	Contact Angle Difference	Wheelset Roll	Rollerset Conicity
	λ	Δ	Γ	λ_R
Wheelset 1				
Creep Tests	0.213	9.32	0.111	0.108
Dynamic Tests	0.213	9.32	0.111	0.0
Wheelset 2				
Creep Tests	0.152	3.95	0.120	0.030
Dynamic Tests	0.152	3.95	0.120	0.0
Ideal CNA Profile	0.178	9.00	0.050	-

INSTRUMENTATION

The creep and dynamic response tests involved steady and sinusoidal forces applied to the A-truck while the vehicle-roller rig operated at constant speed. The instrumentation provided for these tests was intended to measure the applied forces and the resulting displacements of the vehicle components. To accomplish these measurements, 31 transducers were installed on the vehicle and RDU. The majority of these transducers were concentrated on the A-truck due to recording limitations. Several redundant measurements were made to provide for instrumentation or recording failures.

Utilization of the data from these tests, particularly in the creep force identification portion of our work, required accurate knowledge of the initial positions of the displacement transducers. Although this requirement was clearly identified in the test requirements document [2-1], the locations of several important transducers were not determined accurately enough to support an evaluation of creep forces.

The instrumentation can be grouped into the following three categories:

- Forcer system
- Truck and car
- Roller rig

The transducer labels, locations, and descriptions are summarized in Table 2-6 and shown in Figures 2-8 and 2-9.

Forcer System

The forces and actuator displacements were measured for each actuator. The forces were determined from pressure measurements, and the displacements from LVDT's built into the actuators. This instrumentation provided the truck frame lateral displacement and yaw angle relative to the ground.

Truck and Car

This instrumentation measured the wheelset lateral and yaw displacements on the A-truck, the primary and secondary suspension lateral and longitudinal displacements, the secondary roll displacements and selected B-truck motions. The wheelset lateral and yaw measurements

Table 2-6. Instrumentation Description and Location

Channel	Description	Transducer Location
D1	Longitudinal motion of wheelset #1 south side	15 5/8" from rail vertically 13 5/8" from bolster center laterally 52 7/16" from bolster center longitudinally
D2	Longitudinal motion of wheelset #1 north side	10 5/8" from rail vertically 18 7/16" from bolster center laterally 50 3/16 from bolster center longitudinally
D3	Same as D1 except wheelset #2	10 5/8" from rail vertically 18 5/8" from bolster center laterally 50 3/16" from bolster center longitudinally
D4	Same as D2 except wheelset #2	14 5/8" from rail vertically 15 9/16" from bolster center laterally 52 7/16" from bolster center longitudinally
D5	Lateral displacement wheelset #1	15" from wheel center downward 3 7/8" from roller outward 45" from bolster center longitudinally
D6	Lateral displacement wheelset #2	15" from wheel center downward 3 5/8" from roller outward 45" from bolster center longitudinally
D7	Lateral displacement B-truck	8 1/8" from rail vertically 20 1/8" from bolster center laterally (right side) 60 3/16" from bolster center longitudinally
D8	Lateral displacement B-truck	6 5/8" from rail vertically 25 1/8" from bolster center laterally 59 4/16" from bolster center longitudinally
D9	Relative longitudinal displacement Across the primary cheveron - wheelset #1, south side	14 1/8" from rail vertically 18 5/8" from bolster center laterally
D10	Same as above - except north side	20 5/8" from rail vertically 18 5/8" from bolster center laterally
D11	Same as D9 except wheelset #2	20 3/8" from rail vertically 18 5/8" from bolster center laterally
D12	Same as D10 except wheelset #2	11 3/8" from rail vertically 18 5/8" from bolster center laterally
D13	Relative lateral displacement across the primary chevron wheelset #1	13 3/8" from rail vertically 53 11/16" from bolster center longitudinally
D14	Same as D13 except wheelset #2	16 1/8" from rail vertically 55 11/16" from bolster center longitudinally
D15	Relative lateral motion across the air springs, front truck	3 1/2" down from top of bolster 58" from bolster center laterally 2 1/4" from bolster center longitudinally
D16	Same as D15 - except rear truck	1" down from top of bolster 58" from bolster center laterally 1 3/4" from bolster center longitudinally
D17	Relative longitudinal measurement between car body and bolster, truck #1	9" from car body down vertically 53" + 1/4" from bolster center laterally 31" from center of doors longitudinally (west) 45 1/4" from bolster center longitudinally (west)
D18	Same as D17 - except truck #2	9 1/2" from car body down vertically 53" + 1/4" from bolster center laterally 65" from center of doors longitudinally (east) 44" from bolster center longitudinally (east)
D19	Relative longitudinal measurement between truck frame and bolster truck #1	27 1/4" from rail vertically 29" from bolster center laterally
D20	Same as D19 - except truck #2	25 1/2" from rail vertically 29" from bolster center laterally
D21	Relative bolster to car body vertical, A-truck	6" upward from bottom of car 11.25" from bolster center longitudinally (west) 58.56" outboard from car centerline
D31	Lateral displacement of actuator #1	15" from rail vertically 25 1/8" from bolster center laterally 61" from bolster center longitudinally
D32	Same as above - except actuator #2	15" from rail vertically 25 1/8" from bolster center laterally 61" from bolster center longitudinally
D22	Relative bolster to car body vertical,	6" upward from bottom of car 11.25" east of bolster center longitudinally 58.56" outboard from car centerline

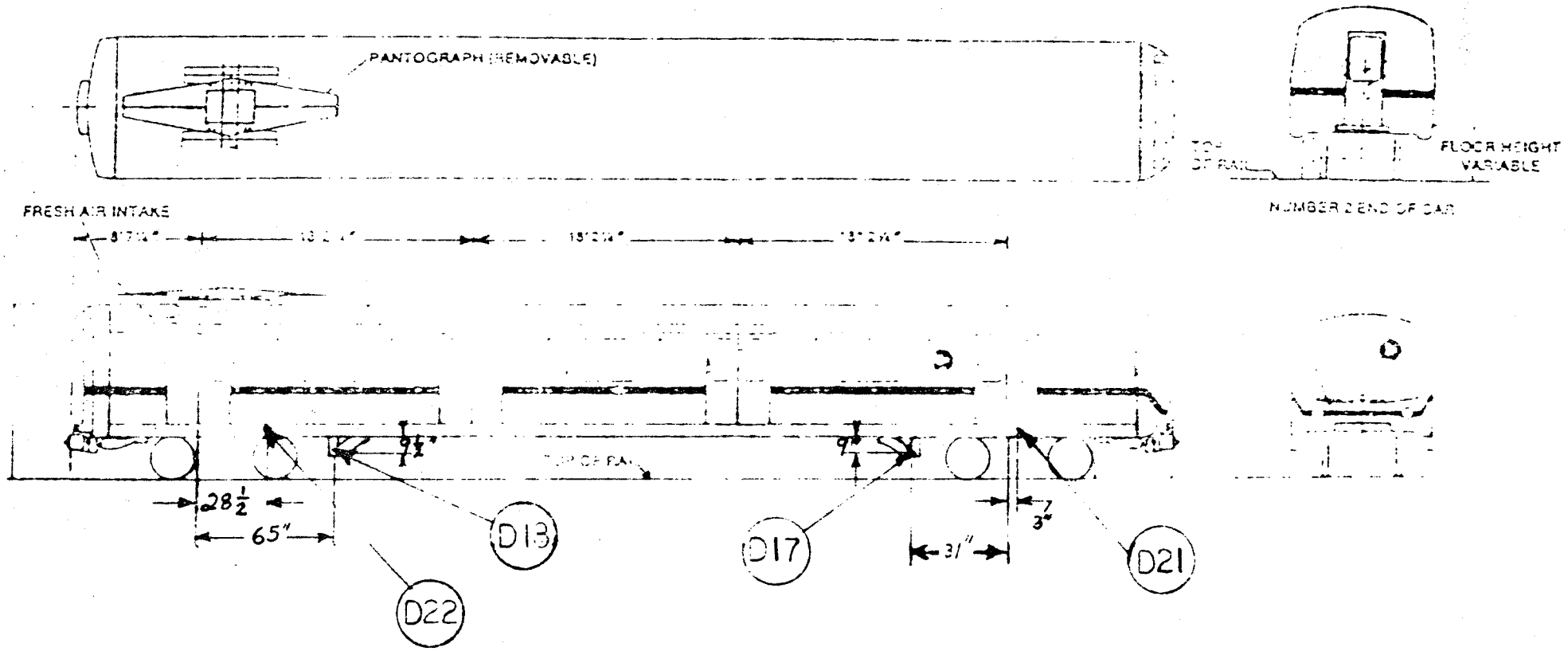

Figure 2-8. SOAC Transducer Locations

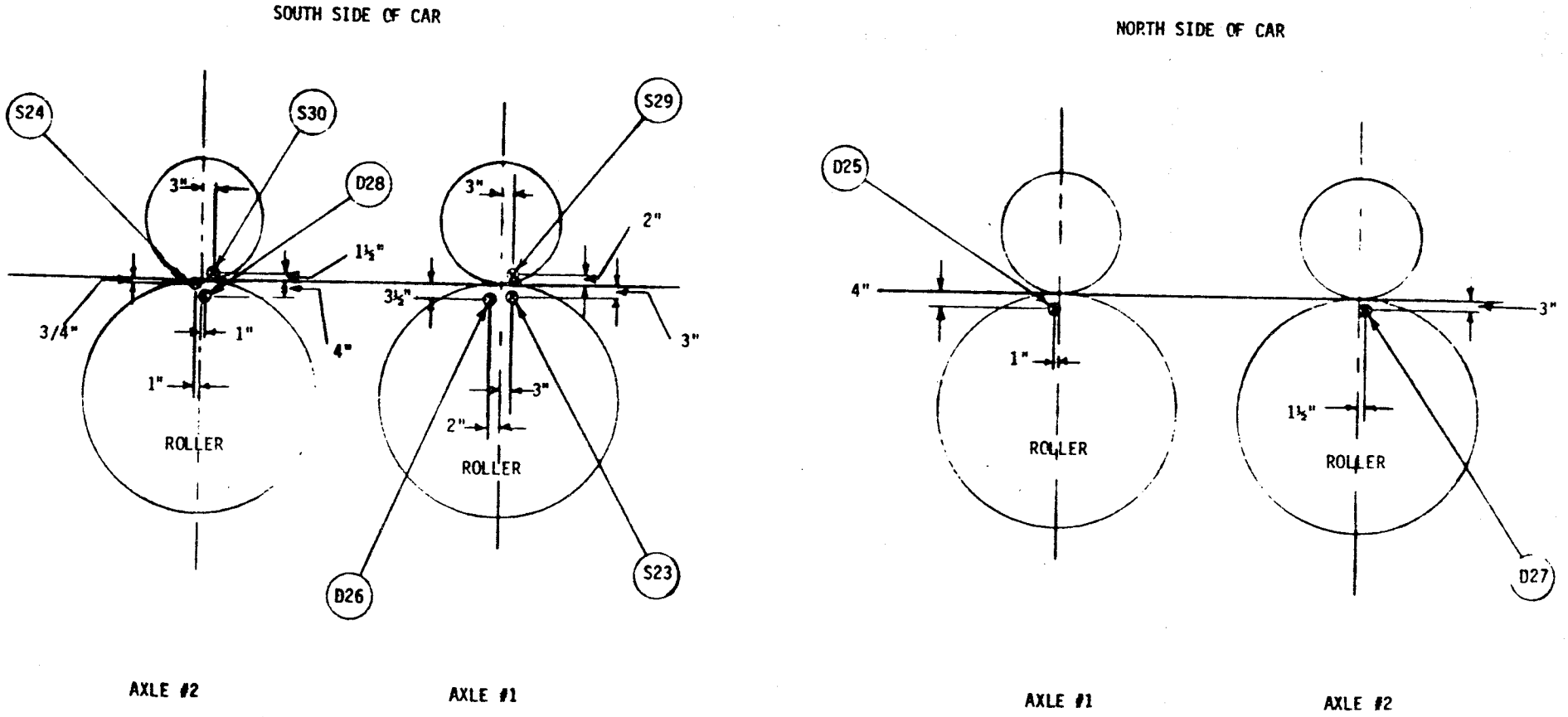

Figure 2-9. Wheel and Roller Transducer Locations on A-Truck.

are absolute measurements that were made from a fixed reference frame, in this case the centerline of the rollers. LVDT's were used to measure these absolute displacements.

Relative displacements across the four primary suspension chevrons were measured by mounting LVDT's between the side frames and the wheelsets. These were mounted both perpendicular and parallel to the sideframes so that lateral and longitudinal displacements across the primary suspension element could be recorded.

Relative lateral, yaw and vertical motions between the car body and the truck frames were measured for both trucks. LVDT's mounted between truck frame and truck bolster, and truck bolster and car body were used. The relative car-bolster-truck frame yaw measurements were made to determine the state of the nonlinear secondary yaw suspension. This nonlinearity occurs due to Coulomb friction between bolster and truck frame at the centerplate. Relative motion between the bolster and the truck frame only occurs when the friction level is exceeded. An LVDT was mounted between the bolster and the A-truck frame to monitor the position of the bolster relative to the truck frame. The secondary yaw stiffness is due to the rubber bushings on the anchor rods between the bolster and car body. One longitudinal LVDT was mounted across these bushings to record displacements of this element.

In summary, a total of twenty-two measurements were made on the vehicle. These were 1) two lateral displacements relative to ground , one for wheelset of the A-truck 2) four longitudinal displacements relative to ground, one at each end of each A-truck wheelset, 3) two lateral displacements across the primary elements, one at each A-truck wheelset, 4) four longitudinal displacements across the primary chevrons of the A-truck, 5) two lateral measurements relative to ground for the A-truck frame, 6) two longitudinal measurements between the truck bolsters and the carbody, one on each truck, 7) two longitudinal measurements between the bolsters and the truck frame, one on each truck, 8) two lateral measurements between the truck bolster and the car body, one on each end, and 8) two bolsters to car body vertical displacements, one at each truck.

Roller Rig

The rotational speeds of each rollerset were recorded from signals available in the RDU control system, and the lateral displacements of the top of each roller were measured with LVDT's. Thus, four speed measurements and four displacement measurements were recorded to evaluate the RDU dynamics.

TEST CONDUCT

The creep force identification and vehicle dynamic response tests were conducted from March 5 to March 9, 1981. Altogether, 32 runs were made, including creep tests, initial condition tests, and forced response tests at different speeds and with different wheel-roller surface preparations. An abbreviated log of this test series is given in Table 2-7, and further details are contained in the Test Engineer's log [12]. Note that the first six runs proved to be learning trials to shake down the test and measurement system.

Creep Force Tests

The creep force tests were designed to find nominal creep force conditions and to investigate the effects of speed and wheel-roller surface condition on these forces. Nominally clean, soapy wet, and greased surfaces were tested. Tests at 15 and 60 mph roller surface speeds were carried out at each surface condition. Creep force data under nominal wheel-roller surface conditions was obtained in Runs 7-11. Creep force Runs 12, 21, and 22 were intended to check whether creep force levels changed overnight (Run 12) or as a result of running for several hours (Runs 21 and 22). Creep force tests with a soap solution applied to the wheel-roller interface were carried out in Runs 25 and 26. The truck displacements with the soap solution differed very little from those measured under dry conditions, prompting additional tests with grease applied directly to the rollers (Runs 27 and 28).

In the nominal test series, efforts were made to obtain clean roller and wheel surface conditions before recording data. Before the first serious run (Run 7), the rollers were cleaned by wiping with acetone, scraping an accumulation of sludge from wheels and rollers, further applications of acetone, and buffing with emery paper. The

Table 2-7. Test Log

Run	Date	Description
1	3/5/81	Hunting Test - No instability at 80 mph.
2	"	Hunting Test/ w Forcing, No instability at 80 mph.
3	"	Hunting Test/Forcing, no instability at 80 mph.
4	3/6/81	Creep Test (15 mph).
5	"	Creep Test (15 mph) Actuators in Phase
6	"	Creep Test (75 mph) Instrumentation Failure.
7	"	Creep Test (15 mph).
8	"	Creep Test (15 mph).
9	"	Creep Test (60 mph).
10	"	Creep Test (60 mph).
11	"	Fr. Freq. Resp., Log Sweep (0.05-20 Hz), 20 mph.
12	3/9/81	Creep Test, 15 mph.
13	"	Fr. Freq. Sweep, 40 mph, large amplitude.
14	"	Fr. Freq. Sweep, 40 mph, small amplitude.
15	"	Fr. Freq. Dwell, 40 mph, 0.5, 1.5, 3.5, 6.5 Hz.
16	"	Fr. Freq. Sweep, 70 mph, large amplitude.
17	"	Fr. Freq. Sweep, 70 mph, small amplitude.
18	"	Fr. Freq. Dwell, 70 mph.
19	"	Initial Condition Test; 10, 20, ... 80 mph, #1 actuator.
20	"	Init. Cond. Test; 10, 20, ... 80 mph, #2 actuator.
21	"	Creep Test, 15 mph.
22	"	Creep Test, 60 mph.
23	"	Lat. Stiffness Test, Actuators Out of Phase.
24	"	Lat. Stiffness Test, Actuators in Phase.
25	"	Creep Test, Soap Solution, 15 mph.
26	"	Creep Test, Soap Solution, 60 mph.
27	"	Creep Test, Greased Rollers, 15 mph.
28	"	Creep Test, Greased Rollers, 60 mph.
29	"	Fr. Freq. Swp, Gr. Rollers, 40 mph, lg. ampl.
30	"	Fr. Freq. Swp, Gr. Rollers, 40 mph, sm. ampl.
31	"	Fr. Freq. Swp, Gr. Rollers, 70 mph, lg. ampl.
32	"	Fr. Freq. Swp, Gr. Rollers, 70 mph, sm. ampl.

sludgy surface deposits were attributed to oil leaks from the rollerset bearings. Although these deposits were difficult to remove initially, they did not appear to build up again during the remainder of the test series. This may be due to the cleansing effects of the wheel-roller creep process. It should be noted that the majority of the cleaning effort was applied to the A-truck wheels and rollers. The surface deposits, for example, were never completely removed from the B-truck wheel and roller surfaces. This has no bearing on the creep force results, but may be important in interpreting the dynamic response test results.

The soap solution used in Runs 25 and 26 was sprayed continuously onto the wheel-roller interface region during the creep tests. Only the A-truck received the soap spray.

The grease used in Runs 27-32 was JT-6 multi-purpose grease. This was applied by hand prior to Run 27. Additional grease was not used for the subsequent runs because wheel and roller surfaces appeared to have an adequate surface film throughout the test series.

In each creep force test, the RDU was first brought up to test speed, the force of the front actuator was slowly increased until one wheel was in flange contact with a roller, and then the force was decreased in roughly ten increments, pausing at each increment to insure that transient effects had died out. Data recording continued throughout the creep test.

Initial Condition Tests

The initial condition tests were intended to evaluate the relative stability of the vehicle at different speeds. Initial condition tests with "clean" wheel-roller surfaces at speeds from 10 to 80 mph were carried out in Runs 19 and 20. Because the transient response decayed very quickly at all speeds, indicating good stability and providing very little useful data, these tests were not repeated with the greased surface condition.

In each initial condition test, the RDU was brought to 80 mph, a force was applied with the actuator until flange contact occurred on one wheel, the force was released with a dump valve near the actuator, and the force was again applied and released after the transient decayed.

This sequence was repeated several times before reducing the speed by 10 mph and repeating the series. In Run 19, the No. 1 actuator, located at the front of the A-truck was used, while the No. 2 actuator was used in Run 20. Data was recorded continuously during each run.

Forced Response Tests

Forced response tests with sinusoidal displacements of the actuator were intended to provide a more complete characterization of the SOAC or RDU lateral dynamic behavior. One test series, Runs 13-18, was conducted with the nominally "clean" wheel and roller surfaces, and a second series, Runs 29-32, with the greased surfaces. Swept sinusoidal forcing with the frequency varying from 0.2 to 10 Hz in a logarithmic manner over a 5 minute time period was used in Runs 13, 14, 16, 17, and 29-32. An attempt was made to identify the most dominant modal frequencies during Runs 13, 14, 16 and 17 and to dwell at these frequencies during Runs 15 and 18. It proved difficult to identify dominant frequencies on the strip chart recordings. As a result, the dwell tests were dropped from the greased roller series.

The No. 1 actuator was used in position control mode for all forced response tests. To study the nonlinear effects in the system, runs were conducted at two different amplitudes. For the larger amplitudes, the actuator position was set just below that needed to cause flange contact at 0.2 Hz. Because this led to violent motion at the kinematic mode frequency, the actuator displacement was reduced during the middle of Runs 13 and 16. The low amplitude runs were conducted with the actuator displacement at approximately 20% of the large amplitude runs. The smaller amplitude was used in the dwell tests as well. All forced runs were conducted at 40 and 70 mph roller surface speeds.

DATA PROCESSING

All the SOAC on RDU test measurements were recorded on analog and digital magnetic tape as the tests were conducted. The digitally recorded data was filtered at 25 Hz and sampled at a 64 sample per second rate. It was later discovered that channel labels had been swapped and at least one channel inadvertently omitted on the digital tape after Run 13. This data was subsequently redigitized from the

analog tapes. During the tests, 14 channels were also displayed on oscillograph paper.

The dynamic response test digital data was subsequently processed at the Transportation Test Center using the DRS [2-13] data processing program. Power spectral densities (PSD's) were computed for selected measurements in all the swept sinusoidal forcing runs (Runs 13, 14, 16, 17, 29, 30, 31, and 32). In addition, transfer functions between selected measurements and the actuator force or actuator displacement were computed. These test results are discussed in Chapter 6.

The transient response test data was also processed using features of the DRS program. Exponentially decaying sinusoids were fitted in the least squares sense to selected transient response signals. These functions provided estimates of the frequency and damping ratio of the least damped modes of vehicle motion. A discussion of these results may also be found in Chapter 6.

Chapter 3

VEHICLE MODELING

INTRODUCTION

The essential elements of the SOAC vehicle are the wheelsets, the truck frames and the car body. These elements interact with each other through the primary and secondary suspensions. The wheelsets additionally interact with the rollersets of the RDU, and the forward truck interacts with the laboratory forcing system in the test series of particular interest here. Figure 3-1 shows a portion of the vehicle schematically and illustrates the element interconnections.

The primary suspension elements are rubber chevrons installed in the truck axle boxes. These chevrons admit relative truck to wheelset motions in the lateral, longitudinal and vertical directions. Because of their nearly linear force-deflection characteristics, we modelled the chevrons as parallel combinations of linear springs and linear dampers.

The secondary suspension elements consist of air springs, bolsters, tierods and dampers. The air springs transmit the weight forces of the carbody to the bolsters. These springs admit vertical, lateral, yaw and roll motions between the car body and the bolsters. The bolsters contact the trucks at centerpins that allow only rotations, and also at friction pads that transmit the carbody loads to the trucks and provide yaw damping when relative motion occurs. Each bolster has two friction pads, one at each end. The tierods provide yaw stiffness between the carbody and the bolsters. Two sets of dampers provide damping between the carbody and the bolsters in the vertical and lateral directions. In the dynamic model we have modelled all the secondary suspension elements linearly. Nearly linear characteristics exist for all these elements with the exception of the friction pads during situations when suspension forces due to yaw motions are sufficiently large to overcome the Coulomb friction forces at the pads. In these operating regions equivalent linearization techniques employing describing functions yield equivalent linear values that represent the secondary yaw suspension characteristics. In the steady-state model we have modelled the friction pads as actual nonlinear Coulomb friction elements.

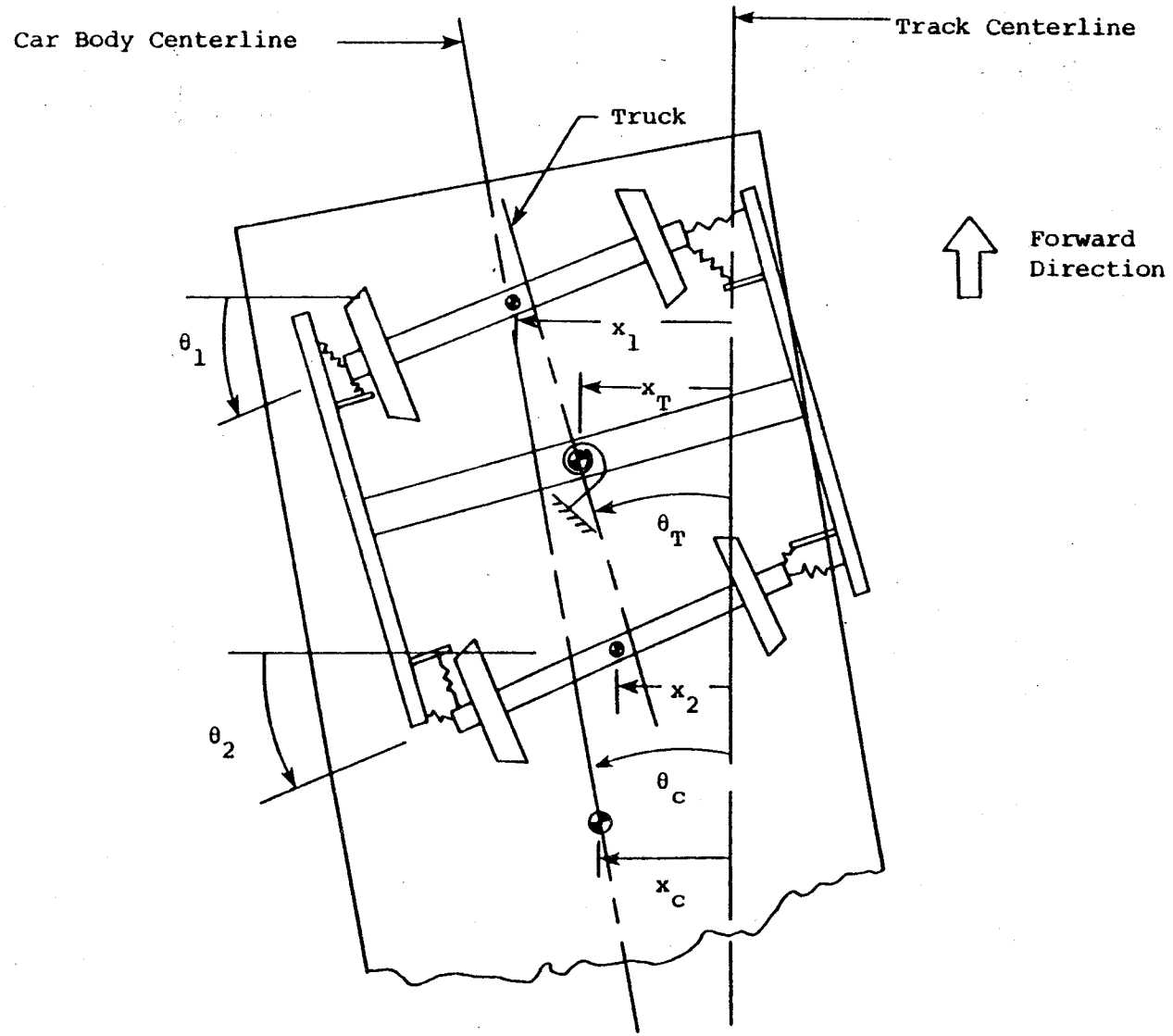

Figure 3-1. Schematic of a Passenger Vehicle.

Two different effects constitute the major differences between operation of a rail vehicle on track and operaton ot the same vehicle on a roller rig. The first effect is the interaction between the vehicle's wheelsets and the roller rig's rollersets. Terms appear in the model's equations of motion that are not present in vehicle-on-track models. In fact the vehicle-on-roller rig equations of motion reduce to the vehicle-on-track equations of motion as the diameter of the rollers becomes large. The second effect is the dynamic forcing that occurs during rail operation but not during roller rig operations. Random rail irregularities including alignment, crosslevel and rolling line offset variations are not normally present in roller rig testing because of good quality control during the roller machining.

In this chapter we present the equations of motion for a wheelset on a roller rig, a truck on a roller rig, and finally an entire vehicle on a roller rig. The wheelset model introduces the roller rig terms into the equations of motion. The truck model brings in the effects ot the primary suspension elements since they support the trucks on the wheelsets, and the vehicle model brings in the effects ot the secondary suspension elements since the carbody to truck forces are transmitted through these elements. The wheelset and truck equations of motion neglect inertial loads since we derived these equations specifically for use in the steady-state creep force characterization study. Reference [14] contains a detailed derivation of the equations of motion of the wheelset and truck. References [15] and [16] also contain derivations of the roller rig terms, although each takes a somewhat different approach than the one used in [14]. For the dynamic analysis we modified an existing 17-DOF passenger car model by including the roller rig terms in the equations of motion. Details of this model have not appeared in the open literature, but its uniqueness lies in the inclusion of the roller rig terms, not in the model itself. Reference [17] contains the derivation of a similar model that does not include the roller rig terms.

WHEELSET MODEL

Forces and moments exerted on a wheelset arise from the creepage forces in the wheel-roller contact patch, the contact forces normal to the contact patch, the primary suspension forces and the axle body forces. We consider each of these sources in the following.

Axis Systems

Three frames of reference are used to describe the motion of a wheelset as shown in Figure 3-2. The $\hat{i}'''$, $\hat{j}'''$, $\hat{k}'''$ frame is an inertial reference frame and is assumed to be fixed with respect to the track or roller center line. The unit vector $\hat{k}'''$ is assumed to be oriented along the roller or track center line, and the $\hat{i}'''$, $\hat{j}'''$ vectors are oriented laterally and vertically according to the right hand rule.

The frame $\hat{i}'$, $\hat{j}'$, $\hat{k}'$ is taken to be a body coordinate system, i.e., the frame is attached to the wheelset. However the wheelset rotates about its axle relative to the frame $\hat{i}'$, $\hat{j}'$, $\hat{k}'$. The frame is aligned with the principal directions of the wheelset inertia tensor at the center of gravity. The problem of describing the orientaton of the wheelset in space reduces to describing the location of the $\hat{i}'$, $\hat{j}'$, $\hat{k}'$ system with respect to the $\hat{i}'''$, $\hat{j}'''$, $\hat{k}'''$ coordinate system.

An auxiliary coordinate system, $\hat{i}''$, $\hat{j}''$, $\hat{k}''$, is an intermediate system, as shown in Figure 3-2. A sequence of rotations that carries the moving reference frame from coincidence with the $\hat{i}'''$, $\hat{j}'''$, $\hat{k}'''$ to the $\hat{i}'$, $\hat{j}'$, $\hat{k}'$ frame is described as follows: A θ rotation about the $\hat{j}'''$ axis brings the axis oriented along $\hat{k}'''$ into coincidence with the $\hat{k}''$ axis and the moving frame into coincidence with the $\hat{i}''$, $\hat{j}''$, $\hat{k}''$ axis system. A ϕ rotation about the $\hat{k}''$ axis brings the axis system into coincidence with the $\hat{i}'$,$\hat{j}'$, $\hat{k}'$ axes. The angles θ and ϕ therefore represent the wheelset yaw and roll motions respectively.

When wheelset motions are small, the unit vectors $\hat{i}'''$, $\hat{j}'''$, $\hat{k}'''$ relate to the $\hat{i}'$, $\hat{j}'$, $\hat{k}'$ unit vectors as follows:

$$\begin{bmatrix} \hat{i}''' \\ \hat{j}''' \\ \hat{k}''' \end{bmatrix} = \begin{bmatrix} 1 & -\phi & \theta \\ \phi & 1 & 0 \\ -\theta & 0 & 1 \end{bmatrix} \begin{bmatrix} \hat{i}' \\ \hat{j}' \\ \hat{k}' \end{bmatrix} \qquad (3.1)$$

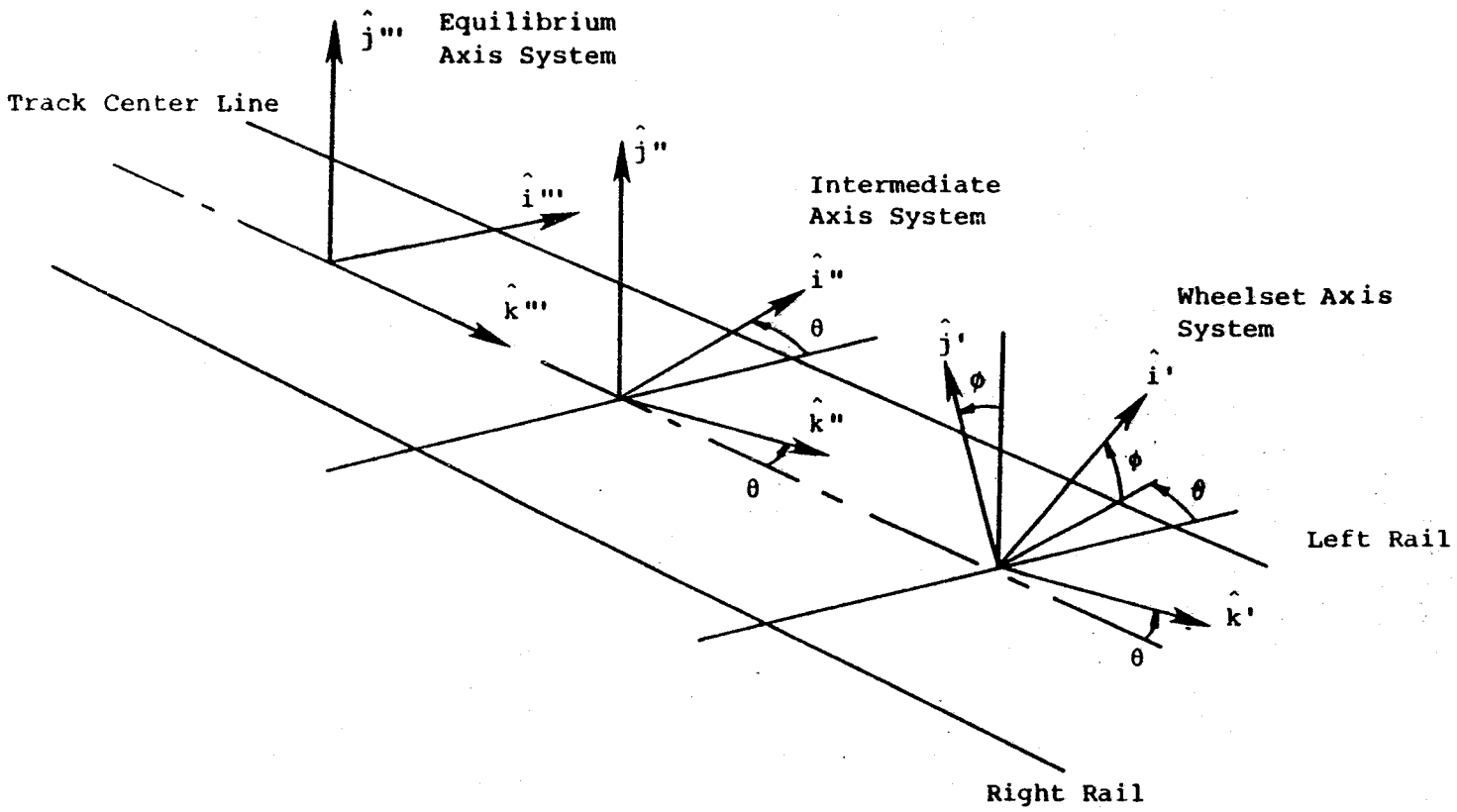

Figure 3-2. Wheelset-Roller Coordinate Systems.

An orthogonal triad of unit vectors, $\hat{e}_1$, $\hat{e}_2$, $\hat{e}_3$ is used to define the directions of the forces of contact. A separate axis system is taken at each wheel for each wheelset, as shown in Figure 3-3. The axis systems for each wheel are distinguished by means of the subscripts L and R which refer to the left and right wheels respectively. The $\hat{e}_{1L}$ and $\hat{e}_{3L}$ axes lie in the plane of contact between the wheel and roller while $\hat{e}_{2L}$ lies along the normal to the contact plane. The $\hat{e}_{1L}$ axes coincides with the lateral direction while the $\hat{e}_{3L}$ is directed longitudinally. The vectors $\hat{e}_{1R}$, $\hat{e}_{2R}$ and $\hat{e}_{3R}$ are similarly defined for the right wheel contact point. Assuming small contact angles, δ_L and δ_R, contact axes can be transformed to the wheelset body axes by:

$$\begin{bmatrix} \hat{e}_{1L} \\ \hat{e}_{2L} \\ \hat{e}_{3L} \end{bmatrix} = \begin{bmatrix} 1 & \delta_L & 0 \\ -\delta_L & 1 & 0 \\ 0 & 0 & 1 \end{bmatrix} \begin{bmatrix} \hat{i}' \\ \hat{j}' \\ \hat{k}' \end{bmatrix}$$

$$\begin{bmatrix} \hat{e}_{1R} \\ \hat{e}_{2R} \\ \hat{e}_{3R} \end{bmatrix} = \begin{bmatrix} 1 & -\delta_R & 0 \\ \delta_R & 1 & 0 \\ 0 & 0 & 1 \end{bmatrix} \begin{bmatrix} \hat{i}' \\ \hat{j}' \\ \hat{k}' \end{bmatrix} \qquad (3.2)$$

The contact axes can be transformed to the $\hat{i}'''$, $\hat{j}'''$, $\hat{k}'''$ axes by the use of Equation (3.1). Hence

$$\begin{bmatrix} \hat{e}_{1L} \\ \hat{e}_{2L} \\ \hat{e}_{3L} \end{bmatrix} = \begin{bmatrix} 1 & +(\delta + \phi) & -\theta \\ -(\delta_L + \phi) & 1 & -\gamma_L \\ \theta & \gamma_L & 1 \end{bmatrix} \begin{bmatrix} \hat{i}''' \\ \hat{j}''' \\ \hat{k}''' \end{bmatrix}$$

$$\begin{bmatrix} \hat{e}_{1R} \\ \hat{e}_{2R} \\ \hat{e}_{3R} \end{bmatrix} = \begin{bmatrix} 1 & -(\delta_R - \phi) & -\theta \\ (\delta_R - \phi) & 1 & \gamma_R \\ \theta & -\gamma_R & 1 \end{bmatrix} \begin{bmatrix} \hat{i}''' \\ \hat{j}''' \\ \hat{k}''' \end{bmatrix} \qquad (3.3)$$

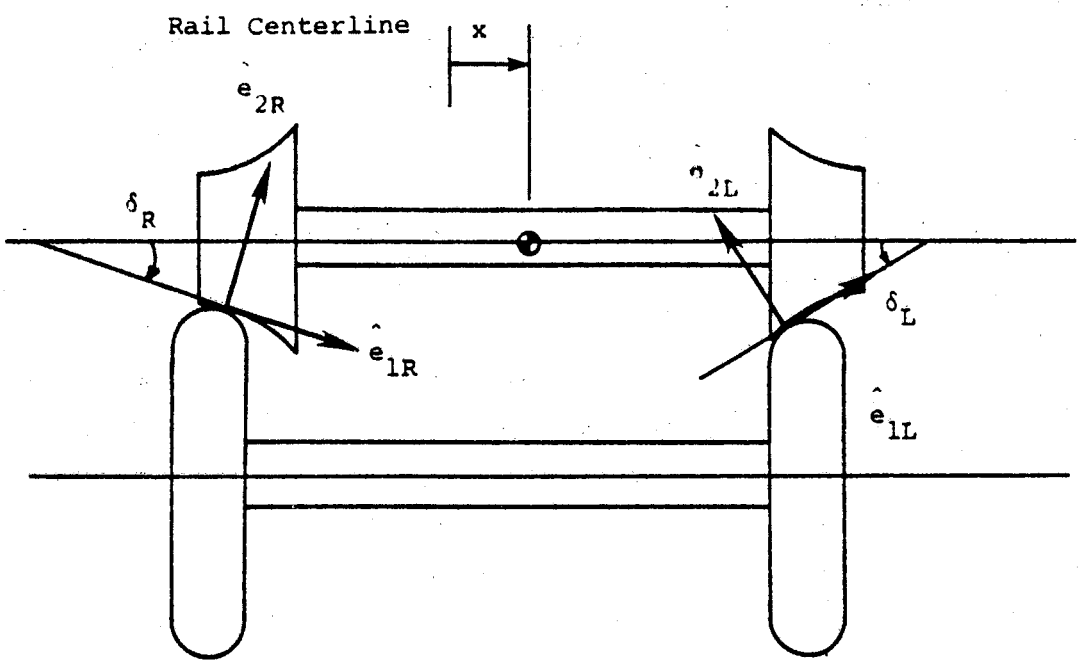

FRONT VIEW

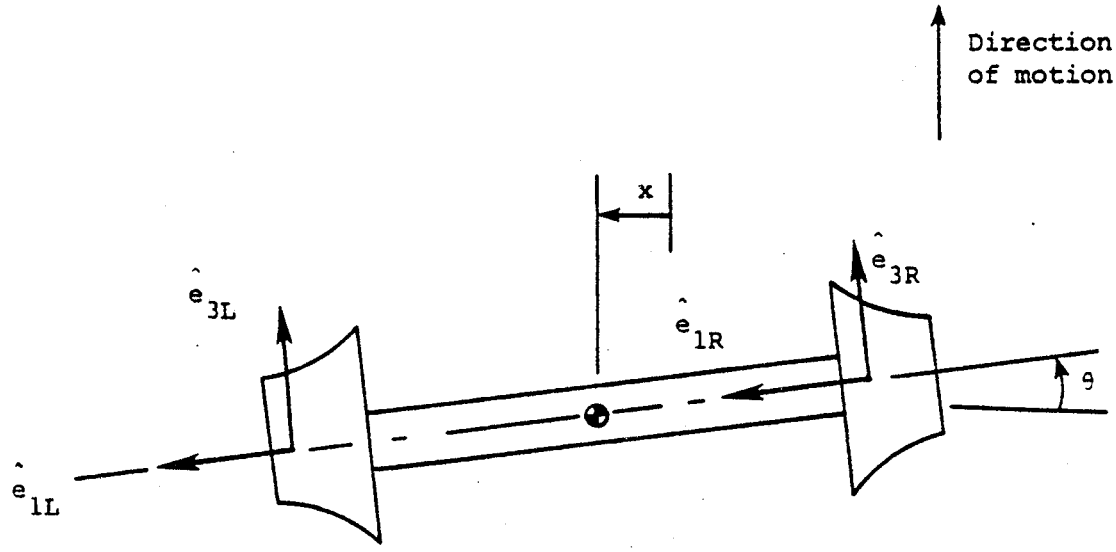

PLAN VIEW

Figure 3-3. Contact Patch Corrdinate Axes.

Creepages and Creep Forces

The theory of Coulomb friction allows for two extremes in the relative motion of two rigid bodies rolling on each other. The bodies are assumed to be either in pure rolling without any slip or completely slipping. However, the work of several investigators has shown that an intermediate stage can occur in which the elasticity of the bodies in contact allows separate regions of rolling and slip within the contact area.

The most complete analysis of the problem has been given by Kalker [18]. His solution includes the case of slip in both the longitudinal and lateral directions and also of spin, i.e., a relative angular velocity between two bodies about the normal to the plane of contact. A solution is given for all values of creepage and spin.

Kalker presented two separate theories, a linear and a nonlinear theory. In the linear theory, which is used in this project, a solution is given for the case where the creepages and spin are vanishingly small. In this theory, the forces and moments exerted by the left roller on the left wheel can be calculated by

$$\begin{aligned} \vec{F}_{1L} &= \{f_{11L}(\xi_{1L}) + f_{12L}(\xi_{2L})\}\hat{e}_{1L} \\ \vec{F}_{3L} &= f_{33L}\,\xi_{3L}\,\hat{e}_{3L} \\ \vec{M}_{L} &= \{f_{12L}(\xi_{1L}) + f_{22L}(\xi_{2L})\}\hat{e}_{2L} \end{aligned} \tag{3.4}$$

where $\vec{F}_{1L}$ and $\vec{F}_{3L}$ are forces in the direction defined by the unit vectors $\hat{e}_{1L}$ and $\hat{e}_{3L}$ respectively and $\vec{M}_L$ is the spin moment in the direction $\hat{e}_{2L}$.

The creep coefficients f_{11L}, f_{12L}, f_{22L} and f_{33L} are functions of the elastic properties of the materials of the surfaces and the normal load. The quantities ξ_{1L}, ξ_{2L} and ξ_{3L} are the lateral, spin and longitudinal creepages along the $\hat{e}_{1L}$, $\hat{e}_{2L}$ and $\hat{e}_{3L}$ directions. Similar equations can be written for the creep forces and moments of the right roller and the right wheel.

$$\vec{F}_{1R} = \{f_{11R}(\xi_{1R}) + f_{12R}(\xi_{2R})\}\hat{e}_{1R}$$

$$\vec{F}_{3R} = f_{33R}\,\xi_{3R}\,\hat{e}_{3R} \qquad (3.5)$$

$$\vec{M}_{R} = \{f_{12R}(\xi_{1R}) + f_{22R}(\xi_{2R})\}\hat{e}_{2R}$$

These forces and moments are shown in Figure 3-4.

Since creep forces occur on both left and right wheels, it is necessary to determine the creepages at both points.

Consider the wheelset on the roller rig as shown in Figure 3-5. Let w_{roll} be the angular velocity of the rollerset about its axle centerline, and let Ω be the angular velocity of the wheelset about its axle centerline. If θ is the wheelset yaw angle, ϕ the wheelset roll angle and β the perturbaton in Ω, then the total angular velocity of the wheelset is

$$\vec{w}_{w} = (\Omega+\dot{\beta})\hat{i}' + \dot{\theta}\hat{j}''' + \dot{\phi}\hat{k}'''$$

Transforming the above equation to the $\hat{i}'''$, $\hat{j}'''$, $\hat{k}'''$ system and neglecting higher order terms,

$$\vec{w}_{w} = (\Omega+\dot{\beta})\hat{i}' + \dot{\theta}\hat{j}' + \dot{\phi}\hat{k}' \qquad (3.6)$$

For the left wheel, the position vector that locates the point of contact can be written as

$$\vec{r}_{LC} = \vec{r}_{CG} + \{(a+\Delta\ell)\hat{i} - r_{L}\hat{j}'\} \qquad (3.7)$$

where $\vec{r}_{CG}$ is the position vector that locates the center of gravity of the wheelset and

$$\vec{r}_{CG} = x\,\hat{i}''' + y\hat{j}''' + z\hat{k}'''$$

and the velocity of the contact point on the left wheel is

$$\dot{\vec{r}}_{LC} = \dot{\vec{r}}_{CG} + \vec{w}_{w} \times \{(a+\Delta\ell\,)\hat{i}' - r_{L}\hat{j}'\} \qquad (3.8)$$

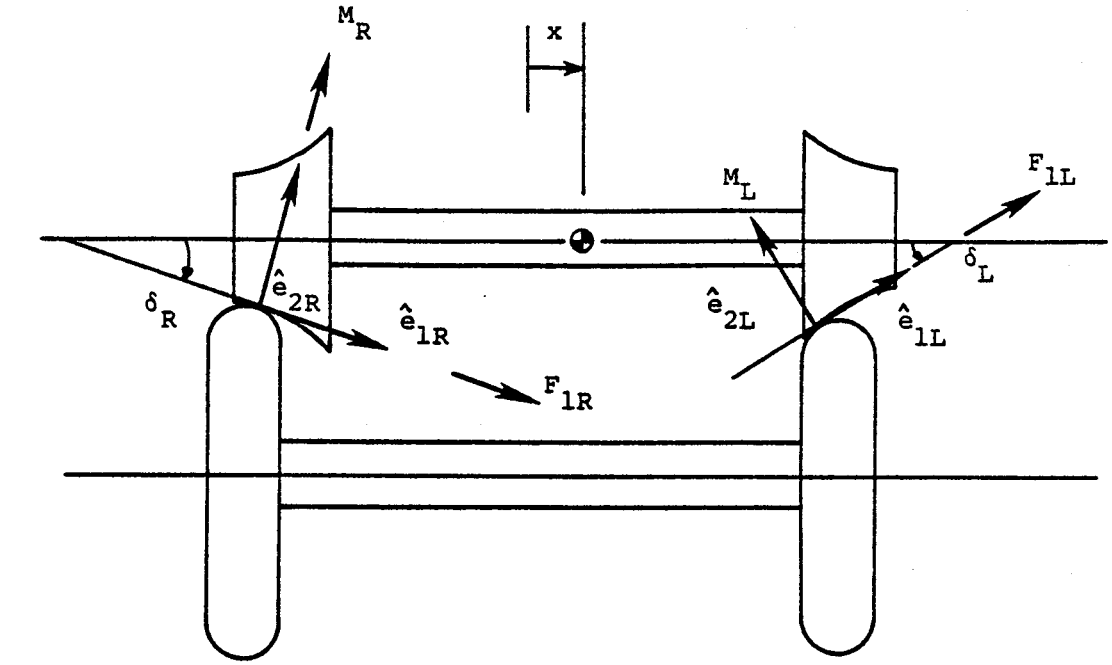

FRONT VIEW

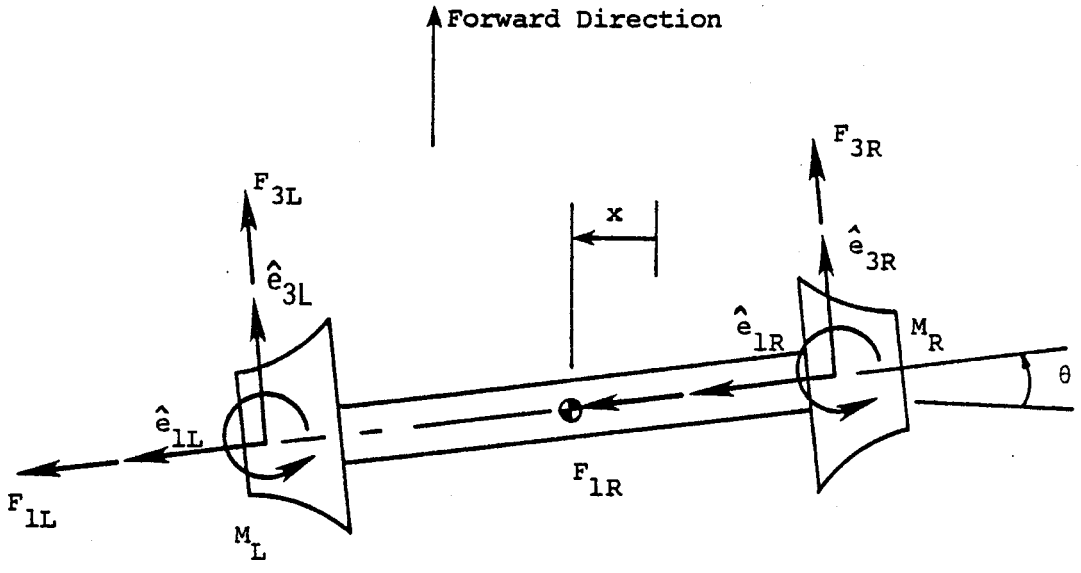

PLAN VIEW

Figure 3-4. Creep Force and Moment Directions for Wheelset on a Roller Rig.

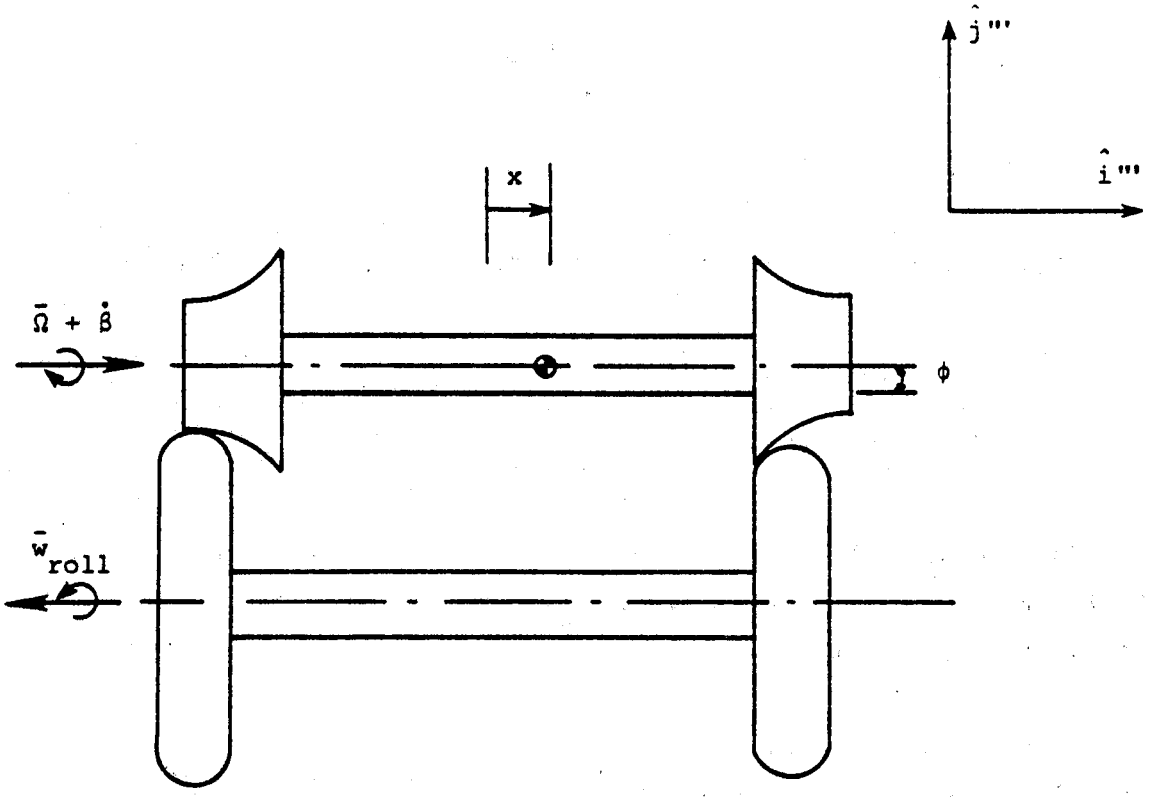

FRONT VIEW

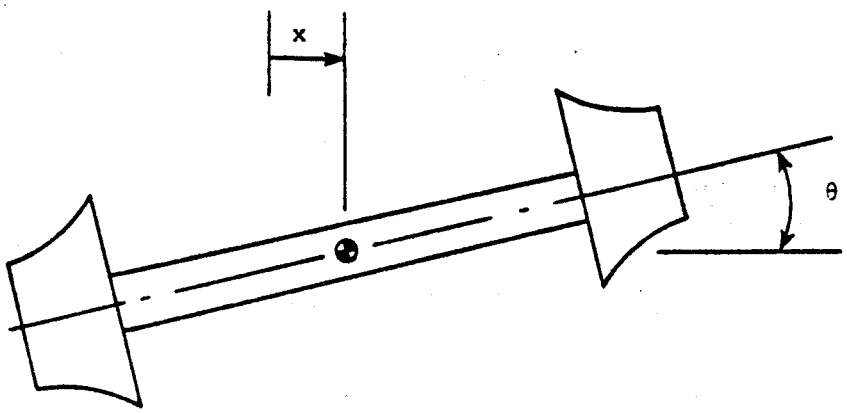

PLAN VIEW

Figure 3-5. Wheelset-Roller Angular Velocities.

Using Equation (3.6), the velocity above becomes

$$\dot{\vec{r}}_{LC} = \dot{\vec{r}}_{CG} + [r_L\dot{\phi}\hat{i}' - \{r_L(\Omega+\dot{\beta}) + \dot{\theta}(a+\Delta\ell)\}\hat{k}' + \dot{\phi}(a+\Delta\ell)\hat{j}'] \tag{3.9}$$

Using Equation (3.9) and transforming to the triple primed system

$$\dot{\vec{r}}_{LC} = (\dot{x}+r_L\dot{\phi} - r_L\Omega\theta)\hat{i}''' + (\dot{y}+\dot{\phi}a + \dot{\phi}\Delta\ell)\hat{j}''' + \{\dot{z} - r_L(\Omega+\dot{\beta}) - \dot{\theta}(a+\Delta\ell)\}\hat{k}''' \tag{3.10}$$

To determine the lateral and the longitudinal creepage at the left wheel, the difference in the velocities of the contact points on the wheels and rollers is

$$\Delta\dot{\vec{r}}_{LC} = \dot{\vec{r}}_{LC} - \vec{w}_{roll} \times \vec{R}_L \tag{3.11}$$

where R_L is the radius of the left roller at the contact point.

$$\Delta\dot{\vec{r}}_{LC} = (\dot{x} + r_L\dot{\phi} - r_L\Omega\theta)\hat{i}''' + (\dot{y}+\dot{\phi}a + \dot{\phi}\Delta\ell)\hat{j}''' + \{\dot{z} - r_L(\Omega+\dot{\beta}) - \dot{\theta}(a+\Delta\ell) + w_{roll}R_L\hat{k}''' \tag{3.12}$$

The total creepage for the left wheel is

$$\vec{\xi}_L = \Delta\dot{\vec{r}}_{LC}/\Omega r_o \tag{3.13}$$

and the lateral creepage along the $\hat{e}_{1L}$ axis is

$$\vec{\xi}_L \cdot \hat{e}_{1L} = [(\dot{x}+r_L\dot{\phi}-r_L\Omega\theta) + (\delta_L+\phi)(\dot{y}+\dot{\phi}a + \dot{\phi}\Delta\ell) - \theta\{\dot{z} - r_L\dot{\beta} - a\dot{\theta} - \Delta\ell\dot{\theta} + (w_{roll}R_L-\Omega r_L)\}]/\Omega r_o$$

In the steady state,

$$\xi_{1L} = -\theta w_{roll} R_L / \Omega r_o \tag{3.14}$$

Similarly, for the longitudinal creepage,

$$\xi_{3L} = \vec{\xi}_L \cdot \hat{e}_{3L} = \{\dot{z} - r_L(\Omega+\dot{\beta}) - \dot{\theta}(a+\Delta\ell) + w_{roll} R_L\}/\Omega r_o$$

and, in steady state

$$\xi_{3L} = (-r_L \Omega + w_{roll} R_L)/\Omega r_o \tag{3.15}$$

To determine the spin creepage on the left wheel, the difference in angular velocity between the wheelset and the roller is

$$\Delta\vec{w} = \vec{w}_w - w_{roll}$$

$$\Delta\vec{w} = (\Omega+\dot{\beta}+w_{roll})\hat{i}''' + (\phi\Omega+\dot{\theta})\hat{j}''' + (\dot{\phi}-\Omega\theta)\hat{k}''' \tag{3.16}$$

Then the spin creepage or creepage along the $\hat{e}_{2L}$ axis is

$$\begin{aligned}\xi_{2L} &= \Delta\vec{w} \cdot \hat{e}_{2L}/\Omega r_o \\ &= \{-(\Omega+\dot{\beta}+w_{roll})(\delta_L+\phi) + (\phi\Omega+\dot{\theta}) - \gamma_L(\dot{\phi}-\Omega\dot{\theta})\}/\Omega r_o\end{aligned} \tag{3.17}$$

In the steady state, this is

$$\xi_{2L} = -(\Omega+w_{roll})(\delta_L+\phi)/\Omega r_o \tag{3.18}$$

Similarly for the right wheel, the creepages in steady state are

$$\xi_{1R} = (\dot{\vec{\Delta r}}_{Rc} \cdot \hat{e}_{1R})/\Omega r_o \tag{3.19}$$

$$= -\theta w_{roll} R_R/\Omega r_o \tag{3.20}$$

$$\xi_{3R} = \dot{\vec{\Delta r}}_{RC} \cdot e_{3R}/\Omega r_o \tag{3.21}$$

$$= (-\Omega r_R + w_{roll} R_R)/\Omega r_o \tag{3.22}$$

$$\xi_{2R} = (\dot{\vec{\Delta w}} \cdot \hat{e}_{2R})/\Omega r_o \tag{3.23}$$

$$= \{(\Omega + w_{roll})\delta_R - w_{roll}\phi\}/\Omega r_o \tag{3.24}$$

Using Equation (3.4) and Equations (3.14) through (3.24) the steady state creep force and moments on the left and right wheels are:

$$\vec{F}_{1L} = [f_{11L}(-w_{roll} R_L\theta) - f_{12L}\{(\Omega+w_{roll})\delta_L - w_{roll}\phi\}]/(\Omega r_o)\hat{e}_{1L} \tag{3.25}$$

$$\vec{F}_{3L} = \{f_{33L}(-r_L\Omega+w_{roll} R_L)\}/(\Omega r_o)\hat{e}_{3L} \tag{3.26}$$

$$\vec{M}_{2L} = \{f_{12L}(-w_{roll} R_L\theta) - f_{22L}\{(\Omega+w_{roll})\delta_L - w_{roll}\phi\}/(\Omega r_o)\hat{e}_{2L} \tag{3.27}$$

and

$$\vec{F}_{1R} = [f_{11R}(-w_{roll} R_R\theta) + f_{12R} \{(\Omega+w_{roll})\delta_R - w_{roll}\phi\}]/(\Omega r_o)\hat{e}_{1R} \tag{3.28}$$

$$\vec{F}_{3R} = f_{33R}(-\Omega r_R+w_{roll} R_R)/(\Omega r_o)\hat{e}_{3R} \tag{3.29}$$

$$\vec{M}_{2R} = \{f_{12R}(-w_{roll} R_R\theta) + f_{22R}(\Omega+w_{roll})(\delta_R-\phi)\}/\Omega r_o\hat{e}_{2R} \tag{3.30}$$

These are as shown in Figure 3-4. The total force on the left wheel at the contact point is

$$\vec{F}_L = \vec{F}_{1L} + \vec{F}_{3L} \tag{3.31}$$

Transforming the Equations (3.14) through (3.24) from the contact point coordinates to the $\hat{i}'''$, $\hat{j}'''$, $\hat{k}'''$ coordinates, the force on the left wheel is

$$\vec{F}_L = [f_{11L}\theta + f_{12L}\{(1 + r_o/R_o)(\delta_L) + r_o\phi/R_o\}/r_o]\hat{i}''' + f_{33L}\{r_L - r_o R_L/R_o\}/r_o\hat{k}''' \tag{3.32}$$

and the moment is

$$\vec{M}_L = [-f_{12L}\theta + f_{22L}\{(1+r_o/R_o)\delta_L + r_o\phi/R_o\}/r_o]\hat{j}''' \tag{3.33}$$

Similarly, for the right wheel, the total force on the wheel is

$$\vec{F}_R = \vec{F}_{1R} + \vec{F}_{3R} \tag{3.34}$$

and after transformation to the triple primed system,

$$\vec{F}_R = [-f_{11R}\theta - f_{12R}\{(1 + r_o/R_o)\delta_R - r_o/R_o\phi\}/r_o]\hat{i}''' + f_{33R}(r_R - r_o/R_o\, R_R)/r_o\hat{k}''' \tag{3.35}$$

and the moment is

$$\vec{M}_R = [-f_{12R}(\theta) - f_{22R}\{(1 + r_o/R_o)\delta_R - r_o\phi/R_o\}/r_o]\hat{j}''' \tag{3.36}$$

In general the creep coefficients on each wheel vary about a nominal value, depending on the normal load and the geometry of the contact region. The variation is small if the curvatures in the contact

region do not change significantly with the wheelset displacement and the normal load. For small motions of the wheelset, this condition is generally satisfied for most wheel profiles. Thus for example, the lateral creep coefficient on the left wheel f_{11L} can be written as

$$f_{11L} = f_{110L} + \Delta f_{11L}$$
$$= f_{110L} (1 + \Delta f_{11L}/f_{110L})$$

where f_{110L} is the nominal value of the creep coefficient and Δf_{11L} is the net variation. If the quantity $\Delta f_{11L}/f_{110L}$ is sufficiently small, that is

$$\Delta f_{11L}/f_{110L} << 1$$

then

$$f_{11L} \simeq f_{110L}$$

Similarly, if the changes in the lateral spin and longitudinal creep coefficients are small enough, so that

$$\Delta f_{12}/f_{120L} << 1$$

and

$$\Delta f_{33}/f_{330L} << 1$$

then

$$f_{12L} \simeq f_{120L}$$

and

$$f_{33L} \simeq f_{330L}$$

If the left and right wheels are identical, then

$$\begin{aligned} f_{110L} &= f_{110R} = f_{11} \\ f_{120L} &= f_{120R} = f_{12} \end{aligned} \tag{3.37}$$

and

$$f_{330L} = f_{330R} = f_{33}$$

The contribution of the spin moments M_L and M_R to the total yaw moment on the wheelset is very small. This is because of the large yaw moment due to the longitudinal creep forces. Therefore, the spin moments M_L and M_R can be neglected in deriving the equations of motion. Using Equation (3.37) in Equations (3.32) through (3.36) and neglecting the spin moment, the resultant creep forces and moments on the wheelset are

$$F_x = 2f_{11}\theta + 2f_{12}\{(1+r_o/R_o)(\delta_L-\delta_R)/2 + r_o\phi/R_o\}/r_o \tag{3.38}$$

$$F_z = 2f_{33}\{(r_L+r_R) - r_o(R_L+R_R)/R_o\}/2 \tag{3.39}$$

$$M_y = -2f_{33}\, a^2[(r_L-r_R)/2a - r_o/R_o(R_R-R_L)/2a]/r_o \tag{3.40}$$

These resultant forces and moments are shown in Figure 3-6.

The rolling radii of the wheelsets and the rollers can be expressed in terms of a mean radius and a perturbation. Thus

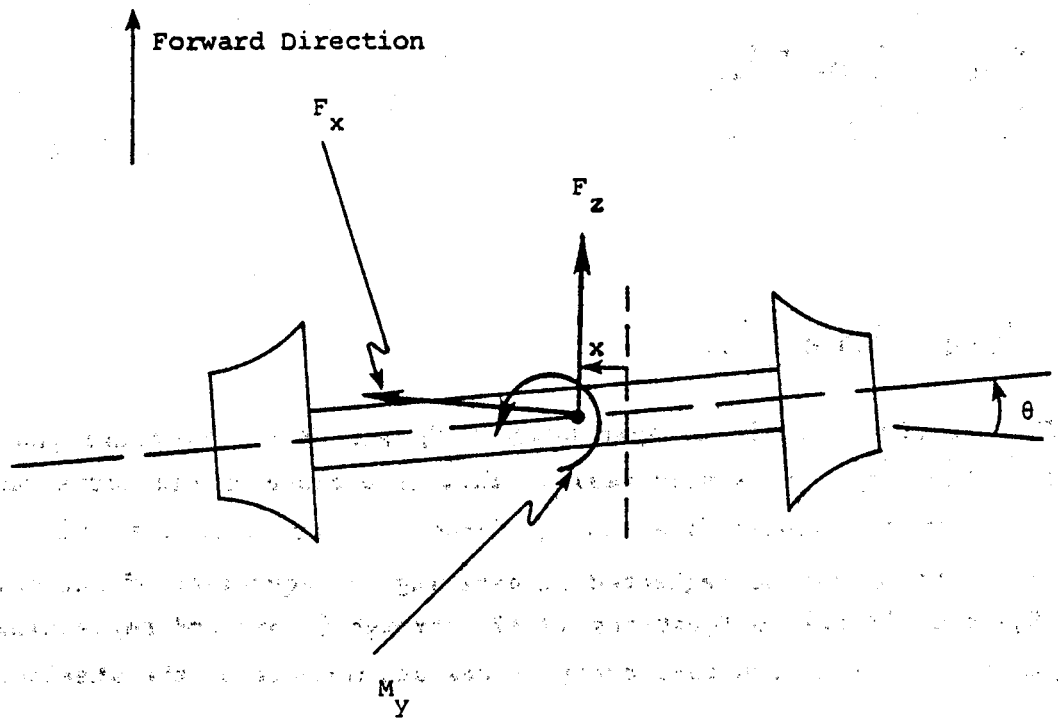

PLAN VIEW

Figure 3-6. Resultant Creep Forces and Moments.

$$
\begin{aligned}
r_L &= r_o + \lambda x \\
r_R &= r_o - \lambda x \\
R_L &= R_o + \lambda_R x \\
R_R &= R_o + \lambda_R x
\end{aligned}
\qquad (3.41)
$$

where λ and λ_R are effective slopes or conicities at the contact points on wheels and the rollers. substituting Equation (3.41) into Equation (3.39) yields

$$F_z = 0$$

Hence, for motions confined to the tread region of the wheels, the net longitudinal drag on the wheelset due to creep is very nearly zero.

Normal Forces

As the wheelset yaws on a pair of rollers, the point of contact ot each wheel on the rail moves away from the top of the rollers and the wheelset is said to decrown. As shown in Figure 3-7, for small yaw angles,

$$a\theta = \gamma(r_o+R_o)$$

or

$$\gamma = a\theta/(r_o+R_o) \qquad (3.42)$$

The decrowning angle γ is consequently a function of the wheelset yaw angle θ; the wheel and roller radii, r_0 , R_0 , and the semi-distance, a, between the contact points. The normal forces exerted by the roller set on the wheelset are shown in Figure 3-7 as well. They can be written as

$$\vec{N}_L = N_L \hat{e}_{2L}$$

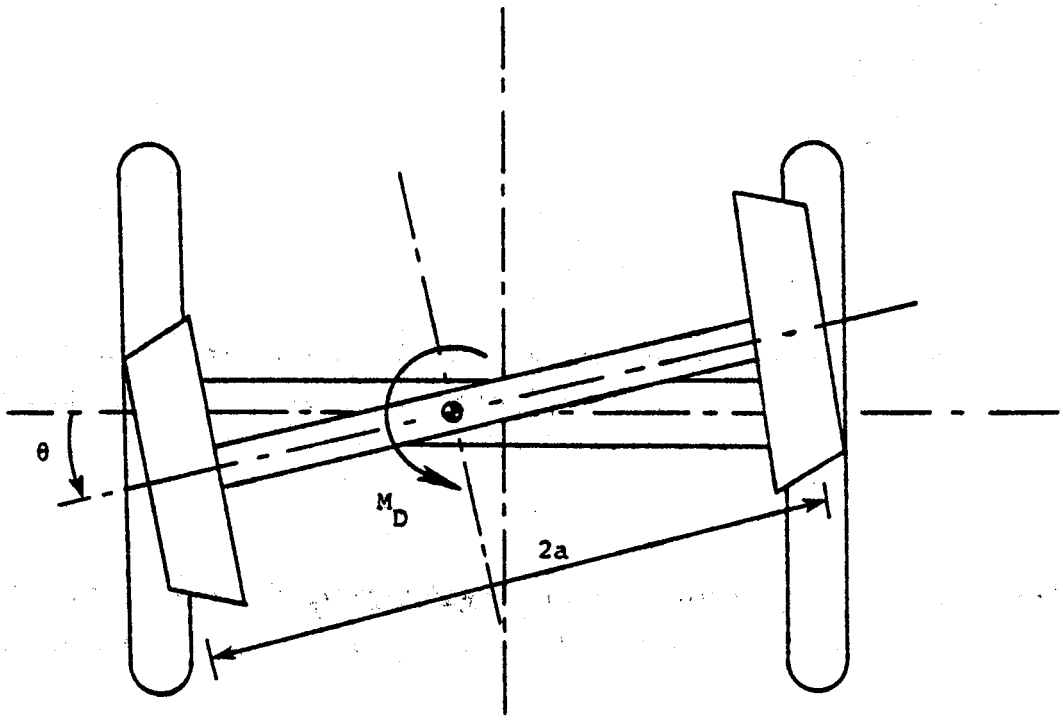

PLAN VIEW

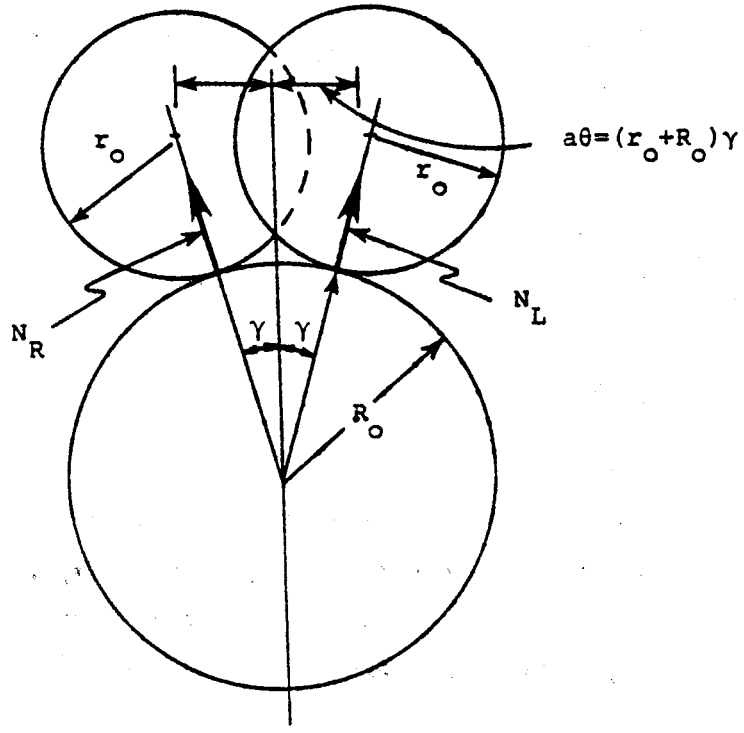

SIDE VIEW

Figure 3-7. Decrowning of Wheelset on Rollers.

and

$$\vec{N}_R = N_R \hat{e}_{2R}$$

Then resolving these forces in the $\hat{i}'''$, $\hat{j}'''$, $\hat{k}'''$ coordinate system,

$$\begin{aligned}\vec{N}_L &= -N_L(\delta_L+\phi)\hat{i}''' + N_L\hat{j}''' - N_L\gamma\hat{k}''' \\ &= N_{Lx}\hat{i}''' + N_{Ly}\hat{j}''' + N_{Lz}\hat{k}'''\end{aligned} \tag{3.43}$$

and

$$\begin{aligned}\vec{N}_R &= N_R(\delta_R-\phi)\hat{i}''' + N_R\hat{j}''' + N_R\gamma\hat{k}''' \\ &= N_{Rx}\hat{i}''' + N_{Ry}\hat{j}''' + N_{Rz}\hat{k}'''\end{aligned} \tag{3.44}$$

Wheel-Roller Geometry Parameters

The wheel-roller geometry parameters, namely $(r_L-r_R)/2a$, $(R_L-R_R)/2a$, $(\delta_L-\delta_R)/2a$, and ϕ appearing in Equations 3.25 to 3.40 are, in general, nonlinear functions of the wheelset lateral displacement. For lateral wheelset excursions such that flange contact does not occur, the effect of wheelset yaw is negligible on these quantities. Therefore, these kinematic quantities are functions of the lateral motion of the wheelset only, and a Mclaurin series can be written for these terms.

Alternatively, at a given value of lateral wheelset displacement, they may be written as

$$\phi = \Gamma(x-x_{01})/a$$

$$(\delta_L-\delta_R)/2 = \Delta(x-x_{02})/2 \qquad (3.45)$$

$$(r_L-r_R)/2a = \lambda(x-x_{03})/a$$

and

$$(R_L-R_R)/2a = -\lambda_R(x-x_{04})/a$$

The quantities x_{0i} are offsets that occur in the wheel rail geometry functions due to differences in the left and right wheel profiles on a wheelset or differences in the left and right roller profiles. These offsets give rise to constant creep forces that act on the wheelset and cause it to shift laterally as well as yaw in its initial state. The parameters Γ, Δ, λ and λ_R are in general functions of the wheelset displacement relative to the initial unloaded position of the wheelset, i.e., $(x-x_0)$. However, as an approximation we have assumed these parameters are constant. Reference [14] provides a justification for this approximation for the SOAC on the RDU.

Suspension Forces

The idealized primary suspension elements between the wheelsets and the truck frame for the SOAC vehicle model are arranged as shown in Figure 3-1. For the SOAC vehicle these suspension forces are produced by means of chevrons placed between the wheelsets and the truck frame. These elements are nearly linear in the range of wheelset and truck motions generally considered and are therefore modelled as linear springs in the lateral and longitudinal directions.

The relative lateral motion between the front wheelset and the truck frame is

$$\delta_{lat} = (x_T + \ell\theta_T + h_T\phi_T - x_1) \qquad (3.46)$$

The relative yaw motion is

$$\theta_{rel} = (\theta_T - \theta_1) \tag{3.47}$$

and the steady lateral suspension force and yaw moment corresponding to these displacements are

$$\begin{aligned} F_{sx} &= 2k_{xp}(x_T + \ell\theta_T + h_T\phi_T - x) \\ M_{sy} &= 2k_{zp}d^2(\theta_T - \theta) \end{aligned} \tag{3.48}$$

Steady State Equations of Motion

The steady state equation of motion for a single wheelset can be written using the free body diagram shown in Figure 3-8.

Summing forces along the $\hat{j}'''$ direction and assuming a small decrowning angle γ

$$m_w g + W_{app} - (N_L + N_R) = 0 \tag{3.49}$$

where W_{app} is the load applied by the vehicle on the wheelset. Or

$$(N_L + N_R) = m_w g + W_{app} \tag{3.50}$$

Summing moments about the $\hat{k}'''$ or roll axis,

$$\begin{aligned} &M_{sz} + (N_L - N_R)a + 2f_{11}r_o\theta + 2f_{12}\{(1+r_o/R_o)(\delta_L - \delta_R)/2 \\ &+ r_o\phi/R_o\} = 0 \end{aligned} \tag{3.51}$$

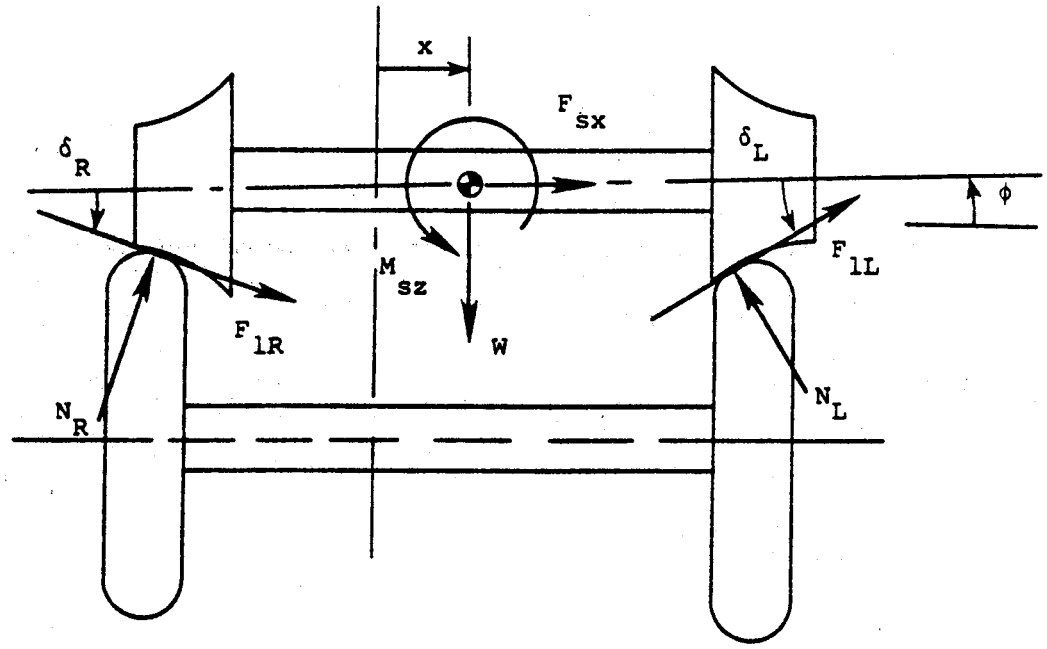

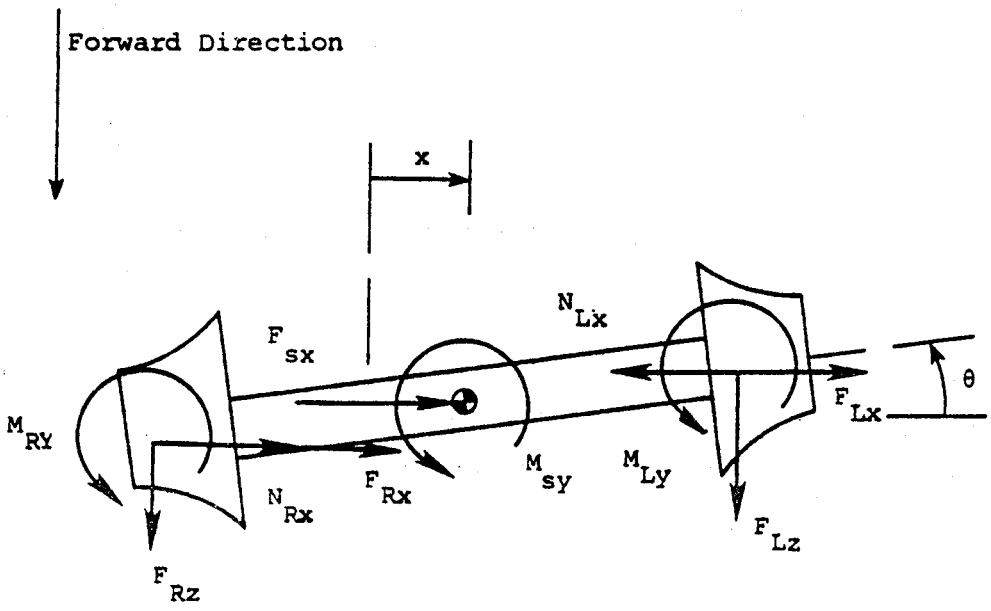

Figure 3-8. Freebody Diagram for a Wheelset on a Roller Rig.

or

$$(N_L-N_R)a = -M_{sz} - 2f_{11}r_o\theta - 2f_{12}\{(1+r_o/R_o)(\delta_L-\delta_R)/2 + r_o\phi/R_o\} \tag{3.52}$$

From Equations (3.51) and (3.52)

$$N_L = [a(m_w g + W_{app}) - M_{sz} - 2f_{11}r_o\theta - 2f_{12}\{(1+r_o/R_o)(\delta_L-\delta_R)/2 + r_o\phi/R_o\}]/2a, \tag{3.53}$$

and

$$N_R = [a(m_w g + W_{app}) + M_{sz} + 2f_{11}r_o\theta + 2f_{12}\{(1+r_o/R_o)(\delta_L-\delta_R)/2 + r_o\phi/R_o\}]/2a. \tag{3.54}$$

From Equations (3.53) and (3.54),

$$(N_L+N_R)\phi = (m_w g + W_{app})\phi \tag{3.55}$$

and

$$N_R\delta_R - N_L\delta_L = -(\delta_L-\delta_R)W/2 \tag{3.56}$$

$$(N_L+N_R)a\gamma = (m_w g + W_{app})a\gamma = Wa^2\theta/(r_o+R_o) \tag{3.57}$$

where

$$W = m_w g + W_{app}$$

Now summing forces in the lateral direction

$$N_{Lx} + N_{Rx} - F_{sx} + F_x = 0 \tag{3.58}$$

Using Equation (3.38) we have

$$-2f_{11}\theta - 2f_{12}\{(1+r_o/R_o)(\delta_L-\delta_R)/2 + r_o/R_o\phi\} + W\{(\delta_L-\delta_R)/2 + \phi\} - F_{sx} = 0 \tag{3.59}$$

Summing moments about the $\hat{j}'''$ or yaw axes through the wheelset center of gravity gives

$$M_{sy} + M_{Ry} + M_{Ly} + \hat{j}''' \cdot [\{(a+\Delta\ell)\hat{i}' - r_L\hat{j}'\} \times \{(N_{Lx}+F_{Lx})\hat{i}''' + (N_{Ly}+F_{Ly})\hat{j}''' + F_{Lz}\hat{k}'''\} + \{-(a-\Delta r)\hat{i}'' - r_R\hat{j}'\} \times \{(N_{Rx}+F_{Rx})\hat{i}''' + (N_{Ry}+F_{Ry})\hat{j}''' + F_{Rz}\hat{k}'''\}] = 0 \tag{3.60}$$

Using Equations (3.57), (3.32), (3.33), (3.35), and (3.36)

$$2f_{12}\theta + 2f_{33}a^2\{(r_L-r_R)/2a - (R_L-R_R)r_o/(2aR_o)\} - Wa^2\theta/(r_o+R_o) - M_{sy} = 0$$

If the wheel-rail geometry parameters are replaced by Equation (3.45), then the equations of motion can be written as

Wheelset lateral equation

$$-2f_{11}\theta - 2f_{12}\{(1+r_o/R_o)\Delta + r_o\Gamma/R_o\}x/ar_o + W(\Delta+\Gamma)x/a - 2k_{xp}(x_T+\ell\theta_T + h_T\phi_T - x) = W - 2f_{12}(1+r_o/R_o)/r_o\}\Delta x_{02}/a + (W-2f_{12}/R_o)\Gamma x_{01}/a \tag{3.61}$$

Wheelset yaw equation

$$2f_{12}\theta + 2f_{33}a(\lambda+r_o\lambda_R/R_o)x/r_o - Wa^2\theta/(r_o+R_o) - 2k_{zp}d^2(\theta_T-\theta)$$
$$= 2f_{33}a(\lambda x_{03} + r_o\lambda_R x_{04}/R_o)/r_o \qquad (3.62)$$

Misalignments

In any large scale physical system, perfect assembly of the constituent parts is never achieved. In the case of the wheelset-roller system, typical misalignments that occur are those due to yaw and lateral misalignments of the rollers and the lateral and yaw misalignments of the wheelsets in the truck frame. These misalignments are shown in Figure 3-9.

The yaw misalignment α_θ modifies the apparent yaw angle between the wheelset and the rollers and significantly affects the wheelset lateral response through its effect on the lateral creep force. For this type of misalignment, the total lateral creep force on the wheelset is

$$F_x = 2f_{12}\{(1+r_o/R_o)(\delta_L-\delta_R)/2 + r_o\phi/R_o\} + 2f_{11}(\theta-\alpha_\theta) \qquad (3.63)$$

The yaw misalignment enters the wheelset yaw equation through the decrowning moment M_D, and the lateral force due to spin creep, F_{spin}. However, there is no effect of this misalignment on the longitudinal creep force that dominates the wheelset yaw equation. The modified decrowning stiffness and spin terms are

$$M_d = Wa^2/(r_o+R_o)(\theta-\alpha_\theta)$$
$$F_{spin} = 2f_{12}(\theta-\alpha_\theta) \qquad (3.64)$$

The roller lateral misalignment α_R affects the wheelset response only if the wheelset is coupled to other wheelsets through a truck frame. For example, if the lateral misalignment occurs at the front

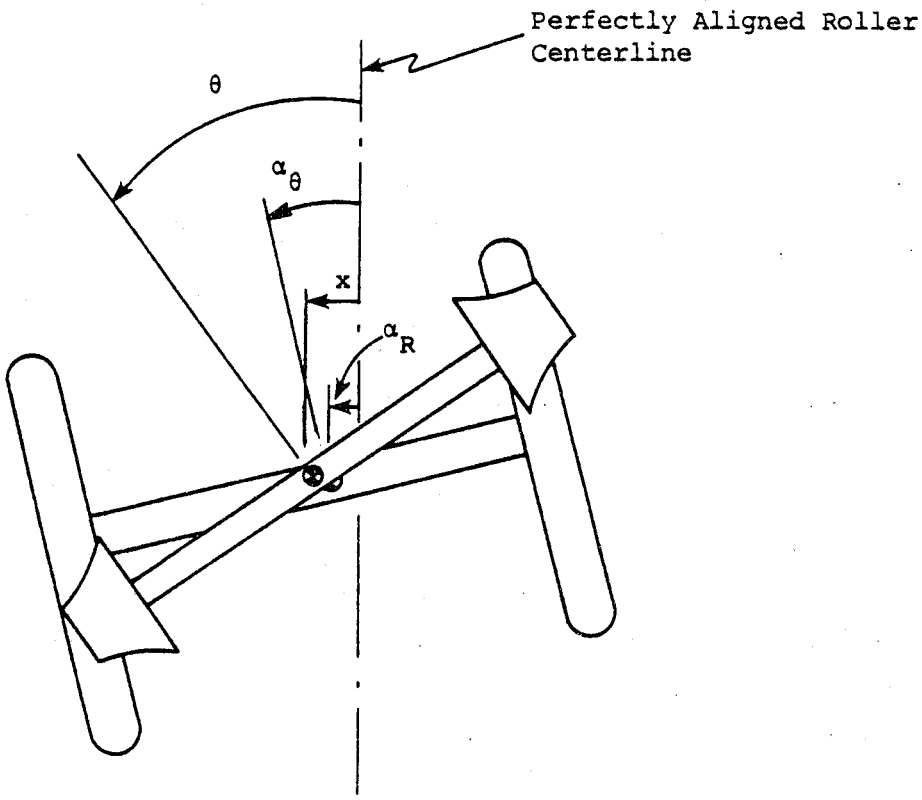

Figure 3-9. Roller Misalignments.

rollers, then forcing is applied to the front wheelset through the wheel-rail geometry. The wheel-rail geometry functions for a lateral misalignment of the rollers are

$$\begin{aligned} \phi &= \Gamma(x-\alpha_R)/a \\ (\delta_L-\delta_R)/2 &= \Delta(x-\alpha_R)/a \\ (r_L-r_R)/2a &= \lambda(x-\alpha_R)/a \\ (R_L-R_R)/2a &= -\lambda_R(x-\alpha_R)/a \end{aligned} \tag{3.65}$$

For both α_θ and α_R, the wheelset equations then become

Wheelset lateral equation with misalignments

$$\begin{aligned} &-2f_{11}(\theta-\alpha_\theta) - 2f_{12}\{(1+r_o/R_o)\Delta + r_o\Gamma/R_o\}(x-\alpha_R)/ar_o \\ &-W(\Delta+\Gamma)(x-\alpha_R)/a - 2k_{xp}(x_T+\ell\theta_T + h_T\phi_T-x) = 0 \end{aligned} \tag{3.66}$$

Wheelset yaw equation with misalignments

$$\begin{aligned} &2f_{33}a(\lambda+r_o/R_o\lambda_R)(x-\alpha_R)/r_o - Wa^2(\theta-\alpha_\theta)/(r_o+R_o) \\ &+ 2f_{12}(\theta-\alpha_\theta) - 2k_{zp}d^2(\theta_T-\theta) = 0 \end{aligned} \tag{3.67}$$

These equations may be solved together with the remaining vehicle equations for the wheelset lateral and yaw displacements due to α_θ and α_R.

For lateral and yaw misalignments, x_{s0} and θ_{s0}, of the wheelset relative to the truck frame, the suspension forces and moments then transmitted to the wheelset are

$$F_{sx} = 2k_{xp}(\delta_{lat}-x_{so}) \tag{3.68}$$

$$M_{sy} = 2k_{zp}d^2(\theta_{rel}-\theta_{so}) \tag{3.69}$$

The equations of motion for a single wheelset with lateral and yaw misalignments of rollers and wheelset relative to the truck frame are therefore

Wheelset lateral equation

$$[2k_{xp}a - 2f_{12}\{(1+r_o/R_o)\Delta + r_o\Gamma/R_o\}/r_o + W(\Delta+\Gamma)]x/a - 2f_{11}\theta - 2k_{xp}\{x_T + \ell\theta_T + h_T\phi_T\} = 2k_{xp}x_{so} - 2f_{12}[(1+r_o/R_o)\Delta + r_o\Gamma/R_o\}/r_o - W(\Delta+\Gamma)]\alpha_R/a - 2f_{11}\alpha_\theta \quad (3.70)$$

Wheelset yaw equation

$$-Wa^2\theta/(r_o+R_o) + 2f_{33}a\{\lambda + r_o\lambda_R/R_o\}x/r_o + 2f_{12}\theta + 2k_{zp}d^2(\theta-\theta_T) = -Wa^2\alpha_\theta/(r_o+R_o) + 2f_{33}a\{\lambda + r_o\lambda_R/R_o\}\alpha_R + 2f_{12}\alpha_\theta - 2k_{zp}d^2\theta_{so} \quad (3.71)$$

The constant terms on the right hand side are due to the misalignments and acts as steady forcing on the wheelset. Therefore, in the linear regime, the response of the wheelset due to the misalignments is superimposed on that due to external forcing.

TRUCK MODEL

A typical truck consists of two wheelsets connected to the truck frame through the primary suspension elements. The truck frame has lateral, yaw and roll degrees of freedom, which, combined with two degrees of freedom for each wheelset gives seven degrees of freedom for the complete model.

The forces external to the model are: (1) creep forces on the wheelsets, (2) secondary suspension forces exerted by the carbody on the

truck frame, and (3) any external forces applied to the truck frame or the wheelsets through mechanical means. The secondary suspension forces and the primary forces and moments that act on the truck model are discussed below and shown in Figure 3-10.

Primary Suspension Forces and Moments

The chevrons that serve as the lateral and longitudinal suspension elements between the wheelsets and the truck frame also provide a vertical suspension and allow a relative roll as well as vertical motion between the wheelsets and the truck frame. If y_i is the relative vertical motion of the truck with respect to the ith wheelset, then the relative vertical motion of the truck with respect to the ith wheelset at the left chevron is

$$\delta_{wiL} = y_i + d(\phi_T - \phi_i) \tag{3.72}$$

and that at the right chevron is

$$\delta_{wiR} = y_i - d(\phi_T - \phi_i) \tag{3.73}$$

and the vertical force of the wheelset on the truck at the left chevron is

$$F_{yL_i} = -k_{y_i}\{y_i + d(\phi_T - \phi_i)\} \tag{3.74}$$

and at the right chevron

$$F_{yR_i} = -k_{y_i}\{y_i - d(\phi_T - \phi_i)\} \tag{3.75}$$

The net vertical force due to deflection from equilibrium is then

$$F_{y_i} = F_{yL_i} + F_{yR_i} = -2k_{y_i} y_i \tag{3.76}$$

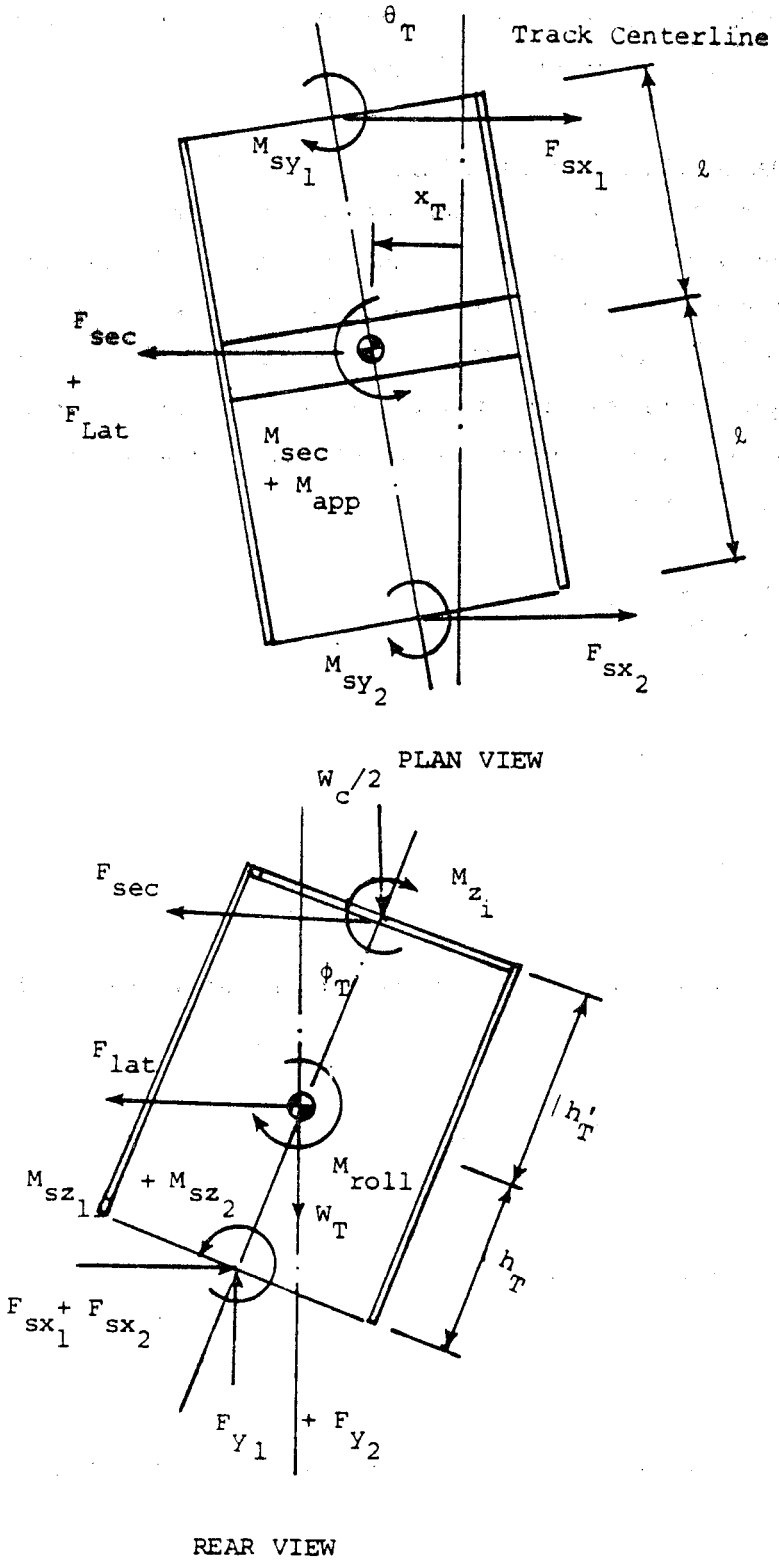

Figure 3-10. Freebody Diagram for the Truck Frame.

The net roll moment exerted by the ith wheelset on the truck is then

$$M_{sz_i} = (F_{yL_i} - F_{yR_i})d = -2k_{y_i} d^2(\phi_T - \phi_i) \tag{3.77}$$

where i = 1, 2.

These forces and moments are shown in Figure 3-10. The lateral forces and yaw moments due to the primary suspension system were previously developed and are given by Equations 3.48.

Secondary Suspension Forces and Moments

The secondary suspension between the truck frame and carbody consists of elements that oppose relative motion between the carbody and the truck in the lateral, vertical, and longitudinal directions.

For the SOAC vehicle, the vertical suspension consists of two air springs mounted on each end of the bolster. These springs have shear characteristics that provide lateral stiffness and damping between the carbody and the truck frame. The yaw suspension consists of interconnections between the bolster and the carbody and between the bolster and truck frame. These interconnections are achieved through the anchor rods and the yaw friction. The anchor rods are placed longitudinally on either side of the bolster and connected to the bolster and the carbody. Rubber bushings in the anchor rods allow relative longitudinal and yaw motion between the bolster and the carbody. The bolster is connected to the truck frame through a yaw pivot located in the truck frame. Friction between the bolster and the truck frame places a limit on the maximum torque that can be transmitted to the truck, before the friction breaks loose. The secondary yaw suspension is therefore modelled as a spring in series with friction and has the torque-deflection characteristics shown in Figure 3-11. The relative yaw displacement between the bolster and the carbody before slip is

$$\theta_{relc} = \theta_c - \theta_T \tag{3.78}$$

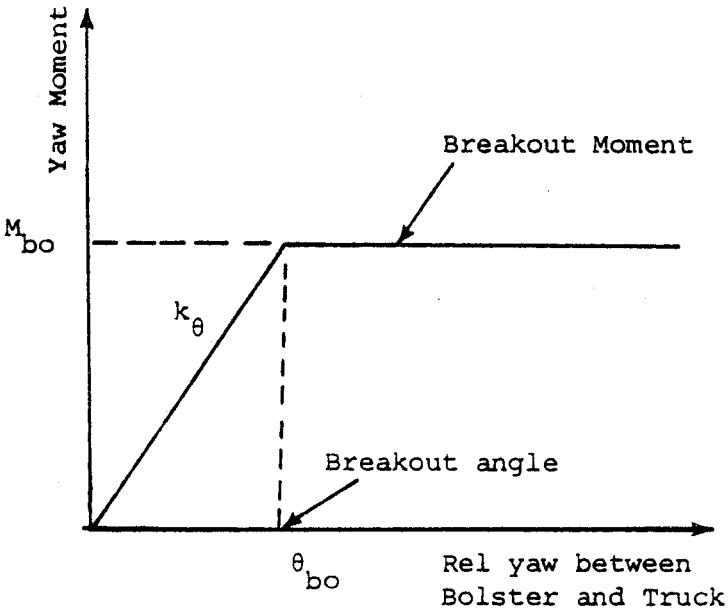

Figure 3-11. Nonlinear Secondary Yaw Characteristics.

where θ_c and θ_T are the respective car and truck yaw angles, and the moment before slip is

$$M_{sec} = k_\theta (\theta_c - \theta_T) \tag{3.79}$$

The relative lateral motion at the air springs, between the carbody and the truck frame is

$$\delta_s = x_c \pm L\theta_c + h_c\phi_c - x_T$$

where $x_c \pm L\,\theta c + h_c\,\phi c$ is the lateral displacement of the point of attachment of the suspension system to the carbody. The lateral suspension force on the truck is then

$$F_{sec} = 2k_{xs} (x_c \pm L\theta_c + h_c\phi_c - x_T) \tag{3.80}$$

where the + refers to the front truck and the - to the rear.

Similarly the vertical force exerted by the car body on one truck is

$$F_{yc_i} = k_{ys}\{y_c \pm d_1(\phi_c - \phi_T)\}$$

$$= W_c/2.$$

The net roll moment exerted by the car on the truck by the two vertical springs located at $\pm d_1$ from the truck centerline is

$$M_z = 2k_{ys}d_1^{\,2}(\phi_c - \phi_T). \tag{3.81}$$

where k_{ys} is the vertical stiffness of each spring and ϕc and ϕT are the carbody and truck roll angles, respectively.

Truck Equations of Motion

The equations of motion for the two wheelsets are as given in Equations (3.70) and (3.71), and these, combined with the truck equations, comprise the complete truck model. Since the truck frame has three degrees of freedom, namely, the truck lateral, x_T, the truck yaw, θ_T, and the truck roll, ϕ_T, the equations of motion of the truck frame can be written for these three motions.

The steady state truck lateral equation is given by summing up all the forces in the lateral direction. Referring to Figure 3-10, then

$$-F_{sx_1} - F_{sx_2} + F_{sec} + F_{lat} = 0 \tag{3.82}$$

where F_{lat} is the net lateral force due to the application of the hydraulic actuators.

Truck Lateral Equation

$$+2k_{xp_1}(x_T+\ell\theta_T-h_T\phi_T-x_1) + 2k_{xp_2}(x_T-\ell\theta_T+h_T\phi_T-x_2) + 2k_{xs}(x_T-x_C - L\theta_c - h_c\phi_c) = F_{lat} + 2k_{xp_1}x_{so_1} + 2k_{xp_2}x_{so_2} \tag{3.83}$$

Summing moments on the truck frame about the $\hat{j}'''$ or yaw axis, gives

$$(F_{sx_2} - F_{sx_1})\ell - M_{sy_1} - M_{sy_2} + M_{sec} + M_{app} = 0 \tag{3.84}$$

or

Truck Yaw Equation

$$-2(k_{xp_2}-k_{xp_1})(x_T+h_T\phi_T)\ell + 2(k_{xp_2}+k_{xp_1})\ell^2\theta_T - 2k_{xp_1}(x_1+x_{so_1})\ell + 2k_{xp_2}(x_2+x_{so_2})\ell + 2(k_{zp_1}+k_{zp_2})d^2\theta_T - 2k_{zp_1}d^2(\theta_1+\theta_{so_1}) - 2k_{zp_2}d^2(\theta_2+\theta_{so_2}) - k_\theta(\theta_c-\theta_T) = M_{app} \tag{3.85}$$

where M_{app} is the net yaw moment due to the hydraulic actuators. Summing moments along the $\hat{k}'''$ or truck roll axis results in

$$-(F_{sx_1}+F_{sx_2})h_T - M_{sz_1} - M_{sz_2} - F_{sec}h'_T + W_c h'_T\phi_T/2 + M_{z_i} + (F_{y_1} + F_{y_2})h_T\phi_T = -M_{roll} \tag{3.86}$$

where M_{roll} is the net roll moment due to the hydraulic actuators.

Truck Roll Equation

$$- 2k_{xp_1}x_{so_1} - 2k_{xp_2}x_{so_2} + [(2k_{xp_1}+2k_{xp_2})h_T - 2k_{xs}h'_T]x_T - 2k_{xp_1}h_T x_1 - 2k_{xp_2}h_T x_2 + (2k_{xp_1}-2k_{xp_2})h_T\ell\theta_T + 2k_{xs}h'_T(x_c+L_c\theta_c) - (2k_{ys}d_1^2 - 2k_{xs}h'_T h_c)\phi_c + [(2k_{xp_1}+2k_{xp_2})h_T^2 + 2k_{ys}d_1^2 + 4k_y d^2 - W_c(h_T+h'_T)/2 - W_T h_T]\phi_T - (2k_y d^2)(x_1\Gamma_1+x_2\Gamma_2)/a = M_{roll} \tag{3.87}$$

Thus, the truck model consists of the lateral and yaw equations for each of the two wheelsets plus the three equations for lateral displacement, yaw angle, and roll angle of the truck frame. Equations (3.70) and (3.71) are the wheelset lateral and yaw equations, and they may be specialized to the front or rear wheelset of a truck by assigning the appropriate subscript to the wheelset variables.

VEHICLE MODEL

The dynamic vehicle model is a set of linear, ordinary, constant-coefficient differential equations consisting of two sets of truck equations and one set of carbody equations. Each set of truck equations has seven degrees of freedom, and the carbody equation set has three degrees of freedom, so the vehicle model has 17 degrees of freedom.

The equations that follow describe a symmetrical carbody on trucks that may have different stiffness and damping characteristics in the front and rear. The primary suspension elements in the front truck are alike for both axles, and likewise they are alike for the rear truck. Each wheelset and rollerset pair may have its own wheel-rail geometry constraint characteristics, but all the pairs must have the same creep-coefficient set. The general form of the model is

$$M\underline{x} + C\underline{\dot{x}} + K\underline{x} = D\underline{F} \tag{3.88}$$

where

M = 17 x 17 mass matrix

C = 17 x 17 damping matrix

K = 17 x 17 stiffness matrix

D = 17 x 2 force distribution matrix

$\underline{x}$ = vector of vehicle displacements

$$\underline{\dot{x}} = \frac{d}{dt}\,\underline{x}$$

$$\underline{x} = \frac{d}{dt}\,\underline{\dot{x}}$$

and

$\underline{F}$ = vector of input forces from actuators

For the study of the SOAC on the RDU we began with an existing 17-DOF passenger car model and modified it by including the roller rig terms discussed earlier in this chapter and the forcing function terms that are specific to the actuator forcing system used during the tests. Since the carbody equations can be obtained in a straightforward manner by application of Newtonian or Lagrangian mechanics, we will not include the details of the derivation here.

Several of the dynamic equations are rather long. Therefore we will present the equations of motion by writing the equations for the individual matrix elements and giving definitions of the displacment and force vectors. The displacements represent linear or rotary perturbation motions with respect to an inertial reference frame that has positive axes as shown in Figure 3-12.

The displacement vector is defined as

x_1 = leading wheelset lateral, leading truck

x_2 = leading wheelset yaw, leading truck

x_3 = trailing wheelset lateral, leading truck

x_4 = trailing wheelset yaw, leading truck

x_5 = truck frame lateral, leading truck

x_6 = truck frame yaw, leading truck

x_7 = truck frame roll, leading truck

x_8 = leading wheelset lateral, trailing truck

x_9 = leading wheelset yaw, trailing truck

x_{10} = trailing wheelset lateral, trailing truck

x_{11} = wheelset yaw, trailing truck

x_{12} = truck frame lateral, trailing truck

x_{13} = truck frame yaw, trailing truck

x_{14} = truck frame roll, trailing truck

x_{15} = carbody lateral

x_{16} = carbody yaw

x_{17} = carbody roll

Figure 3-13 shows schematically a top view of the leading truck frame and shows the actuator force definitions used in the model. The force vector elements are therefore

F_1 = leading actuator force

F_2 = trailing actuator force

Since the actuator forces act directly on the leading truck, the forces will enter only the leading truck lateral and yaw equations of motion. We have assumed in this analysis that the actuators are located vertically at the truck frame center of gravity, so that no forcing terms appear in the truck roll equation. The non-zero elements of the force distribution matrix are therefore

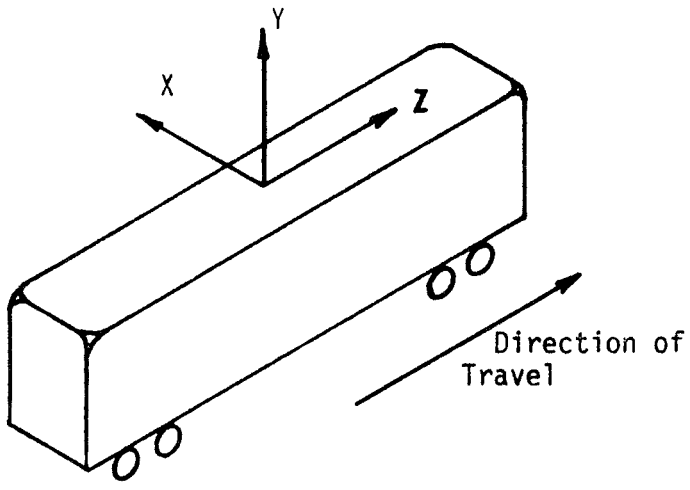

Figure 3-12. Inertial Reference Frame for Vehicle Dynamics Model

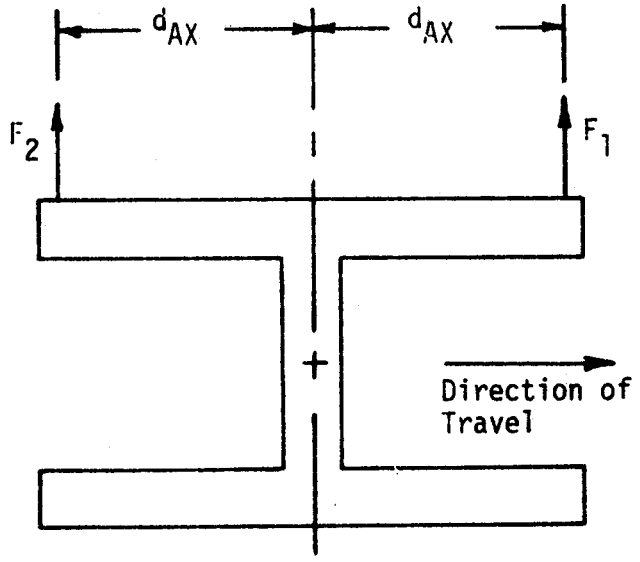

Figure 3-13. Schematic View of Leading Truck Frame Showing Actuator Force Definitions

$D_{5,1} = 1$

$D_{5,2} = 1$

$D_{6,1} = dAX$

$D_{6,2} = -dAX$

where

d_{AX} = half the actuator spacing

The nonzero elements of the system stiffness matrix are

$K_{1,1} = 2k_{xpf} - 2f12\,\Delta 1/(aro) + W(\Delta 1 + \Gamma 1)/a - 2f12(\Delta 1 + \Gamma 1)/(aRo)$

$K_{1,2} = -2f11$

$K_{1,5} = -2k_{xpf}$

$K_{1,6} = -2k_{xpf}\ell$

$K_{1,7} = -2k_{xpf}hT$

$K_{2,1} = 2f33\,\lambda_{w1}a/ro + 2f33\,\lambda_{R1}a/Ro$

$K_{2,2} = 2k_{zpf}d^2 + 2f12 - Wa^2/(r_o + Ro)$

$K_{2,6} = -2k_{zpf}d^2$

$K_{3,3} = 2k_{xpf} - 2f12\,\Delta 2/(aro) + W(\Delta 2 + \Gamma 2)/a - 2f12(\Delta 2 + \Gamma 2)/(aRo)$

$K_{3,4} = -2f11$

$K_{3,5} = -2k_{xpf}$

$K_{3,6} = 2k_{xpf}\ell$

$K_{3,7} = -2k_{xpf}\,hT$

$K_{4,3} = 2f33\,\lambda_{w2}a/ro + 2f33\,\lambda_{R2}a/Ro$

$K_{4,4} = 2k_{zpf}\,d^2 + 2f12 - Wa^2/(r_o + Ro)$

$K_{4,6} = -2k_{zpf}d^2$

$K_{5,1} = -2k_{xpf}$

$K_{5,3} = -2k_{xpf}$

$K_{5,5} = 4k_{xpf} + 2k_{xsf}$

$K_{5,7} = 4k_{xpf}\,hT$

$K_{5,15} = -2k_{xsf}$

$K_{5,16} = -2k_{xsf}\,\ell T$

$K_{5,17} = -2k_{xsf}\,hc$

$K_{6,1} = -2k_{xpf}\ell$

$K_{6,2} = -2k_{zpf}d^2$

$K_{6,3} = 2k_{xpf}\ell$

$K_{6,4} = -2k_{zpf}d^2$

$K_{6,6} = 4k_{xpf}\,\ell^2 + k_{\theta sf} + 4k_{zpf}d^2$

$K_{6,16} = -k_{\theta sf}$

$K_{7,1} = -(2k_{xpf}hT + 2k_{ypf}d^2\,\Gamma_1)/a$

$K_{7,3} = -(2k_{xpf}hT + 2k_{ypf}d^2\,\Gamma_2)/a$

$K_{7,5} = 4k_{xpf}hT - 2k_{xsf}h'T$

$K_{7,7} = 4k_{xpf}\,h^2T + 4k_{ypf}d^2 + 2k_{ysf}d1^2$

$K_{7,15} = 2k_{xsf}\,h'T$

$K_{7,16} = 2k_{xsf}\,h'T\,\ell T$

$K_{7,17} = -2k_{ysf}d1^2 - 2k_{xsf}hThc$

$K_{8,8} = 2k_{xpr} - 2f12\Delta 3/(aro) + W(\Delta 3+\Gamma 3)/a - 2f12(\Delta 3+\Gamma 3)/(aRo)$

$K_{8,9} = -2f11$

$K_{8,12} = -2k_{xpr}$

$K_{8,13} = -2k_{xpr}\ell$

$K_{8,14} = -2k_{xpr}hT$

$K_{9,8} = 2f33\lambda w3a/ro + 2f33\,\lambda R3a/Ro$

$K_{9,9} = 2k_{zprd}^2 + 2f_{12} - Wa^2/(r_o+Ro)$

$K_{9,13} = -2k_{zprd}^2$

$K_{10,10} = 2k_{xpr} - 2f12\Delta 4/(aro) + W(\Delta 4+\Gamma 4)/a - 2f12(\Delta 4+\Gamma 4)/(aRo)$

$K_{10,11} = -2f11$

$K_{10,12} = -2k_{xpr}$

$K_{10,13} = 2k_{xpr}\ell$

$K_{10,14} = -2k_{xpr}hT$

$K_{11,10} = 2f33\lambda w4a/ro + 2f33\,\lambda R4a/Ro$

$K_{11,11} = 2k_{zprd}^2 + 2f_{12} - Wa^2/(r_o + Ro)$

$K_{11,13} = -2k_{zprd}^2$

$K_{12,8} = -2k_{xpr}$

$K_{12,10} = -2k_{xpr}$

$K_{12,12} = 4k_{xpr} + 2k_{sxr}$

$K_{12,14} = 4k_{xpr}hT$

$K_{12,15} = -2k_{xsr}$

$K_{12,16} = -2k_{xsr}\ell T$

$K_{12,1} = -2k_{xsr}hc$

$K_{13,8} = -2k_{xpr}\ell$

$K_{13,9} = -2k_{zprd}^2$

$K_{13,10} = 2k_{xpr}\ell$

$K_{13,11} = -2k_{zprd}^2$

$K_{13,13} = 4k_{xpr}\ell^2 + k_{\theta sr} + 4k_{zprd}^2$

$K_{13,16} = -k_{\theta sr}$

$K_{14,8} = -(2k_{xprh}T + 2k_{yprd}{}^2\Gamma_3)/a$

$K_{14,10} = -(2k_{xprh}T + 2k_{yprd}{}^2\Gamma_4)/a$

$K_{14,12} = 4k_{xprh}T - 2k_{xsrh'}T$

$K_{14,14} = 4k_{xprh}{}^2T + 4k_{yprd}{}^2 + 2k_{ysrdl}{}^2$

$K_{14,15} = 2k_{xsrh'}T$

$K_{14,16} = -2k_{xsrh'}T\ell_T$

$K_{14,17} = -2k_{ysrdl}{}^2 + 2k_{xsrh}Thc$

$K_{15,5} = -2k_{xsf}$

$K_{15,7} = 2k_{xsfh'}T$

$K_{15,12} = -2k_{xsr}$

$K_{15,14} = 2k_{xsrh'}T$

$K_{15,15} = 2(k_{xsf} + k_{xsr})$

$K_{15,16} = 2(k_{xsf} - k_{xsr})\ell_T$

$K_{15,17} = 2(k_{xsf} + k_{xsr})hc$

$K_{16,5} = -2k_{xsf}\ell_T$

$K_{16,6} = -k_{\theta sf}$

$K_{16,7} = 2k_{xsfh'}T\ell_T$

$K_{16,12} = 2k_{xsr}\ell_T$

$K_{16,13} = -k_{\theta sr}$

$K_{16,14} = -2k_{xsrh'}T\ell_T$

$K_{16,15} = 2(k_{xsf} - k_{xsr})\ell_T$

$K_{16,16} = 2(k_{xsf} + k_{xsr})\ell_T{}^2 + k_{\theta sf} + k_{\theta sr}$

$K_{16,17} = 2(k_{xsf} - k_{xsr})hc\ell_T$

$K_{17,5} = -2k_{xsf}hc$

$K_{17,7} = 2k_{xsfh'}Thc - 2k_{ysfdl}{}^2$

$K_{17,12} = -2k_{xsr}\,hc$

$K_{17,14} = 2k_{xsr}\,h'Thc - 2k_{ysrdl}{}^2$

$K_{17,15} = 2(k_{xsf} + k_{xsr})hc$

$K_{17,16} = 2(k_{xsf} - k_{xsr})hc\ell_T$

$K_{17,17} = 2(k_{xsf} + k_{xsr})hc^2 + 2(k_{ysf} + k_{ysr})dl^2 - W_{chc}$

The nonzero elements of the system damping matrix are

$C_{1,1} = 2c_{xpf} + 2f11/V$

$C_{1,2} = -I_{wx}V\Gamma_1/(aro) + 2f12/V$

$C_{1,5} = -2c_{xpf}$

$C_{1,6} = -2c_{xpf}\ell$

$C_{1,7} = -2c_{xpf}\, hT$

$C_{2,1} = I_{wxV}\Gamma_1/(ar_o) - 2f_{12}/V$

$C_{2,2} = 2c_{zpf}d^2 + 2f_{33}a^2/V$

$C_{2,6} = -2c_{zpf}d^2$

$C_{3,3} = 2c_{xpf} + 2f_{11}/V$

$C_{3,4} = -I_{wxV}\Gamma_2/(ar_o) + 2f_{12}/V$

$C_{3,5} = -2c_{xpf}$

$C_{3,6} = 2c_{xpf}\ell$

$C_{3,7} = -2c_{xpf}hT$

$C_{4,3} = I_{wxV}\,\Gamma_2/(ar_o) - 2f_{12}/V$

$C_{4,4} = 2c_{zpf}d^2 + 2f_{33}a^2/V$

$C_{4,6} = -2c_{zpf}d^2$

$C_{5,1} = -2c_{xpf}$

$C_{5,3} = -2c_{xpf}$

$C_{5,5} = 4c_{xpf} + 2c_{xsf}$

$C_{5,7} = 4c_{xpf}\, hT$

$C_{5,15} = -2c_{xsf}$

$C_{5,16} = -2c_{xsf}\ell T$

$C_{5,17} = -2c_{xsf}hc$

$C_{6,1} = -2c_{xpf}\ell$

$C_{6,2} = -2c_{zpf}d^2$

$C_{6,3} = 2c_{xpf}\ell$

$C_{6,4} = -2c_{zpf}d^2$

$C_{6,6} = c_{\theta sf} + 4c_{xpf}\ell^2 + 4c_{zpf}d^2$

$C_{6,16} = -c_{\theta sf}$

$C_{7,1} = -2c_{xpf}hT - 2c_{ypf}d^2\Gamma_1/a$

$C_{7,3} = -2c_{xpf}hT - 2c_{ypf}d^2\Gamma_2/a$

$C_{7,5} = 4c_{xpf}hT - 2c_{xsf}h'T$

$C_{7,7} = 2c_{ysf}d_1^2 + 2c_{xsf}\, h'^2T + 4c_{xpf}\, hT^2 + 4c_{ypf}d^2$

$C_{7,15} = 2c_{xsf}\, h'T$

$C_{7,16} = 2c_{xsf}\, h'T\ell$

$C_{7,17} = -2c_{ysf}d_1^2 + 2c_{xsf}\, h'Thc$

$C_{8,8} = 2c_{xpr} + 2f_{11}/V$

$C_{8,9} = -I_{wxV}\Gamma_3/(ar_o) + 2f_{12}/V$

$C_{8,12} = -2c_{xpr}$

$C_{8,13} = -2c_{xpr}\ell$

$C_{8,14} = -2c_{xprhT}$

$C_{9,8} = I_{wx}V\Gamma_3/(aro) - 2f_{12}/V$

$C_{9,9} = 2c_{zprd}^2 + 2f_{33}a^2/V$

$C_{9,13} = 2c_{zprd}^2$

$C_{10,10} = 2c_{xpr} + 2f_{11}/V$

$C_{10,11} = -I_{wx}V\Gamma_4/(aro) + 2f_{12}/V$

$C_{10,12} = -2c_{xpr}$

$C_{10,13} = 2c_{xpr}\ell$

$C_{10,14} = -2c_{xpr}\ell$

$C_{11,10} = I_{wx}V\Gamma_4/(aro) - 2f_{12}/V$

$C_{11,11} = 2c_{zprd}^2 + 2f_{33}a^2/V$

$C_{11,13} = -2c_{zprd}^2$

$C_{12,8} = -2c_{xpr}$

$C_{12,10} = -2c_{xpr}$

$C_{12,12} = 2c_{xsr} + 4c_{xpr}$

$C_{12,14} = 4c_{xprhT}$

$C_{12,15} = -2c_{xsr}$

$C_{12,16} = 2c_{xsr}\ell_T$

$C_{12,17} = -2c_{xsrhc}$

$C_{13,8} = -2c_{xpr}\ell$

$C_{13,9} = -2c_{zprd}^2$

$C_{13,10} = 2c_{xpr}\ell$

$C_{13,11} = -2c_{zprd}^2$

$C_{13,13} = c_{\theta sr} + 4c_{xpr}\ell^2 + 4c_{zprd}^2$

$C_{13,16} = c_{\theta sr}$

$C_{14,8} = -2c_{xprhT} - 2c_{yprd}^2\Gamma_3/a$

$C_{14,10} = -2c_{xprhT} - 2c_{yprd}^2\Gamma_4/a$

$C_{14,12} = 4c_{xprhT} - 2c_{xsrh'T}$

$C_{14,14} = 2c_{yprd_1}^2 + 2c_{xsrh'T}^2 + 4c_{xprhT}^2 + 4c_{yprd}^2$

$C_{14,15} = 2c_{xsrh'T}$

$C_{14,16} = -2c_{xsrh'T}\ell_T$

$C_{14,17} = -2c_{xprd_1}^2 + 2c_{xsrh'Thc}$

$C_{15,5} = -2c_{xsr}$

$C_{15,7} = 2c_{xsfh'T}$

$C_{15,12} = -2c_{xsr}$

$C_{15,14} = 2c_{xsrh'T}$

$$C_{15,15} = 2c_{xsf} + 2c_{xsr}$$
$$C_{15,16} = 2(c_{xsf} - c_{xsr})\,\ell_T$$
$$C_{15,17} = 2(c_{xsf} + c_{xsr})h_c$$
$$C_{16,5} = -2c_{xsf}\,\ell_T$$
$$C_{16,6} = -c_{\theta sf}$$
$$C_{16,7} = 2c_{xsf}\,\ell_T h'_T$$
$$C_{16,12} = 2c_{xsr}\,\ell_T$$
$$C_{16,13} = -C_{\theta sr}$$
$$C_{16,14} = -2_{xsr}\,\ell_T h'_T$$
$$C_{16,15} = 2(c_{xsf} - c_{xsr})\,\ell_T$$
$$C_{16,16} = 2(c_{xsf} + c_{xsr})\,\ell_T^2 + c_{\theta sf} + c_{\theta sr}$$
$$C_{16,17} = 2(c_{ysf} + c_{ysr})d_1^2 + 2(c_{xsf} - c_{xsr})\,\ell_T h_c$$
$$C_{17,5} = -2c_{xsf}h_c$$
$$C_{17,7} = 2c_{xsf}h_c h'_T - 2c_{ysf}d_1^2$$
$$C_{17,12} = -2_{xsr}h_c$$
$$C_{17,14} = 2c_{xsr}\,h_c h'_T - 2c_{ysr}d_1^2$$
$$C_{17,15} = 2(c_{xsf} + c_{xsr})\,h_c$$
$$C_{17,16} = 2(c_{xsf} - c_{xsr})\,h_c\,\ell_T$$
$$C_{17,17} = 2(c_{xsf} + c_{xsr})\,h_c^2 + (c_{ysf} + c_{ysr})d_1^2$$

The nonzero elements of the system mass matrix are

$$M_{1,1} = m_w$$
$$M_{2,2} = I_{wy}$$
$$M_{3,3} = m_w$$
$$M_{4,4} = I_{wy}$$
$$M_{5,5} = m_f$$
$$M_{6,6} = I_{Ty}$$
$$M_{7,7} = I_{Tz}$$
$$M_{8,8} = m_w$$
$$M_{9,9} = I_{wy}$$
$$M_{10,10} = m_w$$
$$M_{11,11} = I_{wy}$$
$$M_{12,12} = m_f$$
$$M_{13,13} = I_{Ty}$$
$$M_{14,14} = I_{Tz}$$
$$M_{15,15} = m_c$$
$$M_{16,16} = I_{cy}$$
$$M_{17,17} = I_{cz}$$

The vehicle properties represented symbolically above are defined in the following:

m_c = mass of the carbody

m_f = mass of the truck frame

m_w = mass of the wheelset

I_{cy} = yaw moment of inertia of carbody

I_{cz} = roll moment of inertia of carbody

I_{Ty} = yaw moment of inertia of truck frame

I_{Tz} = roll moment of inertia of truck frame

I_{wy} = yaw moment of inertia of wheelset

I_{wx} = moment of inertia of wheelset about axle centerline

k_{xsf} = secondary lateral stiffness per side, front truck

k_{xsr} = secondary lateral stiffness per side, rear truck

k_{ysf} = secondary vertical stiffness per side, front truck

k_{ysr} = secondary vertical stiffness per side, rear truck

$k_{\theta sf}$ = secondary yaw stiffness per truck, front truck

$k_{\theta sr}$ = secondary yaw stiffness per truck, rear truck

k_{xpf} = primary lateral stiffness per wheel, front truck

k_{xpr} = primary lateral stiffness per wheel, rear truck

k_{ypf} = primary vertical stiffness per wheel, front truck

k_{ypr} = primary vertical stiffness per wheel, rear truck

k_{zpf} = primary longitudinal stiffness per wheel, front truck

k_{zpr} = primary longitudinal stiffness per wheel, rear truck

c_{xsf} = secondary lateral damping per side, front truck

c_{xsr} = secondary lateral damping per side, rear truck

c_{ypf} = secondary vertical damping per side, front truck

c_{ypr} = secondary vertical damping per side, rear truck

$c_{\theta sf}$ = secondary yaw damping per truck, front truck

$c_{\theta sr}$ = secondary yaw damping per truck, rear truck

c_{xpf} = primary lateral damping per wheel, front truck

c_{xpr} = primary lateral damping per wheel, rear truck

c_{ypf} = primary vertical damping per wheel, front truck

c_{ypr} = primary vertical damping per wheel, rear truck

c_{zpf} = primary longitudinal damping per wheel, front truck

c_{zpr} = primary longitudinal damping per wheel, rear truck

a = half the rail gauge

d = half the primary suspension separation

d_1 = half the secondary suspension separation

ℓ = half the truck wheelbase

h_T = vertical distance, primary suspension to truck c.g.

h'_T = vertical distance, truck c.g. to truck bolster

h_c = vertical distance, car bolster to car c.g.

ℓ_T = longitudinal distance, car c.g. to truck c.g.

r_o = wheel radius

R_o = roller radius

f_{11} = lateral creep coefficient

f_{12} = spin creep coefficient

f_{33} = longitudinal creep coefficient

λ_{wi} = conicity of ith wheelset (i = 1,2,3,4)

Δ_i = ith contact angle coefficient

Γ_i = ith roll angle coefficient

λ_{Ri} = conicity of ith rollerset

V = vehicle speed

Chapter 4

CREEP FORCE ESTIMATION

INTRODUCTION

The approach taken in this project to estimation of the creep coefficients is to apply various steady forces and/or moments to the rail vehicle, measure the resulting displacements of the vehicle and then find the creep coefficients using the equation,

$$K \underline{x} = \underline{F} \qquad (4\text{-}1)$$

where:

F = vector of applied forces and/or moments

$\underline{x}$ = vector of vehicle component displacements

K = matrix containing creep coefficients, suspension stiffnesses, and vehicle geometry terms.

Several methods are possible for estimating the creep coefficients, f_{ij}, contained in K. For example, Agarwal [4-1] used a search procedure based on the Hooke and Jeeves algorithm [4-2]. This algorithm searched over possible ranges of the creep coefficients to find those that, when substituted in K, minimized the difference or error between the left and right hand sides of Eqn. 2-1. Direct substitution of test data into the linear, algebraic equilibrium equations and inversion of the resulting matrix may also be used to find the system parameters. a third method involves linear regression. each approach is described below.

Equation (4-1) may describe a complete rail vehicle or only part of a rail vehicle, such as wheelset or two wheelsets of one truck. The particular model used determines in part the particular technique that may be used to find the creep coefficients. For example, Agarwal used a model of a complete rail vehicle that entailed 17 degrees of freedom. These were: (a) lateral and yaw displacements of each of four wheelsets, (b) lateral, yaw, and roll displacements of the car body. Two other models have been used to estimate creep coefficients. These are the single wheelset model and the two wheelset model. All these approaches assume that a steady lateral force and/or yaw movement is

applied to the frame of one of the two trucks. Further discussion of these approaches may be found in [14].

MATRIX INVERSION

The single wheelset model consists of the lateral and yaw equations that may be written in the following form:

$$K_{wl}\begin{bmatrix} x \\ \theta \end{bmatrix} = B_l \begin{bmatrix} x_T + h\phi_T \\ \theta_T \end{bmatrix} + \underline{M}_w + \underline{M}_s \qquad (4\text{-}2)$$

In this equation, x and θ are the wheelset lateral and yaw displacements, x_t, θ_T, ϕ_T are the truck frame lateral, yaw, and roll displacements and, h is the vertical distance from the truck frame to the axle centerline. M_w is a constant vector that includes offsets due to the possibility of the left and right wheels and/or the left and right rails not being mirror images of each other. M_s is a constant vector that includes misalignments of the wheelset in the truck frame and misalignments of the rollers of the RDU. The creep coefficients appear in K_{wl} and in M_w and M_s, as seen in the following equations for the elements of these matrices:

$$K_{11} = -2f_{12}\left\{[1+(r_o/R_o)]\Delta + (r_o/R_o)\Gamma\right\}/ar_o + W(\Delta+\Gamma)/a + 2k_{xp}$$

$$K_{12} = -2f_{11}$$

$$K_{21} = 2f_{33}a[\lambda_w + (r_o/R_o)\lambda_R]/r_o$$

$$K_{22} = +2f_{12} - Wa^2/(r_o+R_o) + 2k_{zp}d^2$$

$$B_{11} = 2k_{xp}$$

$$B_{12} = \pm 2k_{xp}\ell$$

$$B_{21} = 0$$

$$B_{22} = 2k_{zp}d^2$$

where,

the + and - signs are used for the front and rear wheelsets, respectively,

x = wheelset lateral displacement (measured positive to the left from the track centerline)

θ = wheelset yaw displacement (measured positive counter-clockwise)

k_{xp} = lateral primary stiffness per axle box

k_{zp} = longitudinal primary stiffness per axle box

W = total applied load on the wheelset

a = semi-rail gage

r_o = mean rolling radius of wheel

R_o = mean rolling radius of rollers

d = semi-separation distance between the longitudinal primary suspension elements

ℓ = semi-wheelbase

λ_w = effective conicity of wheelset

λ_R = effective conicity of rollers

Δ = contact angle coefficient

f_{11} = lateral creep coefficient/wheel

f_{12} = lateral-spin creep coefficient/wheel

f_{33} = longitudinal creep coefficient/wheel

If the wheelset response is sufficiently linear, two different forcing levels can be used. Because Equation (4.2) must be satisfied at each, and M_w and M_s are constant, the difference in the two equations at the two forcing levels may be written as

$$K_{wl}\begin{bmatrix}\Delta x\\ \Delta\theta\end{bmatrix} = B_1\begin{bmatrix}\Delta(x_T + h\phi_T)\\ \Delta\theta_T\end{bmatrix} \tag{4.3}$$

where the Δ notation indicates the difference between the values of the indicated variable at the two forcing levels. Thus, the sometimes difficult task of obtaining M_w and M_s, and the problem of finding the initial conditions for the wheelset and truck displacements may be avoided. In the actual creep coefficient estimation work we neglected the contribution that truck frame roll makes to wheelset lateral displacement, since the contribution is small.

The three creep coefficients (lateral, longitudinal, and lateral-spin) appear explicitly in Equation (4.3). The pure spin creep coefficient appears in the yaw moment equation, but the yaw moment due to spin is negligible compared with that due to the couple formed by the longitudinal creep forces. These two equations are not sufficient to solve for the three creep coefficients. Either of two assumptions could be made to overcome this problem.

The first potential assumption is that

$$f_{11}/f_{11_{th}} = f_{12}/f_{12_{th}} = f_{33}/f_{33_{th}} = n \tag{4.4}$$

where f_{11}, f_{12}, and f_{33} are the estimated values of the lateral, lateral-spin, and longitudinal creep coefficients, respectively. The

creep coefficients with the subscript "th" are the values predicted by Kalker's linear theory [18] for the (assumed) known wheel and rail geometry and loading. With this assumption, either equation of Eqn. (4.3) can be solved for n and the values for f_{11}, f_{12}, and f_{33} can be easily calculated. Most subscale test work [21] suggests that this is a reasonable assumption even in the presence of small amounts of contamination. However, in most cases [21,22,23] the subscale tests were done with newly machined surfaces for which there would be negligible work-hardening. Work-hardening conceivably could cause directionally dependent or anisotropic material properties to develop in the contacting surfaces that might render invalid the assumption of Eqn. (4.4).

A second, less restrictive assumption is that

$$f_{11}/f_{11_{th}} = f12/f12_{th} = n1 \tag{4.5a}$$

and

$$f_{33}/f_{33_{th}} = n2. \tag{4.5b}$$

The rationale here is that the lateral creep force arises due to the effective lateral stiffness of the surface layers of the rail and roller materials. Consequently the lateral and the lateral-spin creep coefficients should be the same fraction of Kalker's theoretical values. The effective longitudinal stiffness of the surfaces may be different from the lateral. When Eqn. (4.5a) and (4.5b) are substituted in Eqn. (4-3) it may be re-written in the form

$$A\begin{bmatrix} n_1 \\ n_2 \end{bmatrix} = \underline{D} \ . \tag{4.6}$$

This equation may be solved explicitly for n_1 and n_2, presuming that the required wheelset and truck displacements are measured and the other vehicle parameters known apriori.

An alternative approach for application of the matrix inversion method is to use a more complex model. The four equations for the two wheelset model may be written as

$$K_{w2}\,\Delta\underline{x} = B_2 \begin{bmatrix} \Delta(\underline{x}_T + h\phi_T) \\ \Delta\theta_T \end{bmatrix} \tag{4.7}$$

where $\underline{x}^T = [\Delta x_1, \Delta\theta_1, \Delta x_2, \Delta\theta_2]^T$ contains the values over two forcing levels for the lateral and yaw displacements of the front and rear wheelsets (subscripts 1 and 2, respectively) of the truck to which forcing is applied. These equations (4.7) are the lateral force and yaw moment equations for each of the two wheelsets.

In general, we would expect that the three creep coefficients for the front wheelset would differ from the three for the rear if there were different surface conditions and/or wheel-rail geometry. Hence, there are six creep coefficients to be estimated from four equations.

Matrix inversion can be used with this model if it is assumed that the three creep coefficients for the front wheelset have the same values as the three for the rear. Thus both front and rear wheelsets are assumed to have identical lateral, lateral-spin and longitudinal creep coefficients. If surface conditions and wheel-rail geometry are closely controlled so that this is reasonable, any three of the four equations of Eqn. (4.7) may be inverted and used to solve for the creep coefficients. It is best if both lateral equations and one yaw equation are used, because the term involving the lateral-spin creep coefficient has a very small effect on the yaw equation. A check on the accuracy of the assumption of identical creep coefficients for the front and rear wheelsets can be made by using the remaining yaw equation to re-estimate the creep coefficients. Close correspondence for the two sets of estimates would lend credibility to the assumption.

LINEAR REGRESSION

Eqn. (4.3) may be rewritten in the following form:

$$\begin{bmatrix}\Delta x\\ \Delta\theta\end{bmatrix} = K_{w_1}^{-1} B_1 \begin{bmatrix}\Delta(x_T + h\phi_T)\\ \Delta\theta_T\end{bmatrix} \tag{4.8}$$

or

$$\begin{bmatrix}\Delta x\\ \Delta\theta\end{bmatrix} = C \begin{bmatrix}\Delta(x_T + h\phi_T)\\ \Delta\theta_T\end{bmatrix}$$

where

$$C = K_{w_1}^{-1} B_1$$

If $[\Delta x, \ \Delta\theta]^T$ and $[\Delta(x_T+h\phi_T), \ \Delta\theta_T]^T$ are measured at several different forcing levels, the elements of C, C_{ij}, may be estimated using linear regression procedures [14,24]. The C_{ij} contain the creep coefficients, the wheel-rail geometric constraint functions, the primary suspension stiffnesses, and the vehicle geometry parameters. Once the four coefficients C_{ij} are found, the three creep coefficients may be found from the equations that define the C_{ij}. This procedure is discussed more fully in [14].

Because there are two equations in Eqn. (4.8) at least three different force levels must be applied to the truck to obtain two sets of measurements of $[\Delta x, \Delta\theta]^T$ and $[\Delta(x_{T+h\phi T}), \Delta\theta_T]^T$. In addition, the wheelset displacement and yaw measurements must be linearly independent or the method fails. The successive sets of measurements obtained in the SOAC creep tests were multiples of one another, ruling out the use of linear regression as a means of estimating the creep coefficients for the actual tests of the SOAC. If two forcers are used in a manner such that the forces are not linearly dependent, this approach should be a powerful method for estimating the creep coefficients of a rail vehicle on the RDU. The accuracy of the regression procedure will improve if a greater number of measurements is obtained.

OPTIMIZATION METHODS

As previously mentioned, Agarwal [19,25] used a complete vehicle model (17 degrees-of-freedom) together with a modified Hooke and Jeeves direct search algorithm to find the creep coefficients from simulated results of steady state forcing tests of a rail vehicle on the RDU. He assumed that the three creep coefficients were the same for all four axles. Additionally, the primary suspension characteristics were assumed equal for all wheelsets as were the secondary suspension characteristics for both trucks.

In the current work, the requirement that the creep coefficients be the same for all wheelsets was relaxed. Instead, the assumptions embodied in Eqn. (4-5) were considered valid, i.e.

$$\begin{aligned} (f_{11}/f_{11_{th}})1 &= (f_{12}/f_{12_{th}})1 = n1 \\ (f_{33}/f_{33_{th}})1 &= n2 \\ (f_{11}/f_{11_{th}})2 &= (f_{12}/f_{12_{th}})2 = n3 \\ (f_{33}/f_{33_{th}})2 &= n4 \end{aligned} \tag{4.9}$$

where the four n_i (i=1 to 4) were considered to be different. The variables n_1 and n_2 refer to the front wheelsets of both the front and rear trucks while n_3 and n_4 refer to the rear wheelsets of the two trucks. Thus, rather than having to find the twelve creep coefficients (one set of three for each of the four axles), the task is reduced to finding the four values of n_i. This would seem to be somewhat restrictive. However, for the forcing proposed, i.e. a lateral force

and a yaw moment on only one truck, the contribution of the unforced truck to the response of the forced truck is very small. Consequently, even if the creep coefficients for the axles of the unforced truck were substantially different from those of the corresponding wheelsets of the forced truck, the estimates for the forced truck would be affected only slightly.

These assumptions are included in the complete vehicle model given in the form,

$$K\Delta\underline{x} = \Delta\underline{F} \tag{4.10}$$

where the Δ notation refers to differences in $\underline{x}$ and $\underline{F}$ at two distinct forcing levels. The vector $\Delta\underline{x}$ has as its elements the displacements in the seventeen degree-of-freedom model previously described. The matrix K contains the creep coefficients as well as the wheel-rail geometry and suspension parameters. The vector $\underline{F}$ has as its elements the forces and moments applied to the vehicle by external means (e.g., hydraulic actuators).

The task of finding the n_i to satisfy Eqns. (4.9) and (4.10) using the values of $\Delta\underline{x}$ and $\Delta\underline{F}$ measured during tests was structured as an optimization problem. The general form of the objective function used was

$$F_o = \sum_{i=1}^{17} w_i \, (x_i - x_{TESTi})^2 \tag{4.11}$$

Where x_i and x_{TESTi} represent components of the calculated and measured displacement vector, respectively. The search procedure used was a modified Hooke and Jeeves algorithm that sought to find the four n_i values of Eqns. (4.9) and (4.10) that minimized F_o. The w_i parameters were weighting factors that are chosen based on whether, for a particular i, the corresponding x_i is a linear or angular displacement. The Hooke and Jeeves search was modified to include the constraint that $0 \leq n_i \leq 1$.

This procedure can also be applied when the vehicle suspension and wheel-rail geometric characteristics are nonlinear provided: (a) the nonlinear characteristics are known, and, (b) initial conditions and vehicle and roller system misalignments are known. This is discussed in more detail in [14].

The optimization approach will work even when fewer than seventeen displacements are measured. In fact, it will work if only the lateral and yaw displacements of the wheelsets of the forced truck are measured. In this case, the summation in Eqn. (4.11) would only be over the four wheelset displacements (lateral and yaw for each wheelset).

SUMMARY

Both matrix inversion and linear regression can be used to estimate the creep coefficients with the single wheelset model. If matrix inversion is used, either of two assumptions must be made: (a) all three creep coefficients are the same fraction of the value calculated from Kalker's theory (n), or (b) the lateral and lateral-spin coefficients are the same fraction of the calculated value (n_1) and the longitudinal coefficient is some other fraction (n_2). Linear regression will, however, give distinct estimates of all three coefficients providing a sufficient number of sets of measurements at different forcing levels are available. A summary of the variables estimated and the required measurements is given in Table 4-1.

As shown in Table 4-1, four measurements are required to estimate n_1 and n_2. These are the wheelset lateral and yaw displacements, and the relative lateral and yaw deflections across the primary suspension elements. To estimate n, only the wheelset lateral, truck yaw, and relative lateral deflection across the primary suspension are required. When linear regression is used with the single wheelset model, the wheelset lateral and yaw and the truck lateral and yaw displacements are required.

The two wheelset model is fairly restrictive as it embodies the assumption that the three creep coefficients are the same for the front and rear wheelsets of the truck. This is not likely to be the case in testing on roller rigs while it may be more likely for tests on actual track. Three of the four equations describing the lateral force and yaw moment balance on the two wheelsets are used to solve for the three creep coefficients.

The use of the complete vehicle model to estimate the creep coefficients from steady state tests of a rail vehicle on a roller rig is quite attractive. The lateral and lateral-spin coefficients are

Table 4-1. Estimated Variables and Required Measurements

MODEL	ESTIMATION PROCEDURE	VARIABLES ESTIMATED	REQUIRED MEASUREMENTS
Single Wheelset	Matrix Inversion	(a) n	(a) x, δ_{LAT}, θ_T
		(b) n_1, n_2	(b) x, θ, δ_{LAT}, δ_{LONG}
	Linear Regression	f_{11}, f_{12}, f_{33}	x, θ, x_T, θ_T
Complete Vehicle	Hooke and Jeeves	(a) $\{n_1,n_2\}_i^T$ $i = 1,2$	(a) x_i, θ_i; $i = 1,2$
		(b) $\{n_1,n_2\}_i^T$ $i = 1,2$ and k_{xp}, k_{zp}	(b) x_i, θ_i; $i = 1,2$ x_T, θ_T

NOTE:

x = wheelset lateral displacement

θ = wheelset yaw displacement

δ_{LAT} = relative lateral displacement across primary suspension

δ_{LONG} = relative longitudinal displacement across primary suspension

θ_T = truck frame yaw displacement

x_T = truck frame lateral displacement

subscript "i" refers to wheelset number

assumed to be the same fraction of the calculated value (say n_1) and the longitudinal coefficient is some other fraction (say n_2). The coefficients are not assumed to be the same for the front and rear wheelsets of the forced truck. To perform this estimation, only measurements of the lateral and yaw displacements of the wheelsets of the forced truck are required. In fact, as shown in [4-3], this technique may also be extended to find the primary suspension stiffnesses if the lateral and yaw displacements of the truck frame that is forced are also measured and used.

Chapter 5

CREEP TEST RESULTS

INTRODUCTION

The creep coefficient estimation procedure used displacement measurements from a number of the 18 LVDT's on the vehicle. Longitudinal displacements for wheelset, primary, and secondary suspension displacements were combined to give the yaw angles used in the procedure.

There were a number of difficulties encountered in recording, analyzing and using the test data. Among these were inadvertent and undocumented switching of data channels, apparent failure of transducers, and unsuccessful measurement of the initial positions of the vehicle components. Unsuccessful measurement of the initial positions precluded using the test data for comparison with nonlinear creep theories and mandated the use of linear models and associated estimation procedures. It was concluded from an extensive study of the data and comparison with simulated test results to use only the following data: (a) the lateral displacements of the two wheelsets of the front truck, (b) the relative lateral deflection across the primary suspension of each wheelset, and, (c) the yaw angle and lateral displacement of the frame of the forced truck. Over most of the range of values of actuator force, these response variables were reasonably linear.

CREEP TEST RESULTS

The estimation procedures used in this work presumed a linear creep force law and zero mean values for all forces and displacements. The first step in our data analysis was to remove unmeasured biases and minimize measurement errors in the data. The range of validity of the linearity assumption was also established. A least squares fit to the displacement-force data was made to eliminate biases and reduce the error. Testing for linearity was more difficult, however, due to the lack of initial condition data for the displacement transducers.

An assessment of the range of linear validity was based on the assumption that the linear creep law holds when motions are confined to the wheel tread region. When the motion goes beyond the tread region, large differences in the tread contact angle occur causing large, restoring, gravitational stiffness forces. This hardening effect is seen in the wheelset lateral displacement vs. force results for Run 8 shown in Figure 5-1. The wheelset response appears to be linear in the ±2000 lb. force range.

Least squares fits were made for all the wheelset lateral and yaw measurements relative to ground, the truck frame lateral and yaw measurements relative to ground, and the relative lateral displacements across the primary suspension elements. Judgments on the range of linear response were made based on the standard deviations of residuals from the mean. Figure 5-2 shows the combinations of data points chosen for the Axle 1 lateral displacement in Run 8. Table 5-1 show the correlation coefficients that describe the accuracy of the fit as well as the standard deviations of the residuals for each combination. For Run 8, combination 4 gives the best estimate of the linearity of the data.

In many cases, there was insufficient data to accurately determine the range of linearity. In Run 12, shown in Figure 5-3, the data points are too widely spaced. Rather arbitrarily, a combination of 3 data points was selected to represent the behavior in this case. This same problem with insufficient data points at lower force values occurred with Runs 10, 21, 22, 25 and 26. This was particularly true of the contaminated surface runs where flange contact was approached with lower applied forces.

Because the misalignments and initial conditions were not measured during the tests, estimation techniques using the difference in measurements were used for obtaining the creep coefficients. The least squared estimates discussed above were then used to regenerate data for each variable at two different forcing levels. For example the mean value of the front wheelset lateral displacement $\bar{x}$, obtained by fitting a straight line to the linear portion of the response, is

$$\bar{x}_1 = a_o + a_1 F \tag{5.1}$$

For a given forcing F_1, $\bar{x}_1$ can be written as

$$\bar{x}_{11} = a_{o_i} + a_{1_i} F_1 \tag{5.2}$$

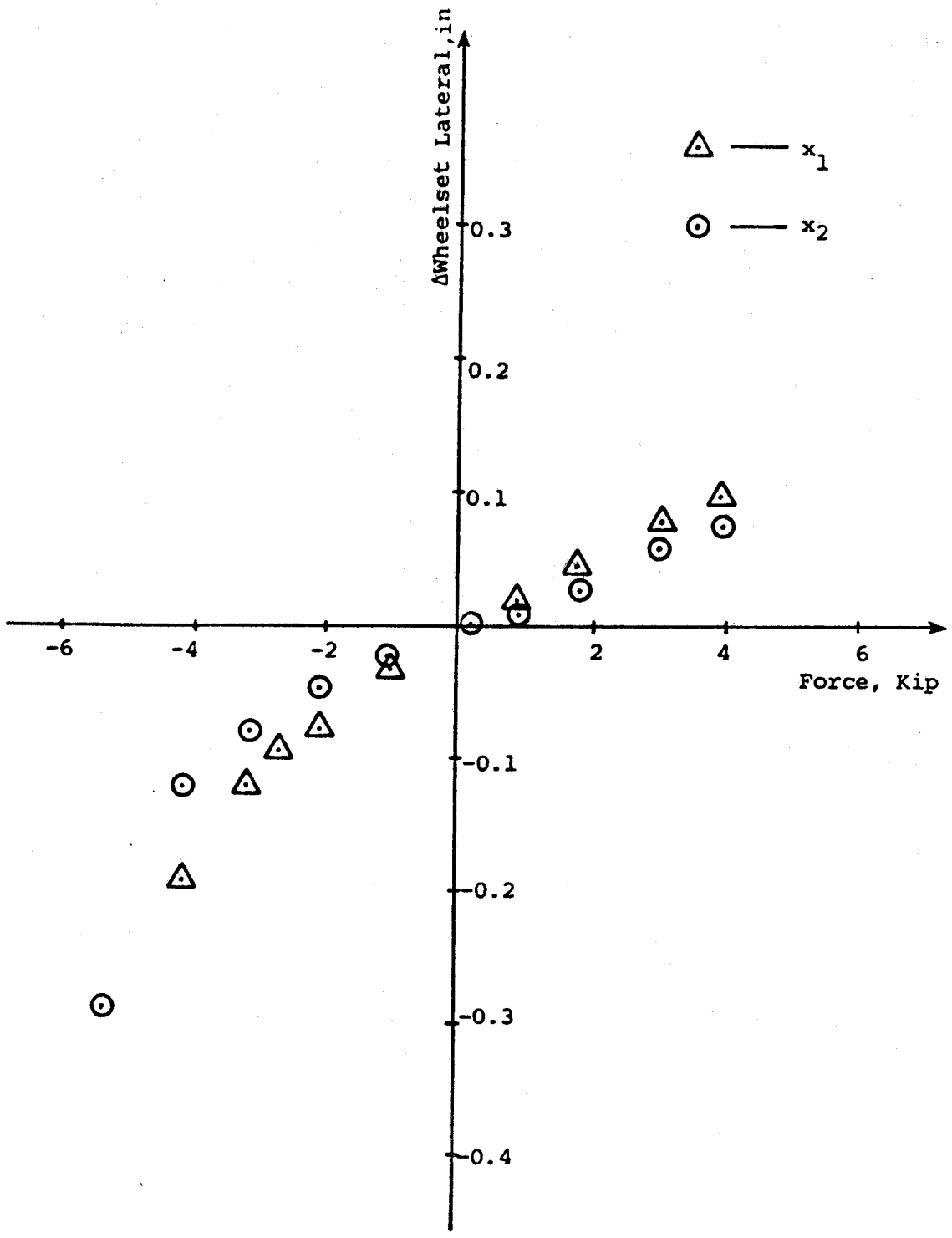

Figure 5-1. Wheelset Lateral Displacement as Function of Actuator Force for Run 8.

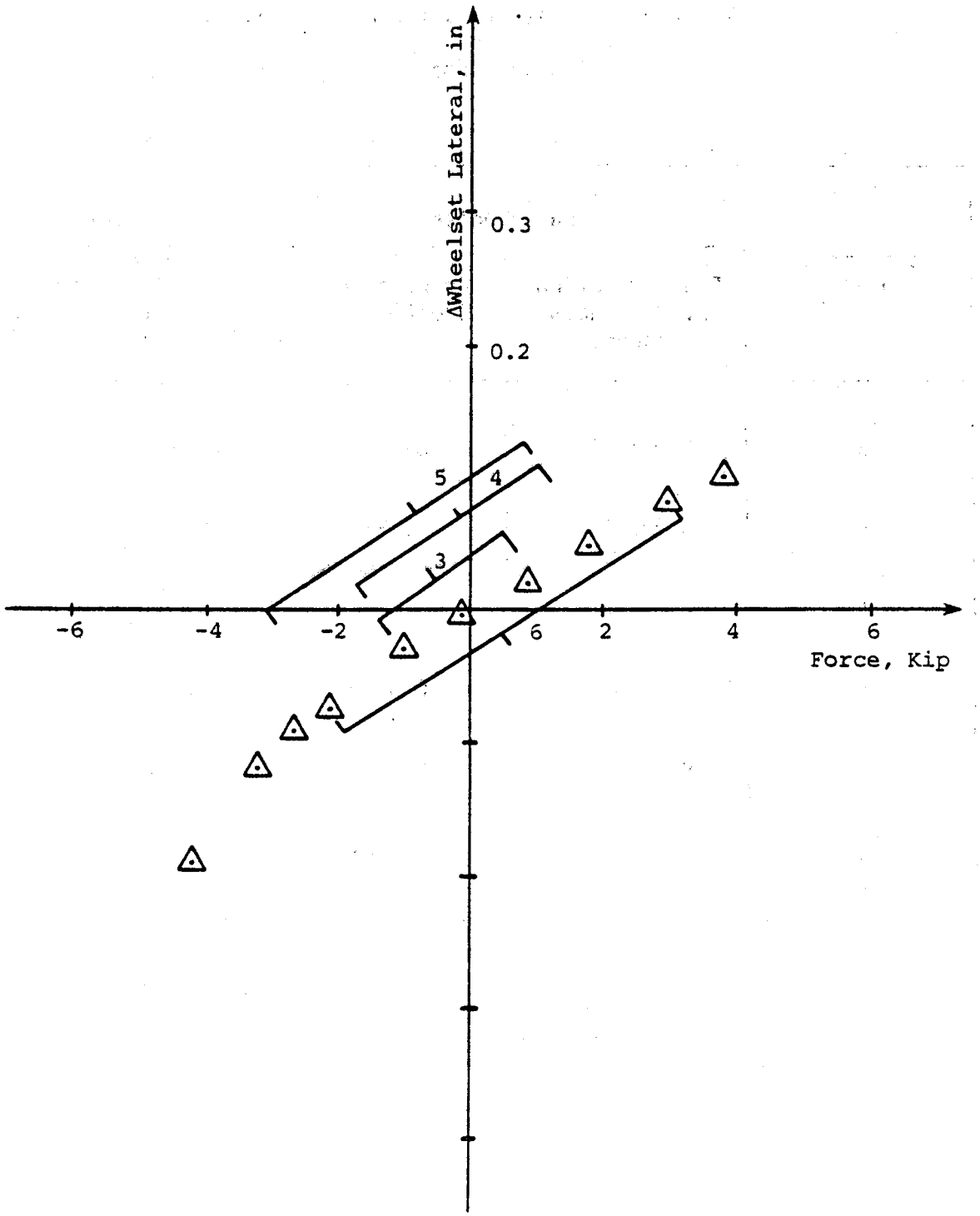

Figure 5-2. Wheelset Lateral Displacement as a Function of Actuator Force for Run 8.

Table 5-1. Statistics for Least Squares Fit to Lateral Displacement Data for Run 8.

Combination Number	Front Wheelset		Rear Wheelset	
	Std. Deviation of Residuals inches	Correlation Coefficient	Std. Deviation of Residuals inches	Correlation Coefficient
3	0.006525	0.9926	0.005055	0.9863
4	0.00611	0.9926	0.00426	0.9987
5	0.00917	0.9905	0.00737	0.9830
6	0.00907	0.9916	0.00657	0.9882
7	0.01641	0.9842	0.01130	0.9804
8	0.01694	0.9849	0.01042	0.9861

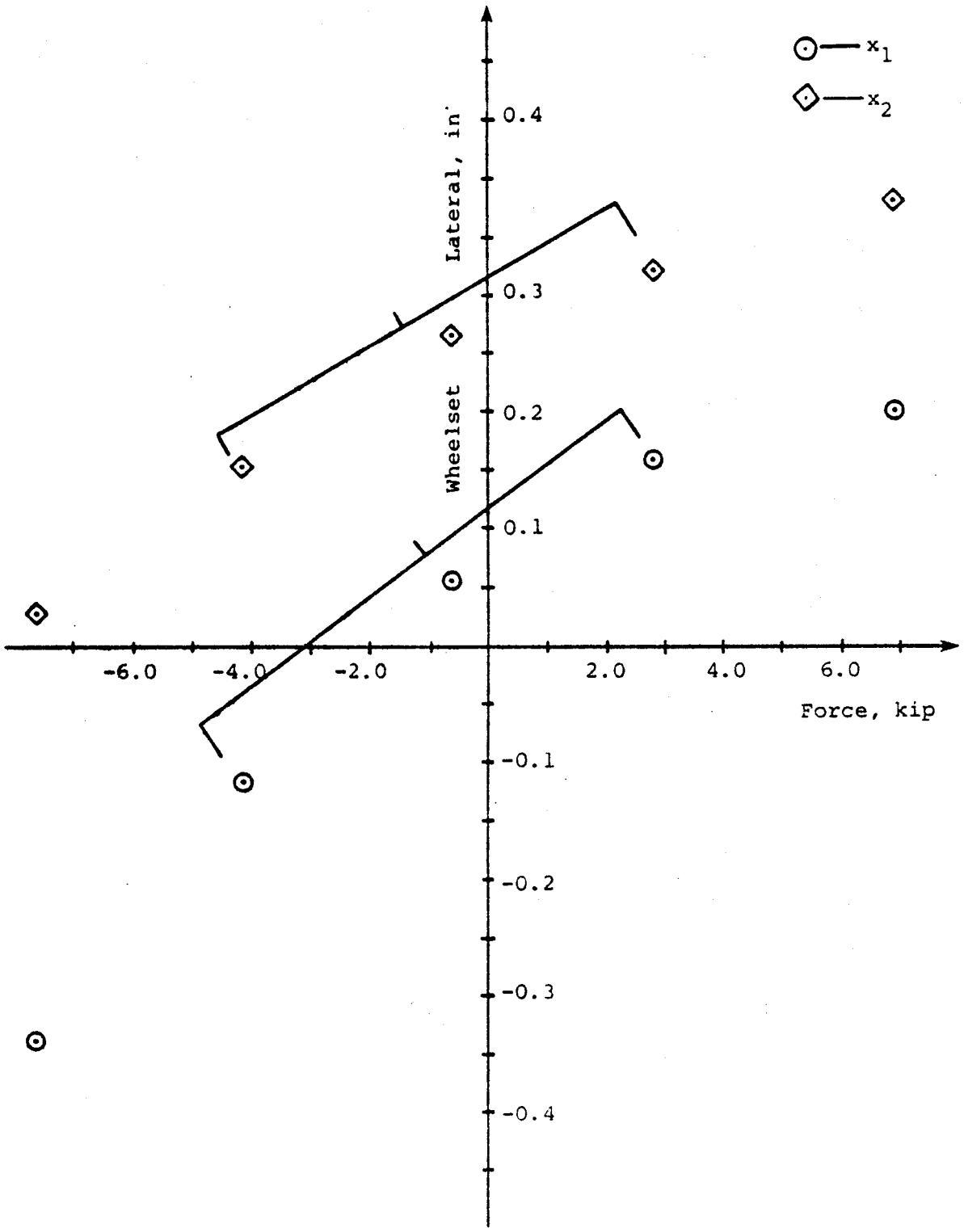

Figure 5-3. Data Point Combinations for Run 12.

and for a forcing level F_2

$$\bar{x}_{12} = a_{o_i} + a1_i F2 \qquad (5.3)$$

Then $\bar{x}_{11}$ and $\bar{x}12$ are two measurements at two different levels of forcing F_1 and F_2 for the variable $\bar{x}_1$. The constant a_{o_i} is the offset of the least squares straight line and $a1_i$ is the slope for the variable $\bar{x}_1$. This procedure was followed for generating the data for all the variables in each run. The two different forcing levels used to generate the data were chosen arbitrarily as + 5kips and - 5kips. This data was then used in the estimation procedures to estimate the creep coefficients.

CREEP COEFFICIENT ESTIMATES

Due to the dubious validity of much of the test data, only the single wheelset model could be used with matrix inversion to estimate the creep coefficients. The measured data for the wheelset lateral displacements, the relative lateral deflections across the primary suspension elements, and the truck yaw angle was used to estimate n (as defined by Eqn. (4.4)) for each wheelset of the forced truck.

As mentioned previously, the lack of initial condition data necessitated the use of linear models and estimation procedures. Accordingly, least squares fits were made to various segments of the data. The differencing procedure described previously was then applied so that the effects of misalignments and initial conditions could be eliminated.

The estimates of the creep coefficients obtained by this approach are listed in Table 5-2. As noted in the table, the values of the longitudinal primary stiffness used in these estimates were half the values obtained by test. These "half test" values were approximately equal to the design value.

It should be noted that while the estimation procedure finds the value of n, this value is based on specific values of the theoretical creep coefficients that are used as input to the estimation procedure. Thus, the procedure actually estimates the values of f_{11}, f_{12}, and f_{33} subject to the assumption that they are all the same fraction of the theoretical values. If different theoretical values are used, a different n would be predicted for the same values of the estimated creep coefficients.

Table 5-2. Estimates of Creep Coefficients

RUN	SPEED MPH	SURFACE	LATERAL, f_{11}, lb/wheel		LATERAL-SPIN, f_{12}, ft-lb/wheel		LONGITUDINAL, f_{33}, lb/wheel	
			FRONT	REAR	FRONT	REAR	FRONT	REAR
8	15	CLEAN	0.847×10^6	1.75×10^6	0.735×10^4	1.52×10^4	1.05×10^6	2.16×10^6
10	60	CLEAN	0.794×10^6	1.59×10^6	0.689×10^4	1.38×10^4	0.98×10^6	1.96×10^6
12	15	CLEAN	0.847×10^6	1.43×10^6	0.735×10^4	1.24×10^4	1.05×10^6	1.76×10^6
21	15	CLEAN	0.688×10^6	1.96×10^6	0.597×10^4	1.70×10^4	0.849×10^6	2.42×10^6
22	60	CLEAN	0.741×10^6	1.48×10^6	0.643×10^4	1.29×10^4	0.915×10^6	1.83×10^6
25	15	SOAP	0.582×10^6	1.19×10^6	0.505×10^4	1.03×10^4	0.719×10^6	1.47×10^6
26	60	SOAP	0.503×10^6	1.14×10^6	0.436×10^4	0.988×10^4	0.621×10^6	1.40×10^6
27	15	GREASE	0.423×10^6	1.01×10^6	0.368×10^4	0.873×10^4	0.523×10^6	1.24×10^6
28	60	GREASE	0.397×10^6	0.980×10^6	0.345×10^4	0.850×10^4	0.490×10^6	1.21×10^6

*NOTE: Longitudinal primary stiffness = 8.70×10^5 lb/ft (per axle box), front;

= 9.70×10^5 lb/ft (per axle box), rear.

The values of the transverse curvatures of the wheels and rollers calculated by the wheel-rail geometry program [11] were different from the design values. The major difference was that the transverse radius of curvature of the top of the roller head was estimated to be much smaller than the 14 inch design value (on the order of 1.0 to 4.0 inch) over the range of contact positions corresponding to wheel tread contact. The estimated values of transverse curvatures for the wheel profiles were much closer to the specified values.

These differences in the specified or design value and the estimated value of the roller head transverse curvature lead to very different values of the theoretical creep coefficients. These theoretical values are given in Table 5-3.

CLEAN SURFACE RESULTS

Using the design values of the creep coefficients from Table 5-3, the values of n for the clean surface runs (8, 10, 12, 21, 22) can be calculated from Table 5-2. These ranged from 0.13 to 0.16 with a mean of 0.148 for the front wheelset and from 0.27 to 0.37 with a mean of 0.31 for the rear wheelset. Using the estimated actual curvatures, the corresponding values were from 0.56 to 0.69 with a mean of 0.64 for the front wheelset and from 1.18 to 1.62 with a mean of 1.36 for the rear wheelset. These values obtained using the specified curvatures are lower than we had anticipated. However,they are reasonably consistent and do not show any significant change due to speed. The values of n obtained using the estimated curvatures are closer to the range we expected. However, the values of n that are greater than 1.0 for the rear wheelset are unrealistic. These discrepancies illustrate the difficulty in obtaining reliable estimates of curvature from measurements of the wheel and rail (or roller) profiles. It is probable that the actual values of n lie in between those cited above.

We were not surprised that the values of n for the front wheelset differed from those for the rear. Neither wheelset-roller combination could be said to be perfectly clean due to the problems noted earlier. The efforts to clean the front and rear wheelsets and rollers of the forced truck differed due to the difference in the accessibility of the wheelsets. Because the friction coefficients were not measured, we can offer no explanation for the large difference in the values of n estimated for the front and rear wheelsets.

Table 5-3. Theoretical Creep Coefficients for Tread Contact

CREEP COEFFICIENTS	DESIGN VALUES(1)	ESTIMATED VALUES (2) FRONT	REAR
Lateral, f_{11}, lb/wheel	5.29×10^6	1.22×10^6	1.21×10^6
Lateral-spin, f_{12}, ft-lb/wheel	4.59×10^4	0.75×10^4	0.750×10^4
Longitudinal, f_{33}, lb/wheel	6.53×10^6	1.28×10^6	1.28×10^4

(1) Based on specified design curvatures.

(2) Based on curvatures estimated for actual profiles using [2-11]. These are average values over the range of tread contact and for left and right wheels.

CONTAMINATED SURFACE RESULTS

The results (Table 5-2) obtained for Runs 25 and 26, at 15 and 60 mph, respectively, with the soap solution are reasonably repeatable and show no apparent effect of speed. For Run 25, the values of n were 0.11 and 0.225 for the front and rear wheelsets while they were 0.095 and 0.215 for Run 26 (using the design values of the creep coefficients from Table 5-3) Using the creep coefficients from Table 5-3 based on the estimated curvatures, the values of n for Run 25 were 0.48 and 0.98 for the front and rear wheelsets while they were 0.41 and 0.94 for Run 26. Thus, the soap-contaminated surfaces yielded substantially lower creep coefficients than the nominally clean surfaces.

Creep coefficients estimated for the runs with greased wheel and rollers are even smaller than those for the soap solution. The values of n for the front and rear wheelsets are 0.08 and 0.19 for Run 27 and 0.075 and 0.185 for Run 28 using the design value creep coefficients. The corresponding values using the estimated curvatures were: (a) 0.35 and 0.83 for the front and rear wheelsets during Run 27; and, (b) 0.33 and 0.81 for the front and rear wheelsets during Run 28. Again, these shown good repeatability and virtually no effect of speed.

SUMMARY

Estimates of creep coefficients were obtained from tests specifically designed for this purpose of the SOAC on the RDU. The only technique that could be used was based on the assumption that the lateral, lateral-spin, and longitudinal coefficients were all the same fraction of the corresponding theoretical values. This approach was necessary because a limited amount of the measured data was considered reliable.

The estimates of the creep coefficients from the test data show large differences between the values for the front and rear wheelsets of the forced truck. The values for the rear wheelset were consistently larger than those for the front wheelset. These differences may be due to one or more of the following possibilities: a) different surface conditions, b) inaccurate measurement of the roller profiles, or c) gain error in the signals for wheelset lateral displacement, lateral deflection across the primary, or the two truck lateral signals.

The runs with nominally clean surfaces show good repeatability in the estimates of the creep coefficients and no apparent influence of speed at the values tested, 15 and 60 mph. The runs with soaped and greased wheel and roller surfaces gave values of the creep coefficients substantially lower than those for the clean surfaces and also showed good repeatability and no discernable influence of speed.

The values of the theoretical creep coefficients were calculated using the method of [26] and (a) the specified design curvatures of the wheel and roller profiles, and (b) the curvatures estimated from actual profile data by the method of [11]. These values differed primarily because the estimated radii of curvature for the roller profiles were considerably smaller than the design values. Because of the similarity in the values of the estimated curvatures for the four rollers, these are probably closer to the true values. However, due to the difficulty in obtaining good estimates of curvatures, the estimated theoretical values for the creep coefficients in Table 5-3 should be regarded as highly uncertain.

Chapter 6

DYNAMIC RESPONSE TEST ANALYSIS AND RESULTS

INTRODUCTION

The SOAC tests on the RDU provide an unusual opportunity to compare experimental and analytical dynamic response results. During vehicle-on-rail tests, roadbed irregularities including alignment, crosslevel and rolling-line offset variations, provide the force inputs to the vehicle. These irregularities are seldom well measured. In some cases estimates of alignment and crosslevel power spectra are known, and virtually nothing is known about rolling line offset variations. In the SOAC tests on the RDU the roller irregularities were sufficiently small that no important vehicle motions resulted from them. Furthermore, the excitation forces provided by hydraulic actuators are well known because the actuator forces and displacements were measured directly. From these tests we have measurements of vehicle response to known excitation forces.

In order to compare experimental and theoretical dynamic response results for the SOAC vehicle, two different test series and two corresponding analyses were conducted. Initial condition tests provided measurements of the SOAC's dynamic response after release from an initial displacement. The corresponding theoretical analysis, an eigenvalue-eigenvector study, provided the natural frequencies and damping ratios of the vehicle model for comparison. The forced-response tests provided measurements from which PSDs and transfer functions were computed. The corresponding theoretical analysis, a forced-response study, provided the same results for the vehicle model.

TTC personnel performed all of the experimental data reduction and supplied us with the results that are included in this chapter.

EIGENVALUE-EIGENVECTOR ANALYSIS

To obtain theoretical results to compare with the initial condition test results we performed an eigenvalue-eigenvector analysis using the complete vehicle model described in Chapter 3. The eigenvalues that

result from this analysis can be thought of as the natural frequencies and damping ratios of the vibration modes of our model. They can also be interpreted equivalently as the locations of the roots of the characteristic equation in the complex plane. The eigenvectors can be interpreted as the system mode shapes, meaning the relative magnitude and phase relationships among the 17 displacement coordinates. To obtain these results we used the unforced or homogeneous part of the vehicle model:

$$M\ddot{\underline{x}} + C\,\dot{\underline{x}} + K\underline{x} = 0 \tag{6.1}$$

We rewrote these equations in first-order form by making the transformation

$$\begin{aligned} y_{2i-1} &= x_i \\ \dot{y}_{2i} &= \dot{x}_i \end{aligned} \tag{6.2}$$

so that the system equations take the form

$$\dot{\underline{y}} = A\,\underline{y} \tag{6.3}$$

where

A = the 34 x 34 system dynamic matrix

The eigenvalue problem is defined by

$$\det(A - \lambda I) = 0 \tag{6.4}$$

where

λ = the set of 34 complex eigenvalues

I = the 34 x 34 identity matrix

The eigenvector problem is defined by

$$A\underline{v} = \lambda\underline{v} \tag{6.5}$$

where

$\underline{v}$ = the complex eigenvector associated with the eigenvalue

The result of this analysis is a set of 34 complex eigenvalues and 34 associated complex eigenvectors. Our computer implementation of this problem uses a Q-R algorithm to find the λ's and $\underline{v}$'s in an iterative manner.

In the dynamic analysis we used the creep coefficient and primary suspension parameters estimated from the creep tests and the measured, estimated, or manufacturer-supplied values for all other vehicle parameters. Our computer implementation of the SOAC model requires that the set of primary suspension stiffnesses be the same for axles 1 and 2. We therefore used average values of the primary stiffnesses at axles 1 and 2 estimated from the creep tests. We used identical sets of parameter values for A-truck and B-truck. Chapter 2 contains tables showing all the parameter values we used. We made no attempt to adjust any of the values of parameters used in the analysis based on the results of the dynamic tests.

Figure 6-1 shows the eigenvalues of the SOAC model for the clean roller condition. We have chosen to display the eigenvalues on a root-locus plot. We computed the eigenvalues at 10-mph speed intervals as shown on the figure. At any particular root location, the distance from the origin to the root equals the natural frequency of a system mode in rad/sec. The cosine of the angle between the real axis and a line from the origin to the root equals the damping ratio. Figure 6-1 actually shows only the lowest nine root-locus branches for the SOAC model. The remaining eight are of higher frequency and of less interest. For reference purposes Figure 6-2 shows the frequency and damping ratio of branches 4 and 5 of Figure 6-1, the kinematic mode of the vehicle.

The root branch labeled 1 is associated with the lower center carbody roll mode of the vehicle. Its location is not a function of speed, and this mode is very weakly coupled to other system modes. This mode has the lowest natural frequency of any of the system modes for speeds above 10 mph. The natural frequency is 0.50 Hz (3.14 rad/sec).

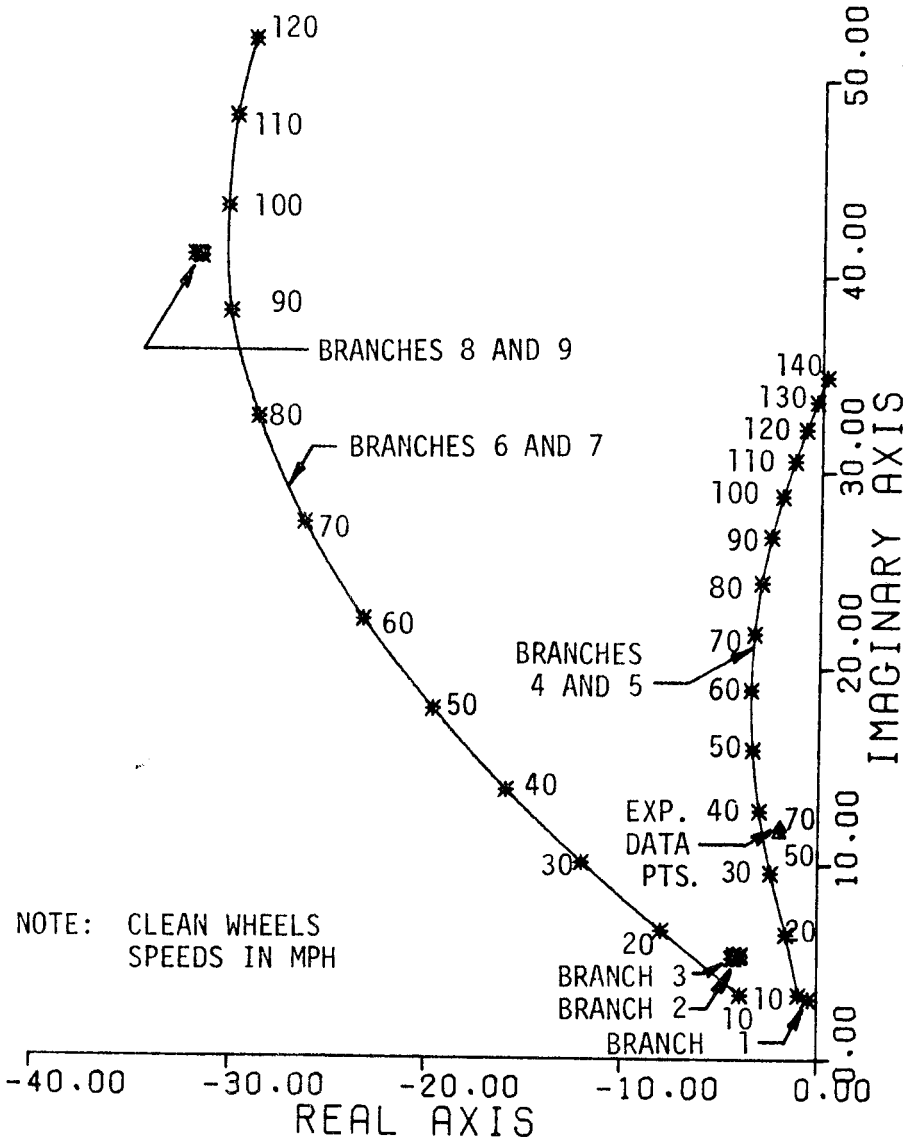

Figure 6-1. SOAC on RDU Model Root Locus

The damping ratio of this mode is 0.14, making it the least-damped system mode for speeds below 80 mph.

Root-locus branch 2 is associated with the carbody yaw mode. In very near proximity is branch 3 which is associated with the carbody lateral mode. Both modes 2 and 3 contain considerable carbody roll as well. Modes 2 and 3 are nearly independent of speed in frequency, damping ratio, and shape. Their natural frequencies are both about 1.0 Hz, and their damping ratios 0.66 and 0.68.

Branches 4 and 5 represent the lowest-frequency kinematic or speed dependent modes of the system. They are so alike in frequency and damping ratio that they overplot one another. These modes become the least damped at speeds above 80 mph, and the system goes unstable as these roots cross into the right half plane at a speed of about 133 mph. Modes 4 and 5 contain large amounts of wheelset and truck lateral and yaw displacements. In fact all system variables except carbody yaw and truck roll have fairly large amplitudes. The natural frequency of these modes is nearly proportional to speed, and the damping ratio decreases from about 0.25 at 10 mph to zero at instability, as shown in Figure 6-2.

Branches 6 and 7 also represent kinematic modes, but with much higher frequency and damping than modes 4 and 5. Like modes 4 and 5 there is considerable lateral and yaw motion of the wheelsets and trucks. Unlike modes 4 and 5 however, there is very little body motion but considerable truck roll.

Branches 8 and 9 represent body modes characterized by large amounts of truck roll. They are very nearly alike in natural frequency and damping ratio.

The kinematic mode pairs, 4-5 and 6-7 move apart and become distinct when we use different parameter sets for the front and rear trucks. It is useful to think of one mode of each pair as being associated with one truck. When the trucks are the same the root loci are the same, or very nearly so. When the trucks are different, the root loci are different. Even when both trucks are the same, the mode shapes are somewhat different however.

The initial condition test series described in Chapter 2 was intended to permit natural frequency and damping-ratio estimates by

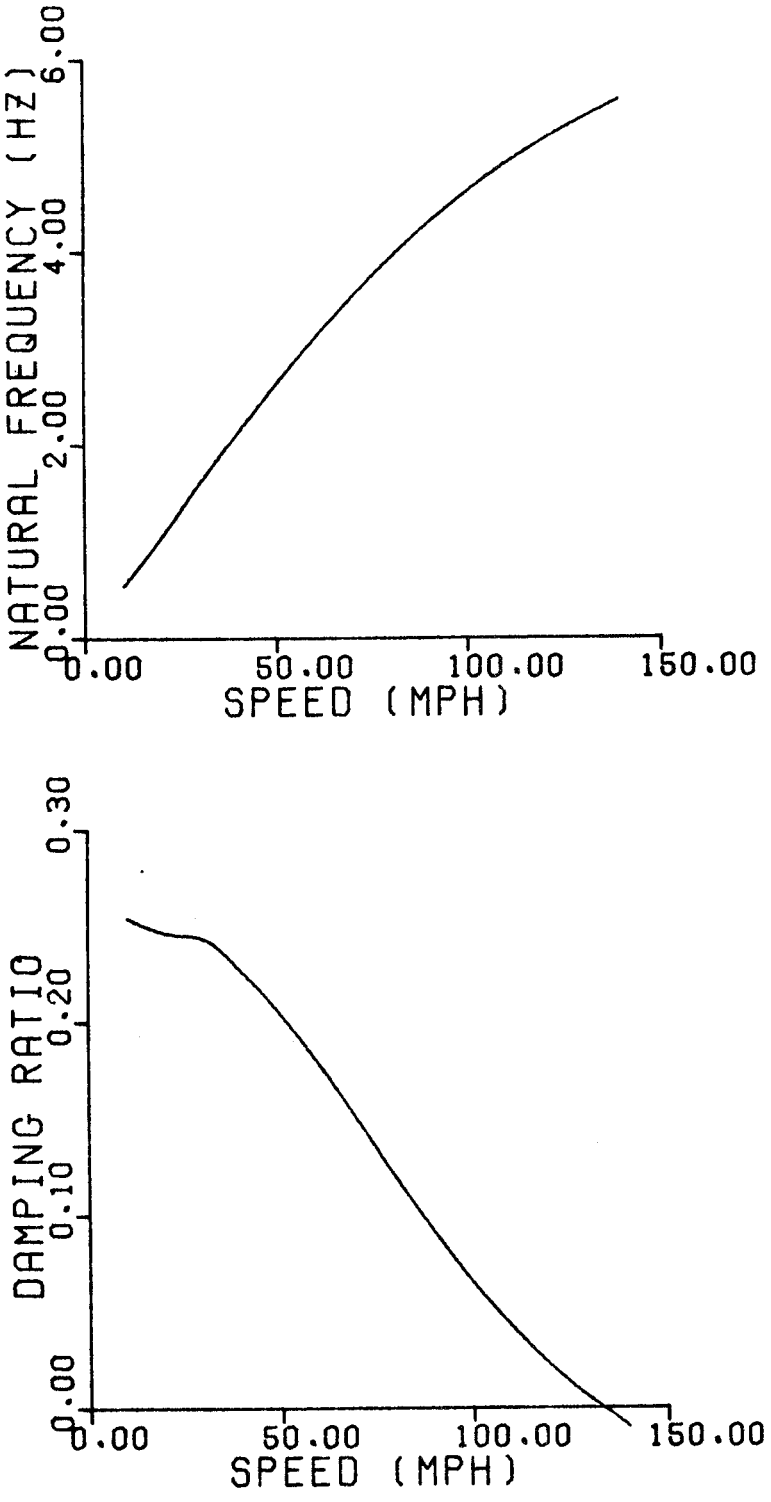

Figure 6-2. Natural Frequency and Damping Ratio of SOAC on RDU Model Kinematic Mode

curvefitting an exponentially decaying sine wave to the time response data. TTC personnel performed two such curvefits on the 50- and 70-mph tests in Run 19. Test data points show in Figure 6-1 as the triangles. The experimental points are not particularly close to the theoretical curves at the test speeds, nor do the data have the proper spacing between them to be kinematic modes, even though the 70-mph point is slightly higher in frequency than the 50-mph point.

We believe that the two experimental points shown in the figure represent a carbody mode of vibration that is unusually high in frequency, about 1.9 Hz, as a result of stiffness added to the SOAC by the roll restraint system employed during the tests.

We conducted a simplified analysis of the carbody yaw mode to investigate the effects of increased stiffness due to the roll restraints. We ignored all other effects in this analysis. For this analysis we used the model shown in Figure 6-3, in which

k_1 = secondary lateral stiffness
k_2 = stiffness of restraint rods
θ = yaw angle
2b = wheelbase
α = angle of restraint rods

The restraint rods are intended to prevent the vehicle from rolling off the RDU during testing. There are two rods on each side of the vehicle. Bellville springs provide the compliance, and the rods can only be tensioned. TTC personnel reported that the restraint systems had 1/2-inch clearance at each rod, so that the carbody had to move enough to close the clearance before any force was transmitted to the carbody.

We assumed that the restraint rods acted on the carbody at the same locations as the secondary suspension, a reasonable but not completely accurate assumption. We assumed that the 1/2-inch clearance at each rod was not present, primarily because we had no convenient way to determine the actual motions of the carbody.

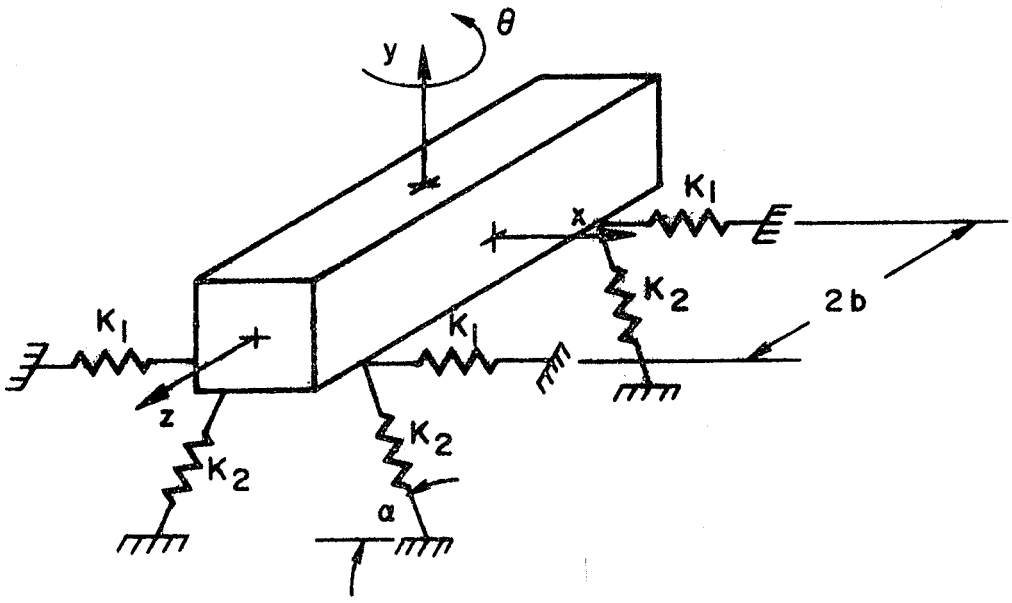

Figure 6-3. Simple Yaw Model of SOAC

The effective spring rate of the restraining rods in the x-direction of Figure 6-3 is

$$k_{2x} = k_2 \cos^2\alpha \tag{6.6}$$

for small displacements. So with

$$\alpha = 76.75^o$$

and

$$k_2 = 440{,}000 \text{ lb/ft}$$

Then

$$k_{2x} = 23{,}100 \text{ lb/ft}$$

The linear homogenous equation of motion for the simplified yaw model is

$$I\ddot{\theta} + 4cb^2\dot{\theta} + (4k_1 + 2k_{2x})b^2\theta = 0 \tag{6.7}$$

From the equation of motion the natural frequency is

$$\omega_n = [(4k_1 + 2k_{2x})b^2/I]^{1/2} \tag{6.8}$$

and the damping ratio is

$$\xi = 2cb/[I(4k_1 + 2k_{2x})]^{1/2} \tag{6.9}$$

where

I = the yaw moment of inertia
c = secondary lateral damping

Values of these parameters used in our theoretical analysis are

$I = 8.58 \times 10^5$ slug ft^2
c = 2366 lb sec/ft
k_1 = 10,500 lb/ft
b = 27 ft

Table 6-1 shows the natural frequencies and damping ratios computed using these values. The simplified yaw model gives results for the

Table 6-1. SOAC Yaw Mode Characteristics

	Natural Frequency (Hz)	Damping Ratio
Yaw mode from 17-DOF model with $K_{2x} = 0$	1.06	0.60
Yaw mode from simplified model with $K_{2x} = 0$	0.95	0.67
Yaw mode from simplified model with $K_{2x} = 23{,}100$ lb/ft	1.38	0.46

unrestrained case that are quite close to the results from the full 17-DOF model The simplified model can therefore be used with some confidence to examine the effects of the restraining system. This examination shows a substantially higher natural frequency and lower damping ratio would exist during use of the restraining system. Clearly for a more accurate analysis we need to modify our 17-DOF model to include the restraining-rod springs. To conduct such an analysis we would need to know the actual amplitudes of carbody motion during the tests, information not now available to us.

We conducted the simplified yaw model analysis in an attempt to explain the unusually high frequency body mode found during the initial condition tests. Although a number of uncertainties still exist, and the measured natural frequency and damping ratios don't match the computed values well, we can still draw some conclusions from this study. We think the least-damped mode of oscillation identified in the initial condition tests is a body mode rather than a kinematic mode. It is possibly, although not certainly, a carbody yaw mode whose unusually high frequency resulted from additional stiffness introduced by the roll

restraining system. We also think, based on this analysis, that the value of secondary lateral damping we have been using is too high. This value was derived from information supplied by the truck manufacturer and has not been verified in the SOAC test series.

An important result of the eigenvalue eigenvector analysis is the high critical speed predicted from the SOAC model. In order to reduce the SOAC's stability, the wheel profiles were modified to approximate a CN-A profile rather than the AAR 1/20 profile. In addition the secondary yaw stiffness was decreased by loosening the nuts on the bolster anchor rods. Despite these two destabilizing modifications, the critical speed predicted by our model is about 133 mph, or 53 mph faster than the highest test speed of 80 mph.

We analyzed a number of different operating conditions by using the appropriate parameter values in our model. Table 6-2 summarizes this work. We interpolated between the 10-mph computation intervals to obtain the critical speeds listed. Three significant figures were used so that critical speed differences between the various cases would be more meaningful. This does not imply, however, that the predictions are correct to the nearest mile per hour. We have included the natural frequency and damping ratio of the least-damped kinematic mode at 80 mph, the highest test speed.

TABLE 6-2. SOAC MODEL STABILITY CHARACTERISTICS

NO.	GUIDEWAY TYPE	GUIDEWAY CONDITION	WHEEL PROFILE	CRITICAL SPEED MPH	DAMPING RATIO AT 80MPH(*)	NATURAL FREQUENCY AT 80 MPH(*) IN HZ
1	RDU	CLEAN	CN-A	133	0.12	4.0
2	RAIL	CLEAN	CN-A	143	0.13	4.0
3	RDU	SOAP	CN-A	162	0.18	3.6
4	RDU	GREASE	CN-A	177	0.21	3.4
5	RDU	CLEAN	AAR 1/20	297	0.33	1.8
6	RAIL	CLEAN	AAR 1/20	308	0.34	1.8

*FREQUENCY AND DAMPING RATIO OF LEAST-DAMPED KINEMATIC MODE

Entry No. 1 in Table 6-2 represents the SOAC as tested on clean rollers. Entry No. 2 represents the vehicle on tangent track. Our model shows about a 10-mph difference in critical speed between RDU and track conditions. The parameters used in the model were the same for No's. 1 and 2 except the roller radius, which was set to a large number for No. 2. The difference in damping ratio of the least-damped kinematic mode at 80 mph between the two cases is small.

Entry No's. 3 and 4 represent the SOAC as tested during the soaped and greased wheel runs. No's. 3 and 4 have the same vehicle parameters as No. 1 except for the smaller values of creep coefficients identified for the soaped and greased wheel creep test runs. A decrease in creep coefficients results in an increase in vehicle stability.

Entry No. 5 shows the substantial difference in stability between the SOAC with CN-A wheels and with AAR 1/20 wheels. For entry No. 5 we used the creep coefficients identified in the creep tests. All wheel conicities were 0.05, and all roller conicities were zero.

Entry No. 6 shows that there is about a 10-mph difference in critical speed between RDU and track conditions for the SOAC with AAR 1/20 profile wheels.

We can draw several conclusions based on the results of the eigenvalue-eigenvector study and the associated initial condition response test.

Despite modifications to the SOAC wheel profiles and secondary yaw stiffnesses the vehicle was in a quite stable configuration, even at the top test speed of 80 mph. Our best current estimate of the critical speed for the clean-wheel tests is 133 mph.

Our 17-DOF SOAC model predicts that the vehicle's dynamics on the RDU are very similar to its dynamics on tangent track in its as-tested configuration. The model also predicts similar RDU and tangent track stability when AAR 1/20 wheelsets are used. With the bolster anchor nuts tight the stability increases, but we have no quantitative comparisons to report on this effect.

During the SOAC tests the least-damped mode was a stationary body mode. We think the frequency of this mode, about 1.9 Hz, was higher than normal for a body mode because of increased stiffness introduced by the restraining system.

FORCED RESPONSE ANALYSIS

For the forced response analysis we started with the vehicle equations of motion in the general form given in Chapter 3.

$$M\ddot{\underline{x}} + C\dot{\underline{x}} + K\underline{x} = D\underline{F} \tag{6.10}$$

Since the forced response tests were conducted using a sine wave sweep of the actuator, we are interested in solutions to the general model equations in the frequency domain. If we Fourier transform the model equations by letting

$$j\omega X = \dot{x} \tag{6.11}$$

where

$j = \sqrt{-1}$

ω = the frequency of interest

the transformed model equations are

$$[(K - \omega 2M) + j\omega C]\underline{X} = D\underline{F} \tag{6.12}$$

The solution of the above equation is

$$\underline{X} = [(K - \omega 2M) + j\omega C]-1D\underline{F} \tag{6.13}$$

Or we can write

$$\underline{X} = H\underline{F} \tag{6.14}$$

where

$$H = [(K - \omega 2M) + j\omega C]-1D \tag{6.15}$$

H is the 17 x 2 transfer function matrix that relates all the system variables to the input forces. Any element of H, in general h_{ij}, gives the response of x_i to the force F_j. Our computer implementation performs the complex matrix inversion and multiplication to yield the h_{ij} elements. The complex h_{ij} are then rewritten in terms of magnitude and phase angle.

TTC personnel computed a number of transfer functions using the DRS program as discussed in Chapter 2 of this report. Some of the transfer functions were output displacements, x_i, in terms of input forces, F_j. Other transfer functions were output displacements in terms of input displacements, x_j. In order to compare measurements and predictions we need to compute the displacement input transfer functions in addition to the force input transfer functions discussed above. To obtain these transfer functions, we duplicated the DRS computation process in our computer model.

DRS computes transfer functions using

$$g_{ij} = S_{ji}/S_{jj} \qquad (6.16)$$

where

g_{ij} = transfer function between ith output and jth input

S_{ji} = cross spectral density between jth and ith variables

S_{jj} = power spectral density of jth variable

The spectral densities are computed from

$$S_{ji} = X^*_j X_i \qquad (6.17)$$

$$S_{jj} = X^*_j X_j \qquad (6.18)$$

where

X_i = Fourier transform of the ith variable

X^*_i = complex conjugate of X_i

In general, the X_i are

$$X_i = h_{i1} F1 + h_{i2} F2 \qquad (6.19)$$

By combining Equations 6.16, 6.17 6.18, and 6.19 and cancelling the complex conjugate terms we obtain

$$g_{ij} = (h_{i1} F1 + h_{i2} F2)/(h_{j1} F1 + h_{j2} F2) \qquad (6.20)$$

During the forced response testing, the axle 1 actuator provided the force input and the trailing actuator acted as a damper since it remained attached to the truck frame but not activated. PSDs of the actuator forces showed that F_1 was about an order of magnitude larger than F_2. Time histories showed that the forces were very nearly 180 degrees out of phase. As an approximation we let

$$F_1 = -10\ F_2$$

We then used the g_{ij} transfer function, Equation 6.20, to compute the displacement input transfer functions for the comparisons with experimental transfer functions.

Our computer implementation of the forced-response model has the same set of assumptions and limitations as the free-response model with the additional limitation that the wheelset/rollerset geometric constraint parameters must be the same for all four axles. We therefore averaged the axle 1 and axle 2 parameters and used the average values for all axles. Otherwise, the same parameter sets were used in both analyses.

To compare the theoretical and experimental forced response of the SOAC we used either displacement input or force input transfer functions. We have plotted the predicted transfer functions directly on the experimental transfer function plots furnished by TTC. Transfer functions permit a more convenient comparison than PSDs because of the normalization that occurs when the transfer functions are computed. To compare PSDs we would have to shape the input force frequency spectrum to match the one used in the tests, a process that is not required in order to compare transfer functions.

We have focused on five measured displacement variables for our comparison: axle 1 primary longitudinal, axle 1 primary lateral, carbody lateral with respect to A-truck bolster, carbody vertical with respect to A-truck bolster, and axle 1 actuator.

We have focused on four test runs for the comparisons: Runs 14 and 17, the 40- and 70-mph clean-roller small-amplitude forced runs, and Runs 30 and 32 the 40- and 70-mph greased-roller small-amplitude forced runs. We selected these runs because we thought our model would most nearly represent the SOAC vehicle on these runs. Vehicle nonlinearities, whose influence is greater at larger displacements are more important in the large-amplitude forced runs than in the small-amplitude runs.

When a vehicle is tested on rail, it is usual to find discrete signals at several locations in the frequency spectrum. In rail testing the most prominant signals usually occur at the rail joint excitation frequency and at the wheel rotation frequency. During roller rig testing it is possible to obtain discrete signals at frequencies corresponding to the wheel rotation, the roller rotation, harmonics of the wheel and roller rotations, and sums and differences of any of the above. Table 6-3 shows some of these possible frequencies.

Figure 6-4 shows the carbody vertical and lateral displacement with respect to the A-truck bolster transfer functions. These transfer functions are referred to the actuator 1 force as an input. We have shown the roller rig frequencies on the vertical displacement transfer function. Since these same frequencies occur often, we will not identify them on subsequent plots. We do not know the source of the large 10-Hz peaks.

TABLE 6-3. FREQUENCIES OF WHEEL AND ROLLER EXCITATION

	40 MPH	70 MPH
fw	7.98 HZ	13.97 HZ
fr	3.74 HZ	6.54 HZ
2 fr	7.48 HZ	13.08 HZ
fw - fr	4.24 HZ	7.43 HZ
fw + fr	11.72 HZ	20.51 HZ

fw = wheel rotation frequency

fr = roller rotation frequency

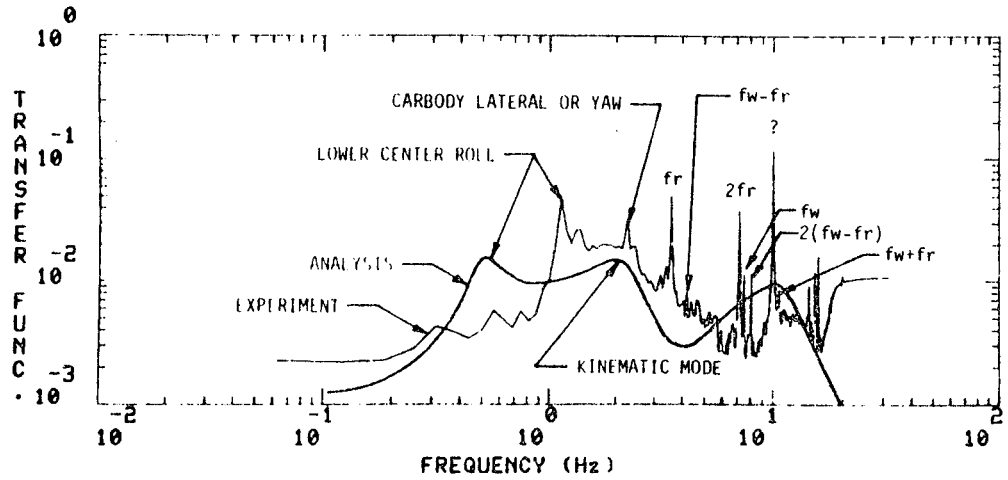

RUN 14
40 MPH
CLEAN
UNITS: IN/KIP
VERTICAL

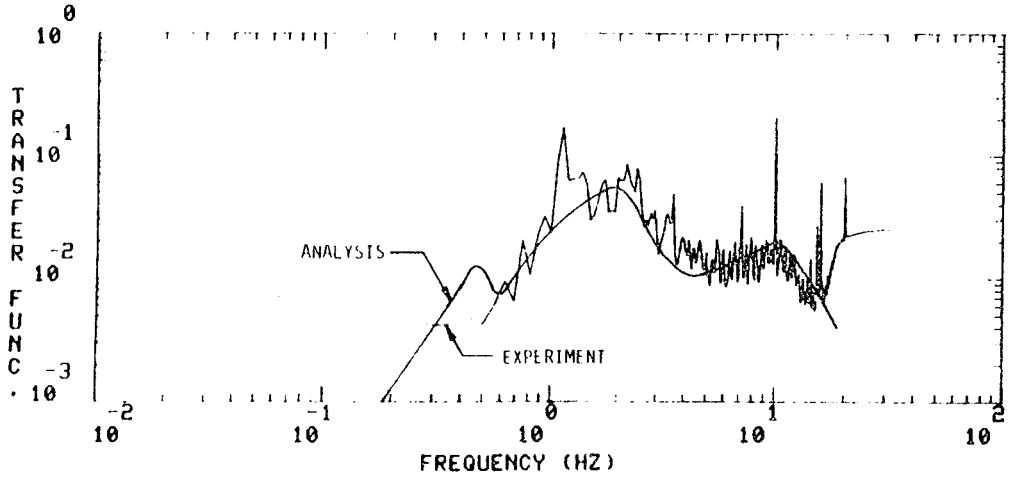

RUN 14
40 MPH
CLEAN
UNITS: IN/KIP
LATERAL

Figure 6-4. Transfer Functions of Carbody to Bolster Lateral and Vertical Displacement Referred to Actuator 1 Force.

Our model predicts a carbody lower center roll mode at about 0.5 Hz. The peak in the theoretical transfer function due to this mode shows prominantly in both Figure 6-4 transfer functions. We think the peak in the experimental transfer functions at about 1.1 Hz is actually the carbody lower center roll, its frequency increased by stiffening from the roll restrain system. We think the peak in the vertical transfer function at about 2.2 Hz is the same carbody yaw or lateral mode that was identified at 1.9 Hz in the initial condition test. These two frequencies appear on many of the transfer function and PSD plots at both 40 and 70 mph for the clean wheel runs. Another pair located at about 1.1 and either 1.6 Hz or 2.0 Hz appears on the plots for the greased wheel runs.

The kinematic mode frequency of 2.1 Hz predicted by our model shows in the Figure 6-4 theoretical plots as a very broad-band resonance. The shapes of the experimental curves follow the theoretical curves very well in the frequency range near 2.1 Hz. The overall levels are about right for both transfer functions.

Figure 6-5 shows the transfer functions of axle 1 absolute longitudinal to actuator 1 displacement for Runs 14, 17, 30 and 32. The overall levels are nearly correct for the 70-mph runs, and the high frequency levels are about right for the 40-mph runs. The analytical predictions are too high for the 40-mph runs at low frequency. Our model shows very little sensitivity to either speed or creep coefficient changes at low frequencies, while the experimental results show very little sensitivity to creep coefficients but a moderate sensitivity to speed at low frequencies. The Run 32 data is of questionable validity above about 7 Hz. Large discontinuities show in the Run 32 PSDs and transfer functions for most variables. The sawtooth pattern that appears in the Run 14 data of Figure 6-5 beginning at about 0.5 Hz and extending to higher frequencies is present in much of the experimental data from the SOAC tests. We do not know the source of this pattern, but we think it is not associated with the dynamic response of the vehicle. Further investigation is required to resolve this issue.

Figure 6-6 shows the transfer functions of axle 1 primary lateral to actuator 1 displacement for Runs 14, 17, 30 and 32. The low frequency levels show the best agreement for Run 32. These levels show

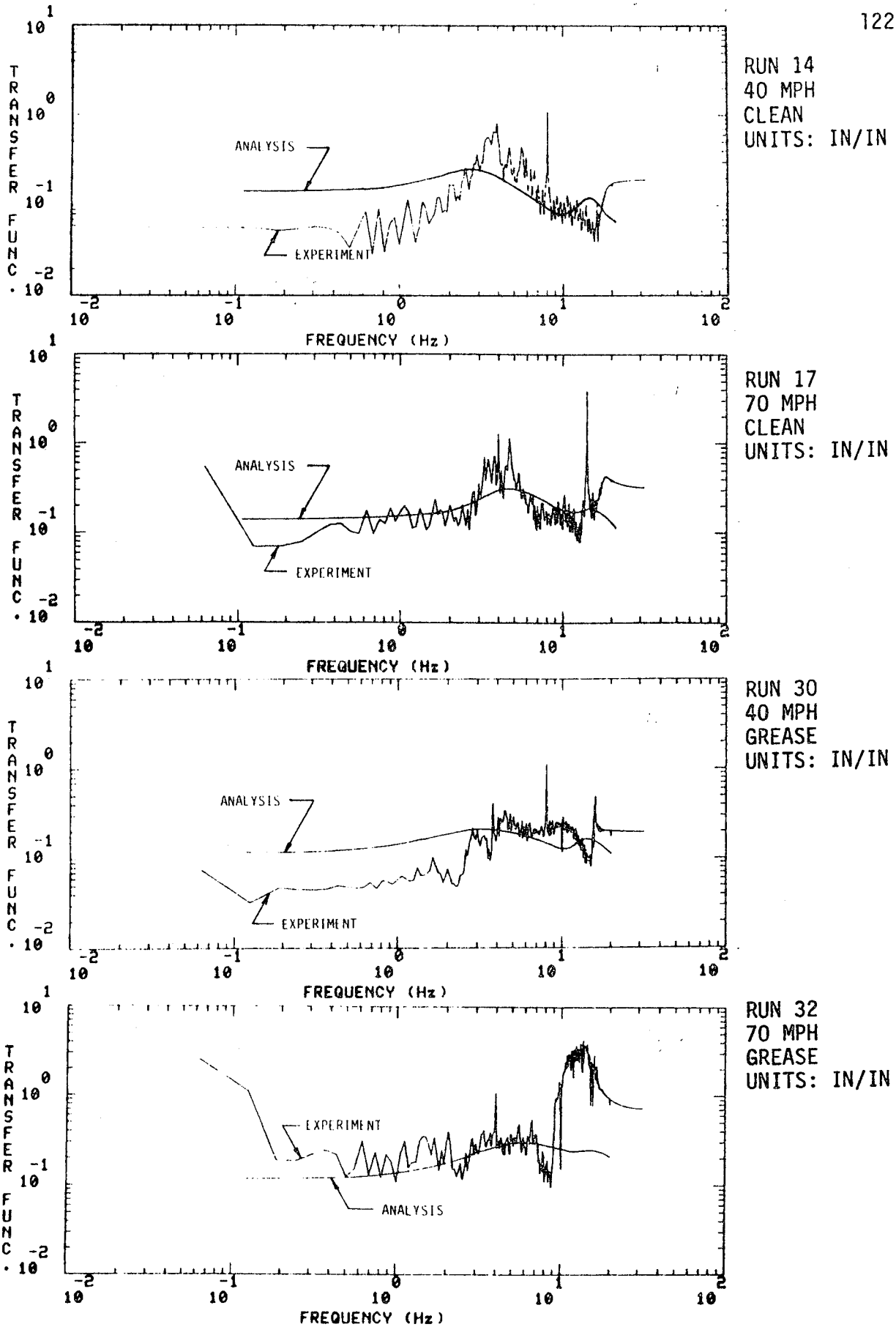

Figure 6-5. Transfer Functions of Axle 1 Longitudinal Displacement to Actuator 1 Displacement.

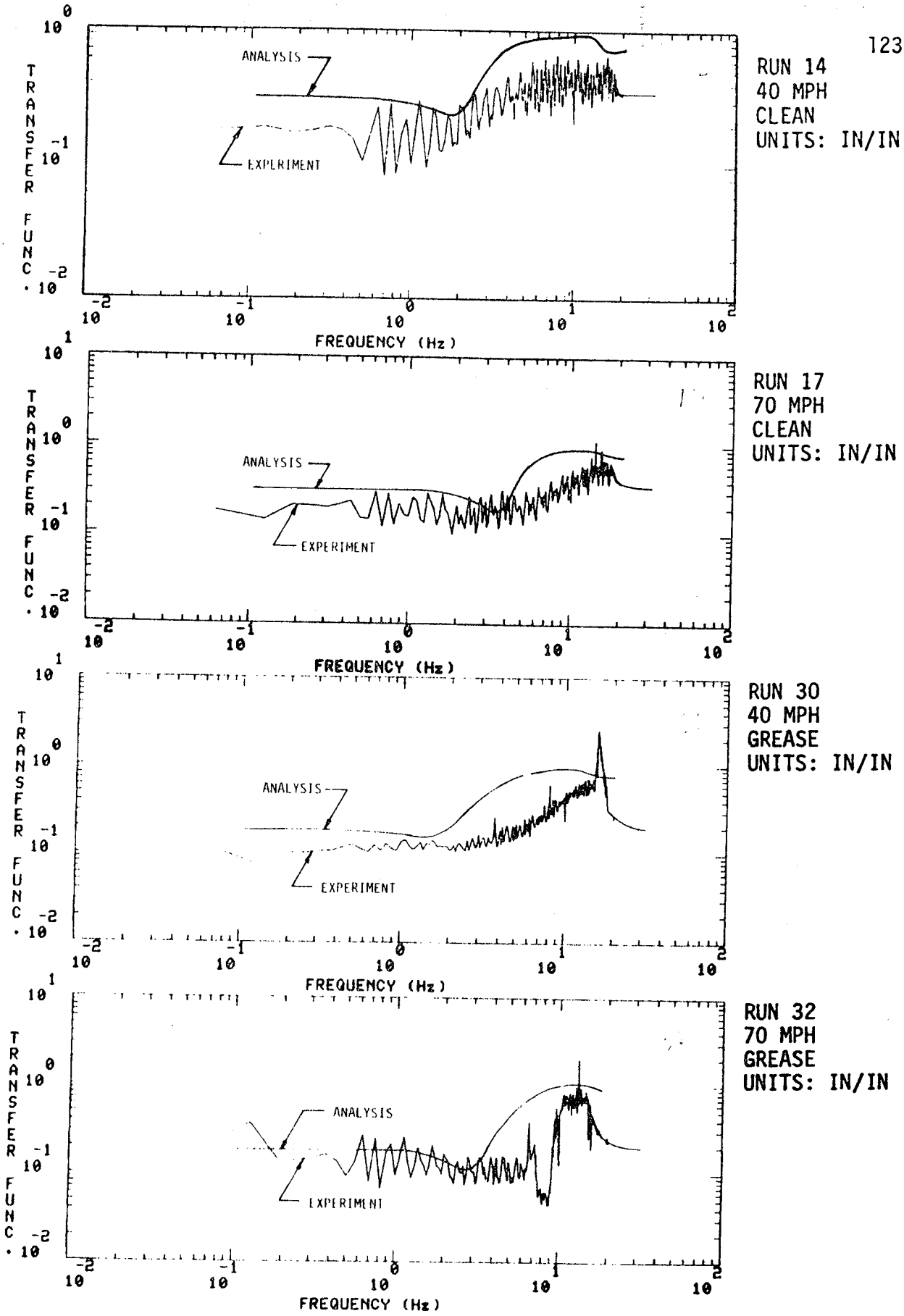

Figure 6-6. Transfer Functions of Axle 1 Primary Lateral Displacement to Actuator 1 Displacement.

fair agreement for Runs 30 and 17, and the worst agreement for Run 14 on which the model prediction is about 1.7 times the experimental value. Our model shows no sensitivity to speed at low frequencies and a moderate sensitivity to creep coefficients. The experimental results show the same trend in creep-coefficient sensitivity as the model, and a small speed sensitivity. For each run, our model shows a moderate dip in transfer function magnitude at the kinematic mode natural frequency followed by an increase in amplitude at higher frequencies. The experimental transfer functions also increase with frequency, but our model fails to predict the shape correctly. The descrepancies in shape may be an indication that the kinematic mode damping is too low in our model predictions.

Figure 6-7 shows the transfer functions of carbody to A-truck bolster lateral displacement referred to the actuator 1 displacement for Runs 14, 17, 30 and 32. These transfer functions exhibit the best overall agreement between theory and experiment of any set that we compared. The agreement would be even better if we adjusted the parameters of our model so that the carbody lower center roll mode had a frequency of 1.1 Hz rather than 0.5 Hz. At the lowest frequencies, below 0.3 Hz, the agreement is not good. The magnitude of these transfer functions should approach a constant value at sufficiently low frequencies, but neither our computations nor the tests were run at a low enough frequency to illustrate this behavior.

Figure 6-8 shows the transfer functions of carbody to A-truck bolster vertical displacement referred to the actuator 1 displacement for Runs 14, 17, 30 and 32. Our model predicts that the low frequency portion of these transfer functions is dominated by the response of the carbody lower center roll mode. Since the lowest-frequency stationary mode in the experimental transfer functions, which we believe to be the lower center roll mode, occurs at about 1.1 Hz, the low frequency agreement is poor for these runs. The trend exhibited in the experimental data showing increased amplitude at very low frequencies must be suspect. It is difficult to conceive of a reasonable model that would exhibit this trend.

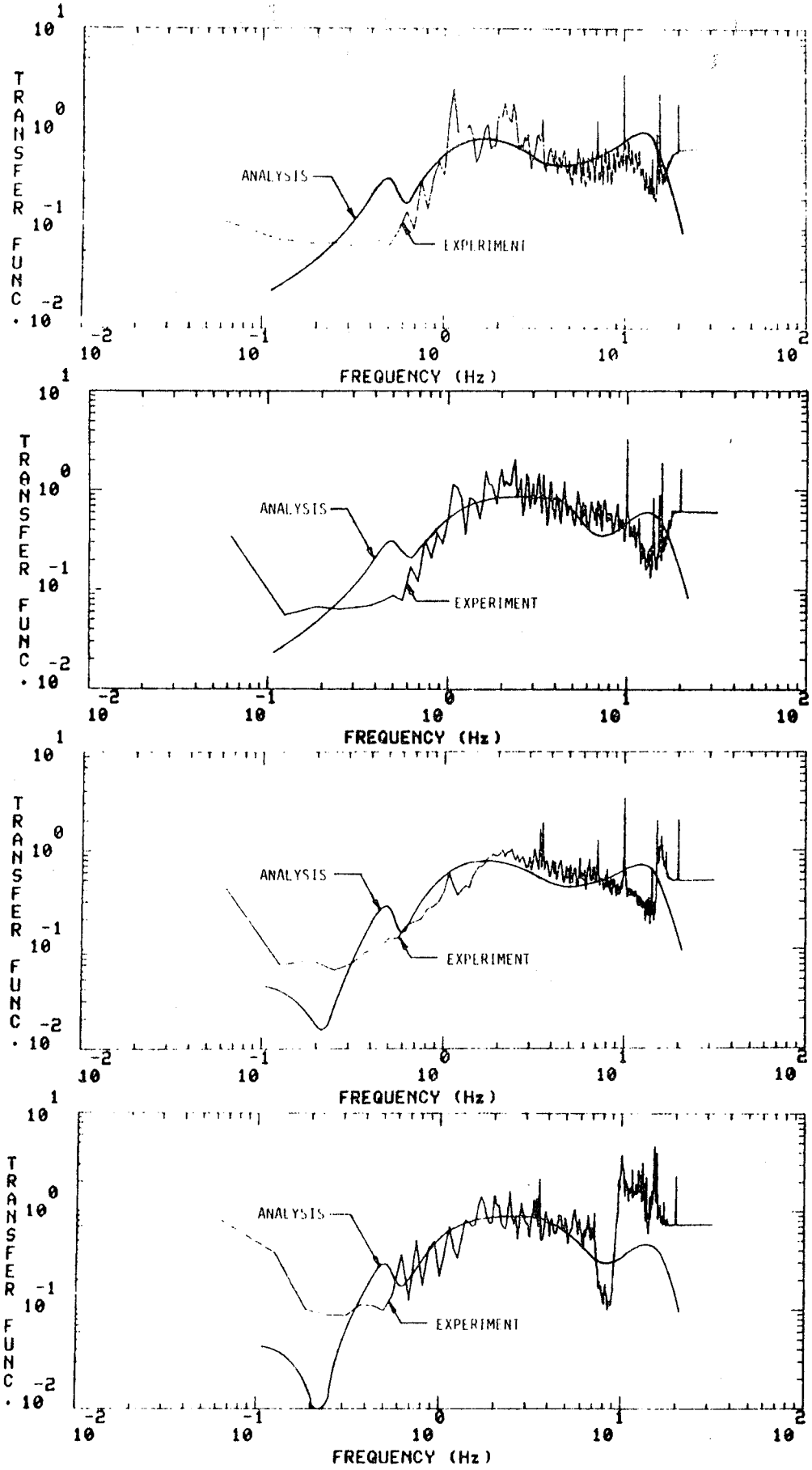

Figure 6-7. Transfer Functions of Carbody to Truck-A Bolster Lateral Displacement Referred to Actuator 1 Displacement.

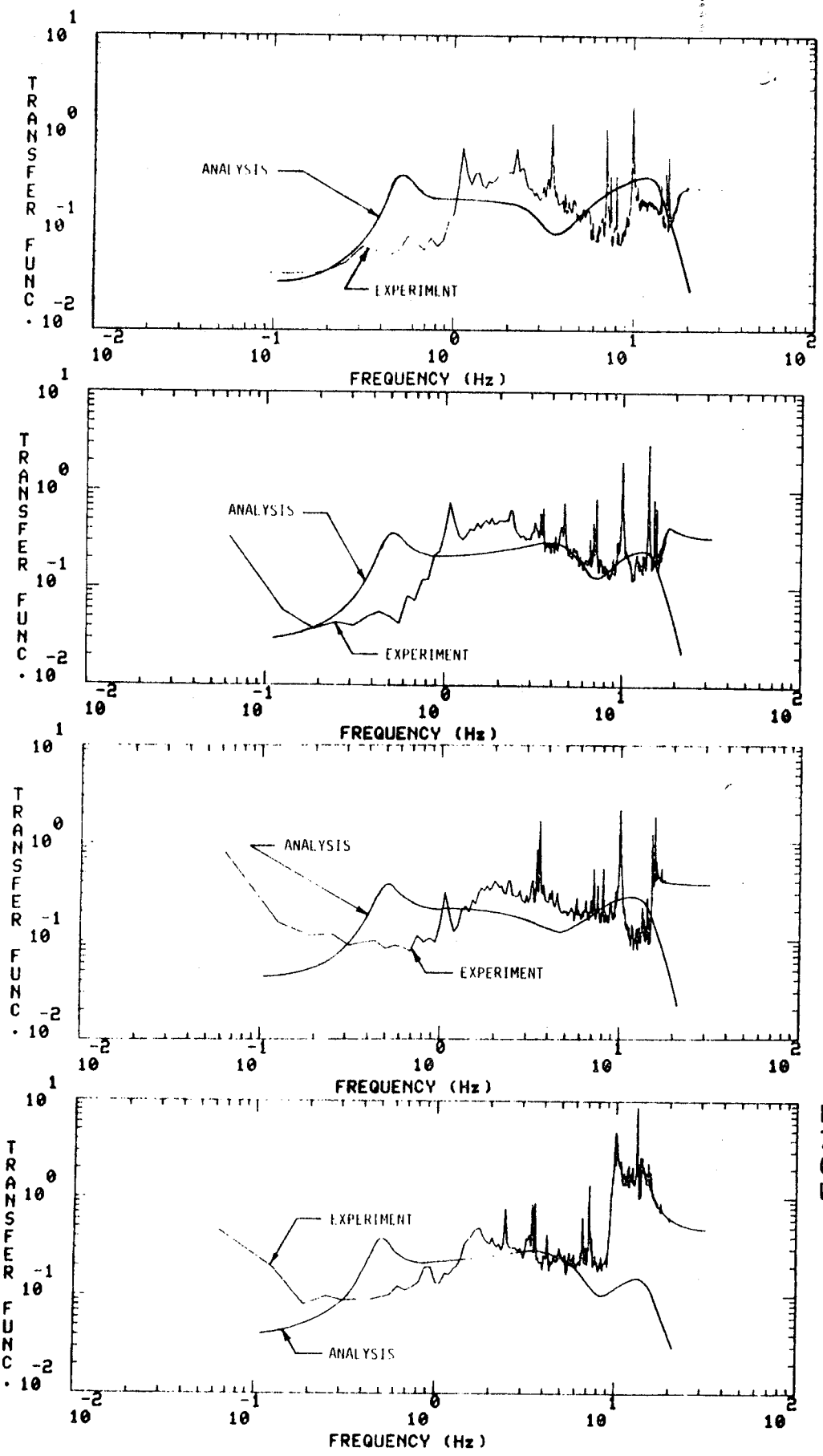

Figure 6-8. Transfer Functions of Carbody to Truck-A Bolster Vertical Displacement Referred to Actuator 1 Displacement.

We also compared the transfer functions of axle 1 actuator force to displacement for Runs 14, 17, 30 and 32. These comparisons are shown in Figure 6-9, and they are interesting for several reasons. At low frequencies both the experimental results and our model predictions show no speed sensitivity and a moderate creep-coefficient sensitivity. The ratio of experimental to analytical values is about 0.65 for all four cases at low frequency. This situation indicates that a single parameter or common product of parameters probably accounts for the difference. The parameter could be a spring rate, a distance or a calibration factor for example. More investigation will be required to resolve the discrepancy. At the kinematic mode frequency our model predicts considerable dynamic activity, while the experimental results show very little activity. Here is another indication that the SOAC vehicle has greater stability than our model predicts. The model's kinematic mode stability is very strongly dependent upon the secondary yaw suspension characteristics. We expect that the model parameters could be adjusted to achieve a significantly better match than is shown in Figure 6-9.

We attempted to compare the analytical and experimental transfer functions of primary longitudinal displacement to axle 1 actuator displacement. Our model predictions are about an order of magnitude higher than the experimental values over much of the frequency range. In addition the analytical and experimental curves have essentially no similarity in shape. Our model predicts that the primary lateral and longitudinal displacements are the same order of magnitude. The experimental results show the primary longitudinal displacements to be about an order of magnitude less than the primary lateral displacements. Since our model and the experimental results show fairly good agreement in the axle longitudinal displacements relative to ground, we expect a measurement problem. We have not at this writing, however, determined the source of the discrepancy.

All rail vehicles contain some nonlinearities, and the SOAC is no exception. Our dynamic analysis of the vehicle is a linear analysis, and we selected the comparison test runs to be ones most likely to approach linear behavior. To make a qualitative assessment of the SOAC nonlinearities we compared the transfer functions and several PSD of

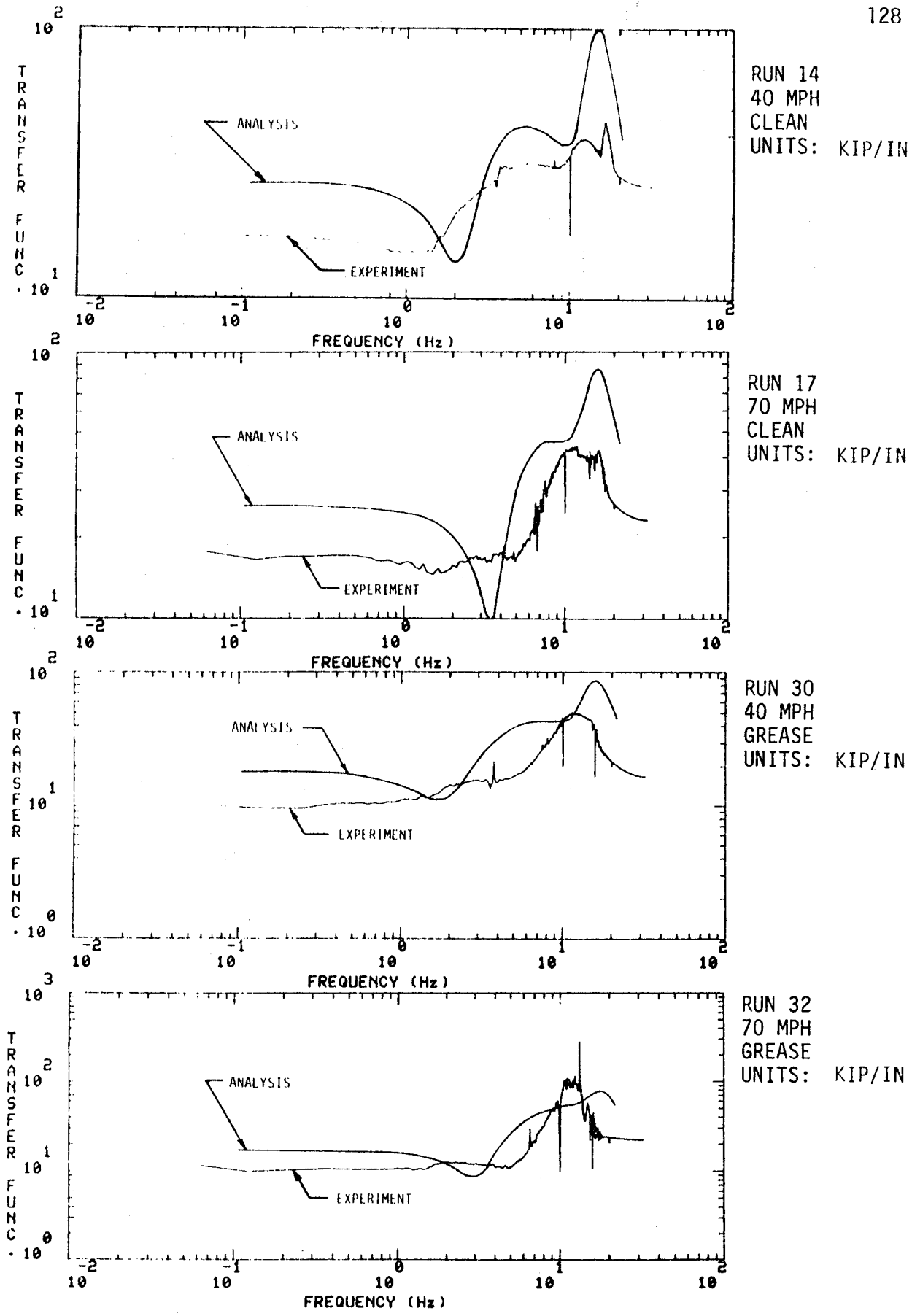

Figure 6-9. Transfer Functions of Actuator 1 Force to Actuator 1 Displacement.

Runs 29 and 30, the greased-roller runs at 40 mph with high and low forcing levels. The actuator force PSD of Run 29 was about an order of magnitude higher than the Run 30 actuator force PSD indicating an absolute force level ratio of about 3 to 1. The transfer functions for the two runs are remarkably similar. The primary difference is that some of the Run 29 transfer functions have slightly higher values in the 8- to 10-Hz range than the corresponding Run 30 transfer functions.

We also compared transfer functions from Runs 16 and 17, the clean roller runs at 70 mph with high and low forcing levels. The transfer functions were very much alike below about 5 Hz. Above 5 Hz the Run 16 data is invalid because of a recording problem, so we could not make a comparison.

All rail vehicles have nonlinear wheel-rail constraint functions as a result of flange-limited lateral travel. We examined the test data for evidence of flange contact. The flange-to-flange clearance predicted by the wheel-rail geometry program is about 0.6 inch. On the large amplitude forced runs the maximum peak-to-peak axle 1 lateral excursion was about 0.6 inch indicating that flange contact was either occuring or nearly occuring. The maximum axle 1 lateral excursion was substantially smaller on the small amplitude forced runs. We conclude that flanging occurred on none of the test runs included earlier in this chapter, but flanging may have occurred on the large amplitude forced runs. The response of the SOAC vehicle does not seem to be heavily influenced by nonlinear effects.

The agreement between the predictions from the forced-response model and the SOAC test results is fairly good considering that we made no attempt to adjust any parameter values on the basis of the dynamic tests. We think that substantially better results can be obtained by the use of parameter estimation techniques.

Based upon the comparisons we have made so far, we think our model underestimates the kinematic mode damping ratios but predicts the frequencies reasonably well. Our model is substantially in error in predicting the body mode frequencies because the model excludes the roll restraint system used during the tests. The low-frequency asymptotic behavior of our model is very similar to the SOAC's behavior, but the need to adjust a few parameters is evident. In several cases, for

example the car to bolster lateral displacement transfer function with respect to actuator force, the analytical and experimental results agree quite well over nearly the entire frequency range of the tests.

The input-output phase relationships for a dynamic system often carry important information about the dynamics of the system. We had hoped to obtain useful information from the phase relationships in this test series. Unfortunately, the phase plots showed considerable oscillation of phase angle between 180° and -180° rendering them of no use for analysis. We have encountered this problem in other rail vehicle test programs, so its occurrence was not entirely unexpected. A solution to this problem would increase the utility of the test data.

MODEL IMPROVEMENTS

A number of possibilities for improvements to the dynamic vehicle model have become apparent during the process of comparing model predictions and test results. These potential improvements fall into two categories: (1) additions that model effects not now accounted for, and (2) adjustments to the model parameter values to obtain better agreement between predictions and test results.

In the creep test portion of this program we identified different sets of creep coefficients for the two wheelset-rollerset pairs on the A-truck. However, both the eigenvalue-eigenvector and forced response implementations of the full dynamic vehicle model require the same creep-coefficient set for all four wheelset-rollerset pairs. Primary suspension stiffness tests conducted at TTC showed differences of about 10 percent between the axle 1 and axle 2 primary stiffnesses. Our dynamic vehicle models require the use of the same primary suspension parameters at all locations. The models could be improved by allowing different creep coefficient and primary suspension parameter sets at each wheelset.

The wheel-roller geometry measurements and subsequent analysis of the measurements with the wheel-roller geometry constraint computer program showed significant differences in the wheel-roller constraint functions for wheelsets 1 and 2. Our eigenvalue-eigenvector vehicle model implementation admits the use of separate constraint functions at each wheelset. However, our forced-response model has no such provision. It could be improved by the addition of this capability.

We previously discussed the poor agreement between our model predictions and the test results for the non-kinematic body modes of vibration. This agreement can be improved by the use of additional suspension elements, springs and perhaps dampers, between the carbody and ground that model the roll restraint system. Greater confidence could be obtained for the validity of the entire model if the analytical-experimental agreement is good at all frequencies of interest, including the body natural frequencies.

The second category of model improvements is model parameter adjustments. As part of this program, tests were conducted to characterize the primary lateral and longitudinal stiffnesses, the

secondary yaw stiffness, and the wheel-roller geometric constraint functions. However, we obtained other important vehicle parameter values form manufacturer's design information or from engineering estimates. We made no attempt to adjust any of these parameters to obtain better agreement between predictions and measurements of the SOAC's dynamic behavior. Making these adjustments would result in better agreement between theory and tests, and therefore lead to a more thorough understanding of the vehicle dynamics. For example, we have very little information on which to base estimates of any of the damping parameters. Furthermore, the secondary lateral stiffness, a very important parameter for dynamic behavior, was set at the truck builder's design value.

A parameter identification analysis of the dynamic tests might also yield better estimates of the behavior of the stiffness elements that were tested statically. In addition, improved values of wheel-roller geometric constraint functions might result.

A further possibility is the identification of some of the B-truck parameters. This truck was largely ignored during the tests. The potential for successful parameter identification is less here, however, because of the relatively small motions that occurred at the B-truck during the tests.

A very important reason to explore parameter identification techniques is that if the vehicle parameters found in the characterization tests can be identified just as well from the dynamic test results, then in future tests it may be possible to eliminate the expensive and time consuming characterization tests.

TESTING METHODS

During the planning stage of the SOAC Demonstration tests we were uncertain about the best way to use the forcing system to obtain the most vehicle action during the forced frequency response tests. At that time the two alternatives being considered were to use the two actuators in phase to force a lateral excursion of the A-truck and to use the actuators out of phase to force a yaw motion. In fact the frequency response tests were conducted with forcing from the axle-1 actuator and damping from the axle-2 actuator, which was not active but still attached to the truck frame.

With the implementation of the forced response SOAC model we are now able to provide quantitative answers to questions about test methods. As an initial study to provide guidance for future tests on the RDU we compared four forcing methods, as shown in Table 6-4. Since the model is linear, any force levels in the same ratios as the ones we used would yield the same results. The common characteristic in the four forcing methods is that the total force capability is constant.

We made computer runs with the SOAC model for each of the forcing methods using parameters representative of the 70-mph clean-roller tests. We swept the forces through a frequency range of about 0.09 to 22 Hz, then integrated the motions of all 17 model variables to obtain the root-mean-square values over the entire frequency range. We normalized the rms values of each model variable for each forcing method by dividing by the lowest rms value. Figure 6-10 shows the normalized rms amplitudes of all the model variables for the four forcing methods. The height of the bars and the density of the shading is proportional to the magnitude of the rms values. Forcing method 4 provides the highest rms values for all variables except X7, which is A-truck roll. Based upon the performance index of maximum rms value, method 4 is clearly the best forcing scheme. Interestingly, method 4 in our study, forcing at axle 1 only, is most nearly like the forcing method actually employed in the SOAC tests. A performance index that included implementation cost would be even more favorable to method 4 since only one actuator need be installed.

TABLE 6-4. FORCING METHODS COMPARED

USING SOAC FORCED RESPONSE MODEL

	METHOD 1	METHOD 2	METHOD 3	METHOD 4
F_1 (LB)	5000	5000	0	10,000
F_2 (LB)	5000	-5000	10,000	0

F_1 is axle 1 actuator force

F_2 is axle 2 actuator force

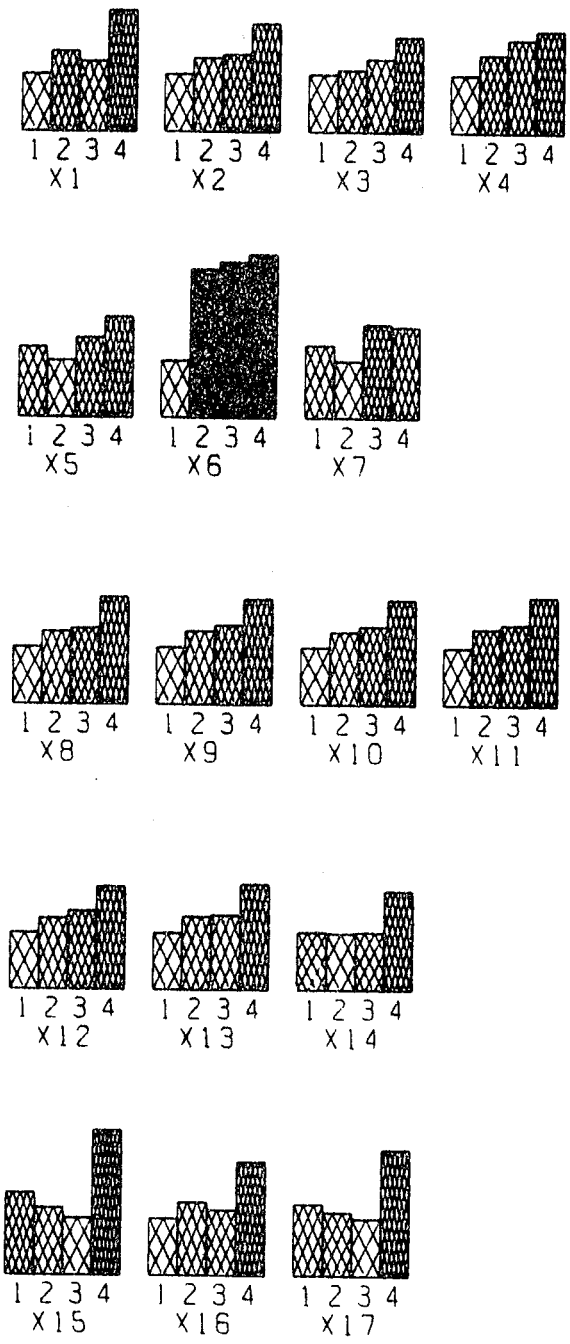

X1 = Wheelset 1 Lateral

X2 = Wheelset 1 Yaw

X3 = Wheelset 2 Lateral

X4 = Wheelset 2 Yaw

X5 = A-Truck Lateral

X6 = A-Truck Yaw

X7 = A-Truck Roll

X8 = Wheelset 3 Lateral

X9 = Wheelset 3 Yaw

X10 = Wheelset 4 Lateral

X11 = Wheelset 4 Yaw

X12 = B-Truck Lateral

X13 = B-Truck Yaw

X14 = B-Truck Roll

X15 = Carbody Lateral

X16 = Carvody Yaw

X17 = Carbody Roll

Figure 6-10. Relative RMS Values of SOAC Model Variables for Four Different Forcing Methods.

The SOAC demonstration test speeds were limited to a maximum of 80 mph by inertial loads in the traction motors. The vehicle proved to be quite stable at 80 mph. To illustrate the dynamic behavior that would be expected as the kinematic mode instability is approached in the forced response test, we ran the SOAC model at speeds up to 130 mph using creep coefficients representative of the clean roller condition. Figure 6-11 shows the transfer function of axle 1 actuator displacement to actuator force for speeds of 40, 70, 100 and 130 mph. The critical speed predicted by the model is about 133 mph. Clearly the task of identifying the kinematic mode frequency and damping is less difficult when test speeds approach the critical speed.

TTC personnel should give serious consideration to not using the roll restrain system on future tests. In this test series it appears that use of the system has significantly changed the carbody modes of the vehicle. If concern that the test vehicle might derail (deroller) dictates use of the restraint system, then perhaps the clearance could be increased from ½ inch to about 6 inches.

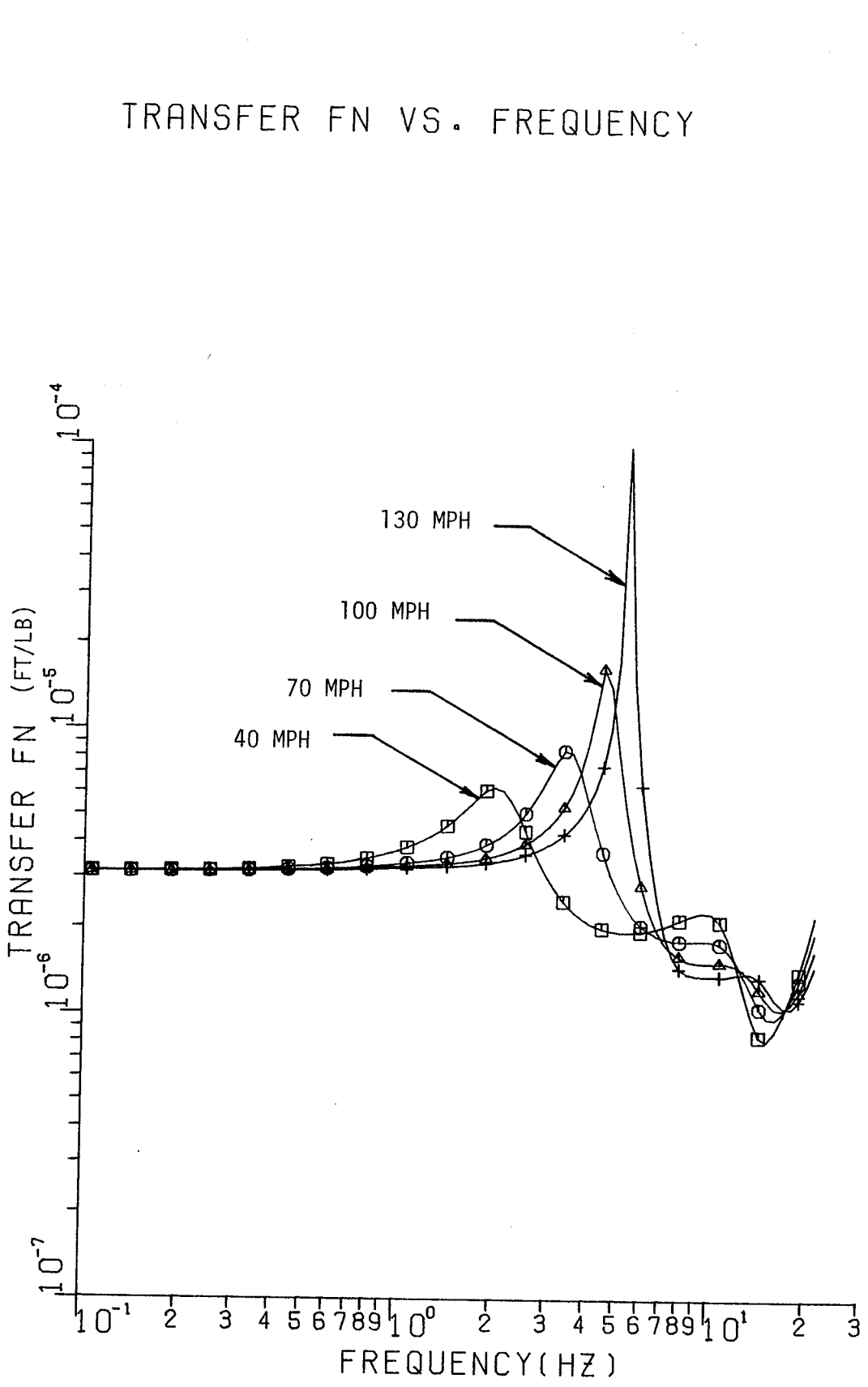

Figure 6-11. Axle 1 Actuator Displacement to Force Transfer Functions from SOAC Model

Chapter 7

SUMMARY, CONCLUSIONS AND RECOMMENDATIONS

SUMMARY

The objectives of the creep and dynamic portions of the SOAC Demonstration Test Program were substantially met. These objectives included vehicle characterization tests, vehicle on roller rig tests, creep force identification and the initial stages of dynamic theory validation. Characterization tests were carried out in the Rail Dynamics Laboratory to determine the primary suspension stiffnesses, the secondary yaw stiffness and friction, the wheel and roller profiles, and the interaxle angular and translational misalignments. With the exception of the primary suspension stiffness data, the results of these tests compared well with design values provided by the vehicle and truck manufacturers. The measured primary lateral stiffness was also close to the design value, but the test value for the primary longitudinal stiffness was about twice the design value.

Four types of tests were performed with the SOAC on the Roll Dynamics Unit on March 5 and 6, 1981. Altogether 32 test runs were made involving 1) creep force identification tests conducted at constant speed with forces applied to one truck with hydraulic actuators, 2) initial condition tests conducted at several speeds by releasing the truck from disturbed positions, 3) swept sinusoidal response tests conducted at constant speed with a sinusoidal, variable frequency force applied to the truck with a hydraulic actuator, and 4) single frequency sinusoidal response tests carried out at constant speed with sinusoidal forcing with the hydraulic actuator. Each test was conducted at more than one speed, with clean and greased wheel-roller surfaces and with different levels of applied forces. The creep identification tests were also carried out with soapy wheel-roller surfaces.

Numerous vehicle component displacements were measured and recorded on magnetic tape in analog and digital form during the tests. This data was reduced by TTC personnel to the forms required for the creep force identification and dynamic theory validation work. The creep force tests results were provided as mean force and displacement values at

different levels of applied forces for each creep test run. Exponentially decaying sinusoidal signals were fit to certain displacement results from the initial condition tests. This provided estimates for the damping and frequency of the least damped mode of vehicle motion. Transfer functions and power spectral densities were computed for most measurements from the swept sinusoidal response tests. The single frequency tests results were not processed further.

The creep force identification procedure utilized linear creep force theory. The objective of this work was identification of the lateral, longitudinal and lateral-spin creep coefficients of this linear model. A single wheelset model was used with a matrix inversion technique to estimate the creep coefficients.

Some of the creep force tests data proved to be unreliable. An extensive study of the data and comparison with simulated test results indicated that the reliable creep test data were the lateral displacements of the front truck wheelsets, the relative lateral deflection across the primary suspension of each wheelset, and the yaw angle and lateral displacement of the forced truck frame. The measured primary longitudinal stiffness, a value twice the design value, also does not agree with simulation results. Simulation indicates that a value approximately equal to the design value is appropriate.

Creep coefficient values at different speeds for the clean, soapy and greased roller conditions were identified from the test data. The values obtained differed from front to rear wheelsets, but were on the same order of magnitude as those given by the linear theory. Good repeatability, from run-to-run was found.

In order to compare experimental and theoretical dynamic response results for the SOAC vehicle, two different test series and corresponding analyses were conducted. Initial condition test results were compared with the results of an eigenvalue-eigenvector analysis. This involves comparing damping ratios and frequencies of the modes of vehicle motion. PSDs and transfer functions obtained from the swept frequency tests were compared with theoretical transfer functions obtained with a frequency domain analysis. Because only a small effort for dynamic theory validation was funded in this contract, our comparison utilized one set of vehicle parameters in the theoretical

analysis. Later stages of the dynamic theory validation will include adjustment and identification of certain vehicle parameters to obtain better agreement between theory and experiment.

The agreement found between predictions from the forced response model and the SOAC test results is fairly good considering that we made no attempt to adjust any parameter values on the basis of the dynamic tests results. We think that substantially better results can be obtained by use of parameter estimation techniques.

The model results predict body mode frequencies very different than those found in the tests. We believe that this difference is due to the effect of the roll restraint system used in the tests but not included in the theoretical model.

CONCLUSIONS

This project demonstrated that the testing methods, creep coefficient identification technique and dynamic theory validation approach all produced useful results. A number of specific conclusions in each area were also reached.

Testing Methods

The actuator configuration used for the forced sinusoidal response tests was found to be nearly optimum. A study of alternative test configurations using two actuators applied to the truck and operated singly, together in-phase, and together out-of-phase indicated that the largest dynamic response is obtained using only the leading actuator on the truck.

The utility of the single frequency sinusoidal response tests was very slight. Because the swept frequency tests did not produce clear resonances or modal frequencies, there was no good way to choose the frequencies for the constant frequency tests. Additionally, the swept frequency tests produced sufficient data to characterize the vehicle response.

Creep Coefficient Identification

The creep coefficient estimates from runs at the same condition showed good repeatability. This lends confidence to the testing and estimation procedures. There was a very small apparent influence of speed on the estimated creep coefficients. This is consistent with the available theory for rolling contact.

Values of the theoretical creep coefficients were calculated using both the specified design curvatures for the wheels and rollers and curvature values estimated from the actual profile data. The latter produced theoretical creep coefficient values smaller than those given by the experiment. It is quite likely that these curvature estimates were in error, and consequently that the magnitude of the estimated theoretical creep coefficients were also in error. This problem illustrates the need for careful determination of wheel and roller (or rail) cross-sectional curvatures in future creep coefficient identification tests.

Dynamic Response

Based upon the comparisons completed to date, it appears that the theoretical model underestimates the kinematic mode damping ratios, but predicts the frequencies reasonably well. The theory is substantially in error in predicting the frequencies reasonably well. The theory is substantially in error in predicting the body mode frequencies because the model excludes the roll restraint system used during the tests. The low-frequency asymptotic behavior of the theoretical model is in most cases very similar to the experimental results, but the need to adjust the model parameters is evident. In several cases, the analytical and experimental transfer functions agree quite well over the entire frequency range of the tests.

The SOAC vehicle possesses a high stability margin at the speeds tested in this program. The dynamic model shows that the roller rig terms are relatively unimportant for the SOAC vehicle, and that the critical speed on the RDU is only about 10 mph lower than it would be on track whose profile is the same as the rollers' profile.

RECOMMENDATIONS

We have gathered a number of recommendations for continued work on this subject and for future testing efforts on the RDU. In future testing on the RDU we suggest that attention be given to the following:

1. Modification or elimination of the roll restraint system. In this test series, it appears that use of the system has significantly changed the carbody modes of the vehicle. If concern exists that the test vehicle might derail (deroller),

then the interference with the vehicle dynamics could be minimized by introducing additional slack into the restraining system.

2. Improvement of the pre-test and post-test instrumentation checks and calibration procedures. Better documentation of instrumentation changes during the test conduct is particularly important.
3. Roller contamination. A method should be devised that will preclude oil contamination of the wheels and rollers by the RDU. Without such a system, conditions approximating clean-rail revenue service can never be achieved on the RDU.
4. Initial condition measurements. Measurements of the vehicle and RDU initial conditions should be made in future tests, These measurements will allow greater flexibility in the selection of creep coefficient identification methods.
5. Coefficient of friction measurement. The test condition coefficients of friction between wheelsets and rollersets should be measured in future tests. Knowledge of friction coefficients is important in the application of nonlinear creep theories.

The dynamic theory verification work was barely started in this project. Continued work with the test data to complete this efforts should prove fruitful. In such future work, the following matters should be addressed:

1. Improvement of the vehicle models to allow for different wheel-rail geometry and creep coefficients on each axle.
2. Inclusion of the vehicle restraint system in the vehicle dynamic model to adequately represent the test situation.
3. Model parameter adjustment to improve agreement. In particular, the vehicle damping properties and the secondary suspension lateral stiffness were not tested for this vehicle. Identification of these parameters from the response data, and verification with different test data should be undertaken. Further evaluation of longitudinal stiffness effects on model results is needed.

REFERENCES

1. Cooperrider, N. K., Law, E. H. and R. H. Fries, "Test Requirements for Creep and Dynamic Tests of the SOAC Transit Car on the Roll Dynamics Unit," prepared for Boeing Services International under contract F-401285-6940, January 13, 1981.

2. _____, "Implementation Plan, Transit Car Demonstration Test Program," Report No. RDU-IP-81-02-03, Rail Dynamics Laboratory, Transportation Test Center, February, 1981.

3. _____, "The Rail Dynamics Laboratory: Capabilities, Tests," Transportation Test Center, January 1982.

4. Horton, M. D., and Muller, G. G., "Drive Train System for Wheel/Rail Dynamics Simulator," prepared for FRA By General Electric Co., under contract DOT-FR-20016, January 23, 1973.

5. Irani, F., "Pre-Test Alignment for SOAC "A" Truck (Motorman's End Only)," private communication, July 1, 1981.

6. Irani, F., "SOAC Lateral Stiffness Test," private communication, June 30, 1981.

7. Nelson, S., "SOAC Longitudinal Stiffness Test," private communication, May 15, 1981.

8. Irani, F., "SOAC Rotational Stiffness Test," private communication, June 30, 1981.

9. Roberts J. A., private communication, December 10, 1980.

10. Cooperrider, N. K., Law, E. H., Hull, R., Kadala, P. and J. M. Tuten, "Analytical and Experimental Determination of Nonlinear Wheel Rail Geometric Constraints," Symposium on Railroad Equipment Dynamics, ASME, 1976, pp. 41-70.

11. Heller, R. and N. K. Cooperrider, "Users' Manual for Asymmetric Wheel/Rail contact Characterization Program," U.S. DOT Report No. FRA-OR&D-78/05, PB 279707, Dec. 1977.

12. Inskeep, D., "SOAC Test Logs," Rail Dynamics Laboratory, March 1981.

13. Chang, E. H., "Data Reduction System (DRS) - User's Manual," Data Processing Department, Transportation Test Center, Pueblo, Colorado, June 30, 1981.

14. Haque, I., "Development and Use of Analytical and Experimental Techniques for the Estimation of Creep Coefficients for a Passenger Vehicle on a Roller Rig," Ph.D. Dissertation, Clemson University, August, 1982.

15. Brickle, B.V., "Roll Dynamics Unit (RDU) Analysis Study; Creepages & Forces Acting on a Wheelset on Rollers," DOT FRA Report, June 1980.

16. Blader, F. B., "Fundamental Differences Between the RDU and an Ideal Track in Determining Vehicle Lateral Dynamics," DOT FR 67001 Reg. No. 10314.

17. Law, E. H., Hadden, J. A. and Cooperrider, N. K., "General Models for Lateral Stability Analyses of Railway Freight Vehicles," Federal Railroad Admin. Rept. FRA-OR&D-77-36 (PB 272372), June 1977.

18. Kalker, J. J., "On the Rolling Contact Between Two Elastic Bodies in the Presence of Dry Friction," Doctoral Thesis, Delft University of Technology, 1967.

19. Agarwal, C., "Determination of Creep Force Characteristics of a Railway Vehicle on a Roller Rig," M.S. Thesis, Department of Mechanical Engineering, Clemson University, December 1980.

20. Kuester, J. L. and J. H. Mize, Optimization Techniques with Fortran, McGraw Hill, 1973.

21. Illingworth, R. "The Mechanism of Railway Vehicle Excitation by Track Irregularities," Ph.D. Thesis, Oxford University (1973).

22. Brickle, B. V., "The Steady State Forces and Moments on a Railway Wheelset Including Flange Contact Condition," Ph.D. Thesis, Loughborough University of Technology (1973).

23. Hobbs, A.E.W., "A Survey of Creep," DYN 52, B.R. Research Department (1967).

24. Graupe, D., Identification of Systems, Van Nestrand Reinhold Company, 1972.

25. Agarwal, C., E. H. Law, N. K. Cooperrrider, "Determination of Creep Force Characteristics of a Railway Vehicle on a Roller Rig," Proc. of 7th Int. Wheelset Congress, Vienna, October, 1981.

26. Hague, Law, Cooperrider, "Users Manual for the Calculation of Kalker's Linear Creep Coefficients," DOT FRA report, May '79.